# APPLICATION OF METAMATERIALS FOR PERFORMANCE ENHANCEMENT OF PLANAR ANTENNAS

**Ph.D. THESIS**

*by*

**DEBASISH PAL**


**DEPARTMENT OF ELECTRONICS AND COMMUNICATION ENGINEERING INDIAN INSTITUTE OF TECHNOLOGY ROORKEE**
**ROORKEE-247667 (INDIA)**
**JUNE, 2016**

# APPLICATION OF METAMATERIALS FOR PERFORMANCE ENHANCEMENT OF PLANAR ANTENNAS

**A THESIS**

***Submitted in partial fulfilment of the requirements for the award of the degree***

***of***

**DOCTOR OF PHILOSOPHY**

***in***

**ELECTRONICS AND COMMUNICATION ENGINEERING**

***by***

**DEBASISH PAL**


**DEPARTMENT OF ELECTRONICS AND COMMUNICATION ENGINEERING**
**INDIAN INSTITUTE OF TECHNOLOGY ROORKEE**
**ROORKEE-247667 (INDIA)**
**JUNE, 2016**

**©INDIAN INSTITUTE OF TECHNOLOGY ROORKEE, ROORKEE- 2016**
**ALL RIGHTS RESERVE**

# INDIAN INSTITUTE OF TECHNOLOGY ROORKEE

## CANDIDATE'S DECLARATION

I hereby certify that the work which is being presented in the thesis entitled **"APPLICATION OF METAMATERIALS FOR PERFORMANCE ENHANCEMENT OF PLANAR ANTENNAS"** in partial fulfillment of the requirements for the award of the Degree of Doctor of Philosophy and submitted in the Department of Electronics and Communication Engineering of the Indian Institute of Technology Roorkee, Roorkee is an authentic record of my own work carried out during a period from July, 2009 to June, 2016 under the supervision of Dr. A. Patnaik, Associate Professor, Department of Electronics and Communication Engineering, Indian Institute of Technology Roorkee, Roorkee, India.

The matter presented in this thesis has not been submitted by me for the award of any other degree of this or any other Institute.

**(DEBASISH PAL)**

This is to certify that the above statement made by the candidate is correct to the best of my knowledge.

**Dr. A. Patnaik**
**Supervisor**
**Date: 25th May 2016**

The PhD Viva-Voce Examination of **Mr. DEBASISH PAL**, Research Scholar, has been held on **17th September 2016.**

**Chairman SRC** **Signature of External Examiner**

This is to certify that the student has made all the corrections in the thesis.

**Signature of Supervisor** **Head of the Department**
**Date: 17th September 2016**

# Acknowledgements

"*Every word of God proves true. He is a shield to all who come to him for protection.*"

First of all, I am extremely grateful to the Almighty God who has always taught me to follow the right path of the life. Without his grace this work could never have come true.

I would like to express my sincere gratitude to my supervisor Dr. Amalendu Patnaik, Associate Professor Department of Electronics and Communication Engineering, IIT Roorkee for his continuous support and valuable guidance in carrying out this research work. His commendable patience, motivation, enthusiasm and immense knowledge have been a source of inspiration in my research and writing of this thesis. This work would not have been possible without him. I have been fortunate enough to get the excellent environment for work with ample facilities and academic freedom from him. I will remain ever indebted to him. I could not have expected having better advisor and mentor for me.

Besides my supervisor, I am very grateful to the other members of my research committee, Dr. M.V. Kartikeyan, Dr. V. Pant and Dr. N. P. Pathak for their suggestions and contributions during my Ph.D. I also offer my sincere thanks to all the faculty and staff members of Electronics and Communication Engineering Department for their needful support. I also express my thanks to the laboratory technicians, Mr. Rajaram, Late. L. Giri and Mr. Gaur for their assistantship in the advanced microwave lab.

The years spent at IIT Roorkee would not have been as wonderful without my friends, including Dr. Omprakash, Dr. M. K. Panda, Dr. Anuradha, Jagannath, Dr. Arjun, Prateek, Ajeet Kumar who contributed through their support, knowledge and friendship in this work.

Special thanks to my friend Dr. Ayan who really helped me in fabrication, testing and thesis writing. I also thank Dr. Anirban Bera for his valuable suggestions. I also express my thanks and gratitude to every member of Klystron group in

CSIR-CEERI Pilani. I also take this opportunity to thank Dr. S. N. Joshi, my sister Mrs. Devyani Monadol, my brother in law Mr. Ashok Mondol, my nephew Anjishnu, my sister Ms. Debolina Dey and my aunt Mrs. Dipali Dey for their continuous mental support and encouragement in tough days of my life.

I take this opportunity to express my regards and obligation to my parents whose support and encouragement I can never forget in my life. It is their blessings where I am today.

I wish to appreciate and thank my beloved son Debarko for his love and his innocent smile which inspired me. Finally, this thesis is dedicated to my parents. Their blessings and love have been a constant support to me throughout my life. For any one I forgot to thank, I am sorry, I just wish them to know that I could not have done this without them.

**DEBASISH PAL**

# Abstract

The ever growing communication system industry and the development of the communication techniques in the last one decade have thrown great challenges to microwave engineers to enhance the performance of the existing systems to cope up with the new wireless communication standards. Antennas, considered as the backbone of the wireless communication system, have to function at par with the other subsidiary microwave circuitry. In this regard, the challenges faced by the antenna engineers are to enhance the performance of the antennas and at the same time to shrink the size of the antenna system. As planar antennas are preferred mostly in wireless industry, because of some of its advantages like light weight, flexibility, conformability etc., constant efforts have been made to enhance its performance, since its inception. The research done in this thesis is an attempt in that direction and the *metamaterial* concept is used for the performance enhancement of planar antennas.

The pioneering work by Veselago in 1968, followed by Pendry in 1996 has made the foundation of the metamaterial concept and since then this artificial material has been adopted by microwave engineers for various activities. Antenna engineers are not exceptions and have used this material for many antenna applications. A glance over the related literature reveals that, most of the works are either results from the full-wave simulators or experimentally verified structures. An analytical approach for metamaterial based planar antenna was absent from the literature. An attempt has been made in this thesis to develop an analytical model and to find out a closed-form expression for the resonant frequency of a metamaterial based planar antenna. Although a specific type of metamaterial (CSRR) structure is used for the analysis, but the same can be extended for other structures also.

After attempting the analysis problem, the design aspect of such structures was explored. The aim was to develop a fast, user-friendly module to fix the design dimensions of metamaterial based antennas, for it to work at desired frequency. The task was approached as an optimization problem and with the help of machine learning approaches, was solved successfully. In order to validate the working of the developed module, few typical cases were considered.

The rest of the work done in this thesis is to use different metamaterial structures

to overcome some of the drawbacks of simple patch antennas. Design of simple multiband patch antennas, enhancement of directivity and design of compact planar antenna structures are the works attempted in this thesis. Laboratory prototype of almost all the antenna structures is made and experimentally measured for cross-verifying the results from the analysis or from the full-wave simulators.

Although some specific metamaterials are used in this thesis, but the concepts developed can be extended to other structures also, giving a scope for future research work. The authors are sure that the work done in this thesis will certainly help the antenna community in a big way.

# Table of Contents

# List of Figures

# List of Tables

# List of Abbreviations

| | |
|---|---|
| AD | Artificial Dielectric |
| ACO | Ant Colony Optimization |
| AMC | Artificial Magnetic Conductor |
| BFO | Bacteria Foraging Optimization |
| CRLH | Composite Right Left Hand |
| CSRR | Complimentary Split Ring Resonator |
| CST | Computer Simulation Technology |
| DNG | Double Negative Material |
| EBG | Electronic Band Gap |
| FSS | Frequency Selective Surface |
| FZ | Fuzzy Logic |
| GA | Genetic Algorithm |
| HIS | High Impedance Surface |
| HPBW | Half Power Beam Width |
| LHM | Left Hand Material |
| MSR | Modified S Shaped Resonator |
| NIM | Negative Index Material |
| NN | Neural Network |
| NRI | Negative Refractive Index |
| OCSRR | Open Complimentary Split Ring Resonator |
| PBG | Photonic Band Gap |
| PM | Plasmonic Media |
| PNA | Performance Network Analyzer |
| PRS | Partially Reflective Screen |
| PSO | Particle Swarm Optimization |

| | |
|---|---|
| RHM | Right Hand Material |
| RS | Rough Sets |
| SPP | Surface Plasmon Polariton |
| SRR | Split Ring Resonator |
| VNA | Vector Network Analyzer |
| WLAN | Wireless Local Area Network |

# 1.

# Introduction

## 1.1 Thesis Prologue

With the rapid advancement of wireless communication technology and systems, the demand for the requirement of accompanied high performance antenna systems is increasing. Continuous efforts have been expended by antenna engineers to enhance the working performance of antenna systems to meet the desired requirement. The work done in this thesis are an attempt to enhance the performance of planar antennas using *metamaterials*. Both analysis and design aspects of metamaterial based patch antennas is considered in this thesis. The results of all the antenna structures, analysed in this thesis, are cross verified with experimental results.

## 1.2 Motivation

Antennas and antenna arrays are an integral part of any wireless communication system. The exponential growth in communication standards, particularly in mobile communication technology, starting from 1G to the present 5G, has thrown tremendous challenges to antenna engineers to think of new designs with improved performance. Compactness of those structures is an added burden. Because of this, a lot of focus is given to the performance enhancement of planar antennas. Although these antennas have many advantages like light weight, low profile, can be flush mounted etc., but at the same time, these structures has some inherent demerits. Ever since the inception of this planar antenna concept, continuous efforts have been made by researchers for its performance enhancement. The work done in this thesis is a small step in that direction. The concept of *metamaterial* has been used, in this thesis, for performance enhancement of patch antennas.

## 1.3 Research Objective

The objectives of our research work are as stated below:

- To develop an analytical model for metamaterial based patch antennas.
- To develop a fast and user-friendly design module for metamaterial based patch antennas.
- To use the metamaterials for removing the demerits of patch antennas for its performance improvement.

In order to meet these research objectives, the following tasks were attempted in this thesis:

a. An equivalent circuit model of a metamaterial based patch antenna is derived in order to find a closed-form expression for its resonant frequency.
b. Machine learning approaches are used to develop a fast and flexible design module for metamaterial based patch antenna.
c. Metamaterial concept is used to design simple multiband patch antennas.
d. Metamaterials are used to enhance the directivity of patch antennas.

## 1.4 Organization of the Thesis

The thesis consists of seven chapters. The first chapter gives an introduction of the work done in the thesis. It also includes the motivation and objectives of the research.

Chapter-2 presents a comprehensive review on electromagnetic metamaterials starting from its definition and classification. Brief history of development of these materials is recalled in this chapter. The interesting characteristics of metamaterials are discussed and the use of these characteristics in various reported applications is highlighted in this chapter.

Chapter-3 of the thesis gives an analytical treatment of a metamaterial based patch antenna. A circuit theoretical approach for a complementary split ring resonator (CSRR) array backed patch antenna is developed in this chapter. The aim is to get a first-hand information of the resonant frequency of such an antenna using a closed-form expression. Mutual coupling between the CSRR array elements and the coupling between the antenna and the metamaterial is considered to derive this closed-form expression.

Because of the complicated structures of the metamaterials, the design of these materials is very cumbersome. In order to overcome this, in Chapter-4, a machine learning based design of metamaterial based patch antennas is attempted. The joint utilization of artificial neural networks and particle swarm optimization helps in developing a user-friendly module for design of metamaterial based antennas.

Chaper-5 and 6 discusses the application of metamaterials for design of multiband microstrip antennas and for enhanced directivity microstrip antennas respectively. Two different types of metamaterial structures are used for these two different applications. Laboratory prototypes of these antennas are made and the measured results are cross verified with EM-simulation results.

Finally chapter-7 summarizes the contributions made in the thesis and the scope for the future work is outlined.

# 2.

# Literature Review

## 2.1 Introduction

*Metamaterials* or more specifically the *Electromagnetic metamaterials* are defined as "artificial effectively homogeneous electromagnetic structures with unusual properties not readily available in nature." [1] An effectively homogeneous structure is a structure whose structural average cell size is much smaller than the guided wavelength.

Obviously, it refers to man-made materials that are purposely designed and engineered to do certain functions. In other words, a metamaterial is the co-existence of materials with well-defined properties that causes new properties due to its composition. These are artificial periodic structures with lattice constants that could be much smaller, in the order or larger than the wavelength of the incident electromagnetic radiation. The concept of metamaterials is a breakthrough mainly due to their ability to guide and control efficiently electromagnetic waves and the material properties. A lot of research focus has been made on these materials with the purpose to study, develop and design metamaterials and their applications. As a result many interesting electromagnetic applications and specifically radiated wave applications have been evolved.

This chapter briefly reviews these metamaterials with special emphasis to their properties and applications. Specific use of these materials for performance improvement of planar antennas is highlighted.

## 2.2 Brief History

The earliest publication on the concept of magnetic refraction can be seen in the lecture notes of Prof. Mandelstam from Moscow University way back in 1945 [2]. In 1951, Malyuzhintes studied Somerfield radiation condition in backward wave media [3]. Sivukhin

observed backward property and investigated negative parameter materials in 1957 [4]. In early 1960s, theoretical studies on backward wave structures, applicable to microwave tubes, were carried out [5-6]. Most significant contributions on electromagnetic metamaterials came from Veselago in 1968. He carried out a methodical analysis of materials with negative permittivity and permeability and coined the term left handed material (LHM) [7]. Veselago pointed out some new features like reverse Doppler effect and backward Cerenkov radiation, in addition to its conventional property of negative refraction.

Still the concept of metamaterials was unable to attract the attention of researchers and scientists due to lack of experimental verification and realization. Pendry (1996) was the first person to realize LHM by using the wire medium whose permittivity was found to be negative [8]. Artificially engineered magnetic plasma with negative permeability was again realized by Pendry and his group in 1999 [9]. In this experiment they demonstrated the concept of Split Ring Resonator (SRR) for magnetic response. Smith then combined these two structures together to realize double negative medium in 2001 [10].

After successful realization of LHM, researchers were attracted towards this fascinating concept and many theoretical and experimental studies were carried out [11-14]. This experiments led to the discovery of super lens and perfect lens [15-20]. During this period an alternative transmission line approach were proposed by two independent groups (Eleftheriades and Caloz-Itoh) for electromagnetic metamaterial structures [21-24]. Usually a transmission line is modelled as distributed series inductances (L) and shunt capacitances (C). As a dual model of conventional transmission line, shunt inductance (L) and series capacitance (C) was proposed by these groups in apprehension to justify LHM. Since the series capacitance is always accompanied by an unavoidable parasitic shunt capacitance, a general composite-right-left-handed (CRLH) transmission line model has been proposed to represent RHM and LHM [24, 25]. Based on this phenomenon, many improved performance microwave components including antennas have been proposed [26-32]. Major disadvantage of electromagnetic metamaterials is its narrow bandwidth.

## 2.3 Classification of Electromagnetic Metamaterials

Different classes of metamaterials have been reported in the literature. These classifications were proposed by Rahamat-Samii [33], Caloz [1], and Engheta [34]. Here we

present some tentative class of metamaterials that exits till date. These classes of metamaterials are as shown below:

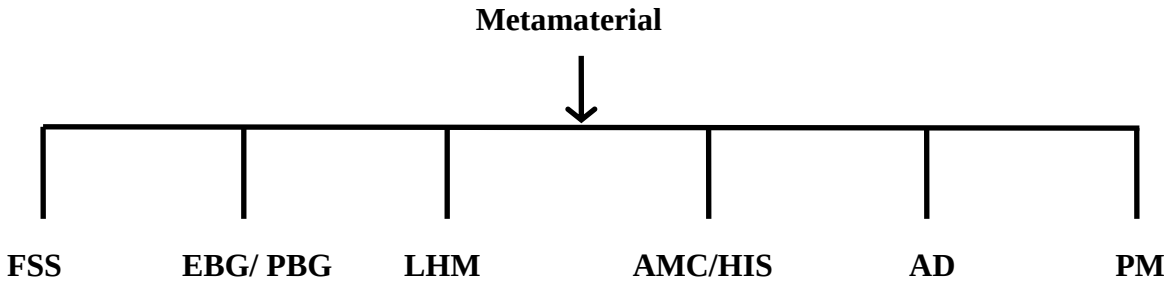


**FSS:** Frequency Selective Surface

**EBG/PBG:** Electronic Band Gap/ Photonic Band Gap

**LHM**: Left Handed Material

**AMC/HIS**: Artificial Magnetic Conductor/ High Impedance Surface

**AD**: Artificial Dielectrics

**PM:** Plasmonic Media

**FSS:** Frequency selective surfaces are large dielectric substrates which consist of conducting elements on one side and the reverse side is devoid of any conducting layer. Conducting elements may be of any shape but all of them must be identical in shape. If the front side of the FSS is illuminated with a range of electromagnetic (EM) waves of various frequencies, some of the waves are transmitted with minimum attenuation, some waves are totally reflected back and some of the waves are partially reflected and partially transmitted. Some of the FSS structure are shown in figure 2.1. Hence this kind of surface performs a selection of frequency among the incident waves on it. So we can view FSS as a filter for plane waves at any angle of incidence [35].

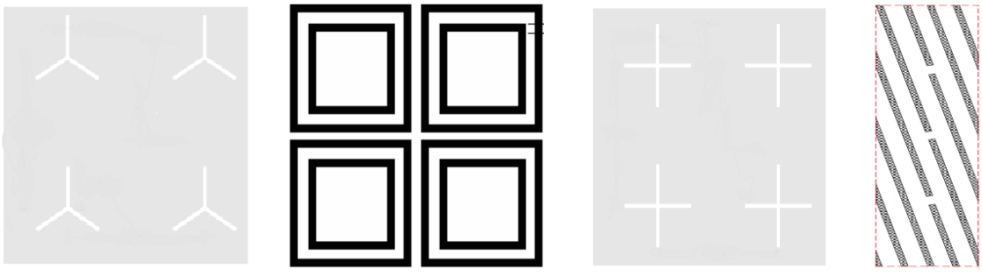

Fig. 2.1. Different types of FSS structures.

**EBG/PBG:** This class of metamaterials are broadly termed as photonic crystals. These are either metallic, dielectric or metalodielectric elements. These materials are used largely to control the propagation of EM waves. EBG structures are said to have two most important properties, (i) these can produce a bandgap and (ii) a localized window for a particular frequency band. Using these properties, this class of materials can be used as a frequency filter or a pass band for a frequency band. A few of EBG structures are shown in figure 2.2. There exists 1D, 2D and 3D EBG structures. 1D and 2D metamaterials are directive in nature. In case of directive EBG structures direction is determined by the periodicity and dielectric constant of the materials [33].

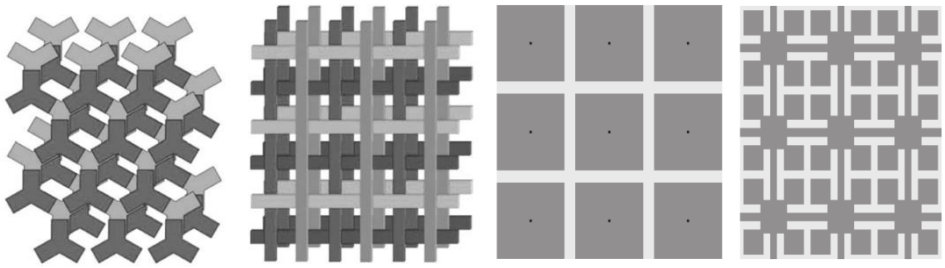

Fig. 2.2. Different types of EBG structures.

**LHM:** Left handed materials have been called by many names, such as negative refractive index (NRI) material, negative-index material (NIM), double-negative (DNG) metamaterial, backward wave media, negative phase velocity (NPV) media, Veselago media etc. These materials are the most famous metamaterials. These have properties of simultaneous negative permittivity and permeability. Composite right/left-handed (CRLH) concept is an artificial transmission line (TL) approach that describes the behaviour (RH or LH) of these medium, depending on the working frequency range. These media can be included in this left-handed class of metamaterials. A typical left handed media is shown in figure 2.3.


Fig. 2.3. Different structures of LHM.

**AMC/HIS:** A HIS or AMC, can be described as a type of synthetic composite that is intentionally structured with a magnetic conducting surface for an allotted but defined range of frequencies. AMC/HIS structures often emerge from an engineered periodic dielectric base along with metallization patterns designed for microwave and radio frequencies. The metallization pattern is usually determined by the intended application of the AMC or HIS structure. Furthermore, two inherent notable properties of this class of metamaterials, which cannot be found in natural materials, have led to a significant number of microwave circuit applications. First, AMC/ HIS surfaces are designed to have an allotted set of frequencies over which electromagnetic surface waves and currents will not be allowed to propagate. These materials are then both beneficial and practical as antenna ground planes, small flat signal processing filters, or filters as part of waveguide structures. For example, AMC (figure 2.4) surfaces as antenna ground planes are able to effectively attenuate undesirable wave fluctuations, or undulations, while producing good radiation patterns. This is because, the material can suppress surface wave propagation within the prescribed range of forbidden frequencies. Secondly, AMC surfaces have very high surface impedance within a specific frequency range, where the tangential magnetic field is small, even with a large electric field along the surface. Therefore, an AMC surface can have a reflection coefficient of +1.

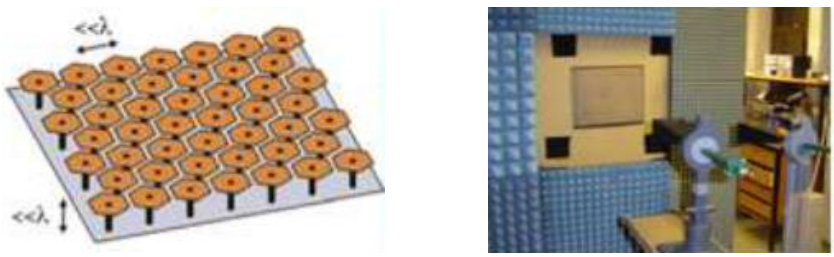

Fig. 2.4. a) A view of AMC structure  b) its testing in anechoic chamber [33].

**AD:** Artificial dielectrics consist of a large number of sub-wavelength conducting obstacles embedded in a homogeneous host medium. Defining such dielectrics as metamaterials makes sense because the conducting properties of metals are being changed to a dielectric-type behaviour in the macroscopic properties. Chiral medias are also included in this class (figure 2.5).The term chiral describes an object, especially a molecule, which has or produces a non-superimposeable mirror image of itself. In chemistry, such a molecule is called an enantiomer or is said to exhibit chirality or enantiomerism. The term "chiral" comes from the Greek word for the human hand, which itself exhibits such non-superimposeability of the left hand precisely over the right. Chiral metamaterials are constructed from chiral in which the effective parameter *k* is non-zero [1].

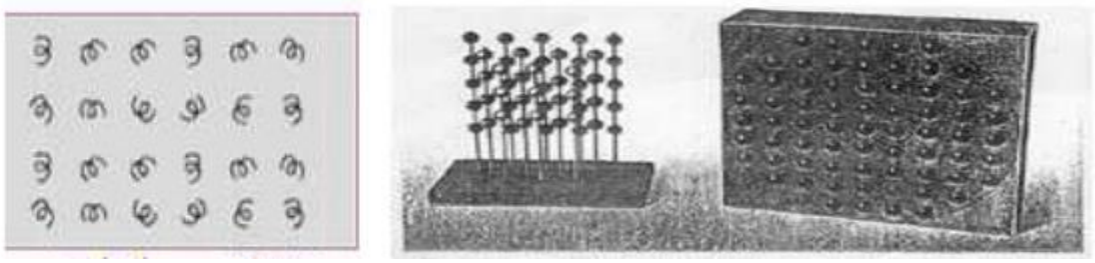

Fig. 2.5 Different types of artificial dielectric structures.

**PM:** Plasmonic metamaterials are materials that exploit surface palsmons, which are produced from the interaction of light with metal-dielectric materials. Under specific conditions, the incident light couples with the surface plasmons to create self-sustaining, propagating electromagnetic wave, known as surface plasmon polaritons (SPPs). Once launched, the SPPs ripple along the metal-dielectric interface and do not stray from this narrow path. Compared with the incident light that triggered the transformation, the SPPs can be much shorter in wavelength. Plasmonic metamaterials (figure 2.6) are tailor made composites of metallic and dielectric materials designed to achieve optical properties not seen in nature. The properties stem from the unique structure of the composites, with features smaller than the wavelength of light separated by sub-wavelength distances. By fabricating such metamaterials, fundamental limits tied to the wavelength of light are overcome. Light hitting a metamaterial is transformed into electromagnetic waves of a different variety of surface plasmon polaritons, which are shorter in wavelength than the incident light. This transformation leads to unusual and counterintuitive properties that might be harnessed for practical use. Moreover, new approaches that simplify the fabrication process of

metamaterials are under development. Furthermore, nanotechnology applications of these nanostructures are currently being researched, including microscopy beyond the diffraction limit [34].

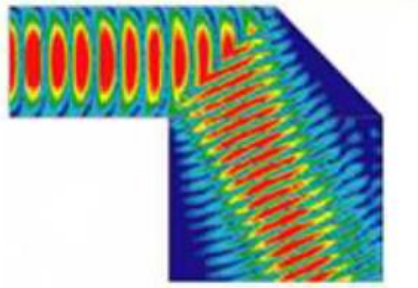

Fig. 2.6. A pictorial view of plasmonic media.

## 2.4 Properties of Electromagnetic Metamaterials

This section describes some peculiar properties of metamaterials which are not usually shown by conventional materials. Few of the following properties are also utilized to enhance the performance of different antenna parameters [1].

1. Reversal of Doppler effect
2. Reversal of Vavilov Cerenkov radiation
3. Reversal of boundary conditions relating the normal components of the electric and magnetic fields at the interface between a conventional RH and LH medium.
4. Reversal of Snell's law
5. Transformation of a point source into a point image by a LH slab.
6. Interchanging of convergence and divergence effects in convex and concave lenses respectively.
7. Formation of left handed triplet of vectors **E**, **H**, **k** in double negative metamaterials

### 2.4.1 Reversal of Doppler effect:

When a moving receiver detects the radiation coming from a source at rest, in an uniform medium, the detected frequency of the radiation depend on the relative velocity of the emitter and receiver. This is well known Doppler's effect. If the receiver moves towards the source, wave fronts and the receiver moves in opposite direction. Therefore the frequency seen by the receiver will be higher than the frequency measured by an observer at rest. However if the medium is left handed material, wave propagation is backward and the wave

fronts moves towards the source. Therefore both the receiver and the wave fronts move in the same direction and the frequency measured at the receiver is smaller than the frequency measured by an observer at rest. This frequency shift is given by

$$\omega = \pm\omega_0 \times \frac{v}{v_p} \tag{2.1}$$

where $\omega_0$ is the frequency of the radiation emitted by the source, $v$ is the velocity at which the receiver moves towards the source, $v_p$is the phase velocity of light in the medium and the ± sign applies to ordinary /left handed media [34].

### 2.4.2 Reversal of Vavilov Cerenkov radiation:

Cerenkov radiation occurs when a charged particle enters an ordinary medium at a velocity higher than the velocity of light in that medium. If the deceleration of this particle is not too high, its velocity can be considered approximately constant over many wave periods. The spherical wavefronts radiated by this particle becomes delayed with regard to the particle motion thus giving rise to a shock wave which travels forward making an angle $\theta$ with the particle velocity. This angle is given by

$$\cos\theta = \frac{c}{nv} \tag{2.2}$$

Where $c/n$ is the velocity of light in the medium and $v$ is the velocity of the particle. If the medium has a negative refractive index, then the wave propagation is backward and the spherical wave fronts corresponding to each frequency harmonics of the radiation move inwards to the source at a velocity $c/|n(\omega)|$. Therefore each wavefront collapses at the advanced position of the particle. Thus the resulting shock wave travels backward at an obtuse angle from the particle motion [34]. Concept of reversal of Cerenkov radiation in left handed media is shown in figure 2.7.

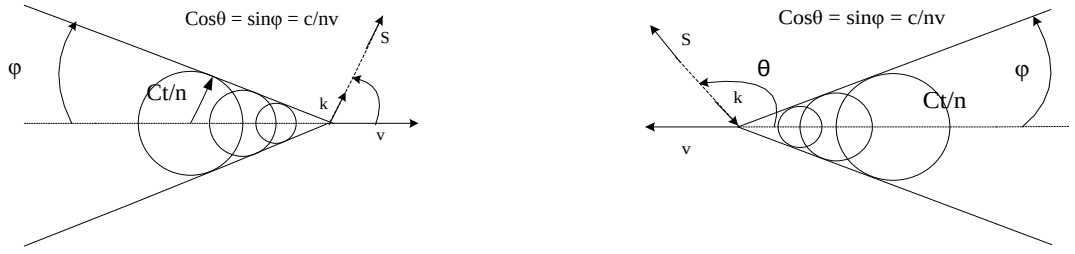


Cerenkov radiation in RH media Cerenkov radiation in LH media Fig. 2.7. Reversal of Vavilov Cerenkov radiation in left handed media.

### 2.4.3 Reversal of boundary condition at the interface between a RH/LH media:

The boundary conditions between two conventional media are:

$$\vec{D}_{1n} = \vec{D}_{2n} \tag{2.3}$$

$$\vec{B}_{1n} = \vec{B}_{2n} \tag{2.4}$$

$$\vec{E}_{1t} = \vec{E}_{2t} \tag{2.5}$$

$$\vec{H}_{1t} = \vec{H}_{2t} \tag{2.6}$$

considering $\rho_s$ and $J_s$ to be zero, that is, supposing no surface charge density and no surface current density. The subscripts *n* and *t* denotes normal and tangential components. Now let us consider a specific case of an interface between a RH and LH media as illustrated in the figure 2.8.

The boundary condition on tangential components does not change since they do not depend on μ and ε. In contrast the boundary conditions on the normal components are necessarily changed, since they involve (μ, ε) with changes in sign. By assuming the left handed media weakly dispersive and that therefore the constitutive relation **D**=ε**E** and **B**=μ**H** are approximately valid, the following boundary conditions at a RH/LH interface can be obtained:

$$\vec{E}_{1n} = -\frac{\varepsilon_2}{|\varepsilon_1|} \times \vec{E}_{2n} \tag{2.7}$$

$$\vec{H}_{1n} = -\frac{\varepsilon_2}{|\varepsilon_1|} \times \vec{H}_{2n} \tag{2.8}$$

$$\vec{E}_{1t} = \vec{E}_{2t} \tag{2.9}$$

$$\vec{H}_{1t} = \vec{H}_{2t} \tag{2.10}$$

Thus the tangential components of $\vec{E}/\vec{H}$ remain continuous while their normal components become antiparallel at the interface between a RH medium and a LH medium [34].

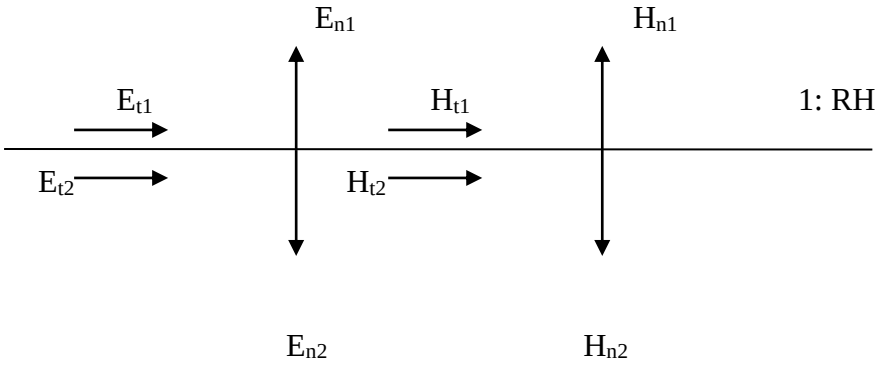


Fig. 2.8 Concept of reversal of boundary condition.

### 2.4.4 Reversal of Snell's law:

Snell's law of refraction is given by

$$n_1 \sin\theta_1 = n_2 \sin\theta_2 \tag{2.11}$$

where $n_1$ and $n_2$ are the refractive index of the two medium and $\theta_1$ and $\theta_2$ are the angle of incidence and angle of refraction respectively. This law is modified at the interface between a RH and LH medium due to the application of a negative sign in the refractive index of the LH medium. Snell's law of refraction may be written in a more general form as

$$S_1|n_1| \sin\theta_1 = S_2|n_2| \sin\theta_2 \tag{2.12}$$

where $S$ stands for the +ve or –ve sign. It can be seen that if the two medium are LH, then Snell's law remains unchanged due to mutual cancellation of the two minus signs of the refractive indices [34]. A wave incident upon the interface between two media with same handedness experience conventional positive refraction characterized by a positive refraction angle, whereas, a ray at the interface between two media of different handedness undergoes negative refraction corresponding to negative refraction angle as shown in figure 2.9.

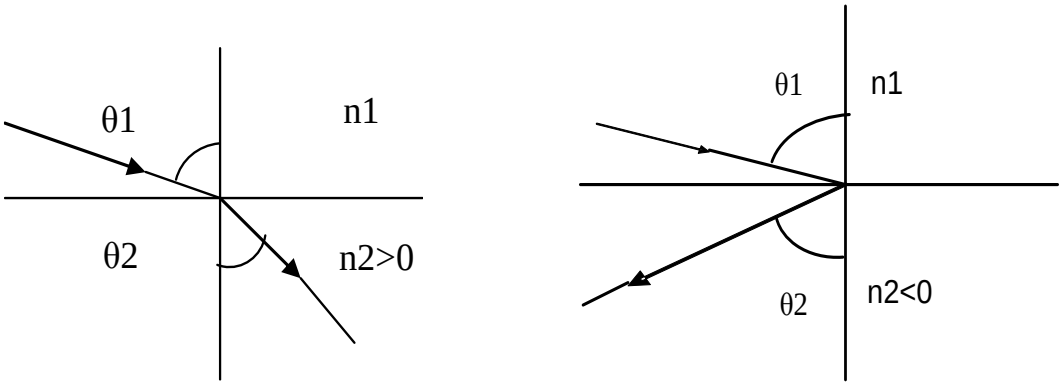


Right handed media Left handed media

Fig. 2.9. Reversal of Snell's law.

### 2.4.5 Transformation of a point source into a point image by a LH slab:

By applying Snell's law twice to a LH slab sandwiched between two RH media, also called a LH lens, it is possible to obtain the double focusing effect, as shown in figure 2.10. Two radiated rays with equal symmetric angles from a source at the distance $l$ from the interface are negatively refracted under an angle of same magnitude to meet at a distance $s$ in the slab. Then they focus again after a second negative refraction in the second RH medium at the distance (d – l) from the second interface where $s$ is given by

$$s = l \times \frac{\tan\theta_r}{\tan\theta_l}, \tag{2.13}$$

the angle $\theta_r$ is the incidence angle and $\theta_l$ is obtained by Snell's law.The above formula shows that if the two media have the same electromagnetic density, that is, refractive indices of same magnitudes, then focus can be obtained at the mirror image of the source $s = l,$ since$|\theta_l| = |\theta_r|$ from Snell's law [34].

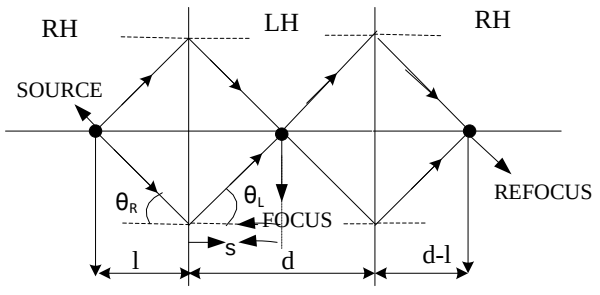


Fig. 2.10. Focusing of a point source into a point image.

### 2.4.6 Interchange in convergence and divergence effect in convex and concave lenses:

Due to their effectively homogeneous nature in the frequency range of interest, metamaterials represent a new paradigm to perform conventional optics in non-conventional materials at microwave frequencies, where in principle, simple ray optics law directly apply. All conventional ray optics may be revisited under the light of the unusual and exotic effects achieved with LH lenses. The diverging effects of the convex lens and the converging effect of the concave lens can be understood from figure 2.11, by applying simple ray optics [34].

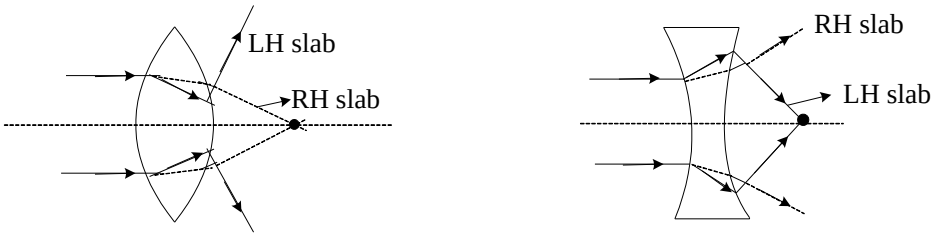


Convex lens Concave lens

Fig. 2.11 Reversal of focusing effect of left handed lenses.

### 2.4.7 Formation of left handed triplet of vectors E, H, k in double negative metamaterials:

In a general media, the vectors **E**, **H**, **k** forms a right handed triplet whereas in case of an electromagnetic metamaterial media having simultaneous negative permittivity and negative permeability [34], these vectors forms a left-handed triplet as shown in the figure 2.12.

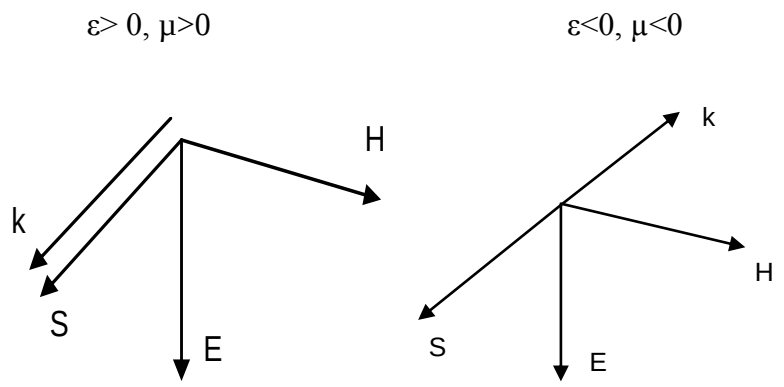


Fig. 2.12. Formation of right handed and left handed triplet of vectors **E**, **H**, **k** in conventional media and left handed media.

## 2.5 Application of metamaterials:

Metamaterials have many applications in microwave engineering [36]. Unusual properties of these novel materials brought revolution in electromagnetism and they gave solution to many critical problems. Apart from antenna, these are used in many microwave applications like waveguides, planar circuits, filters, LED, cavity, imaging systems, microwave couplers, wave propagation applications etc. Fig. 2.13 shows a list of such applications of metamaterials.

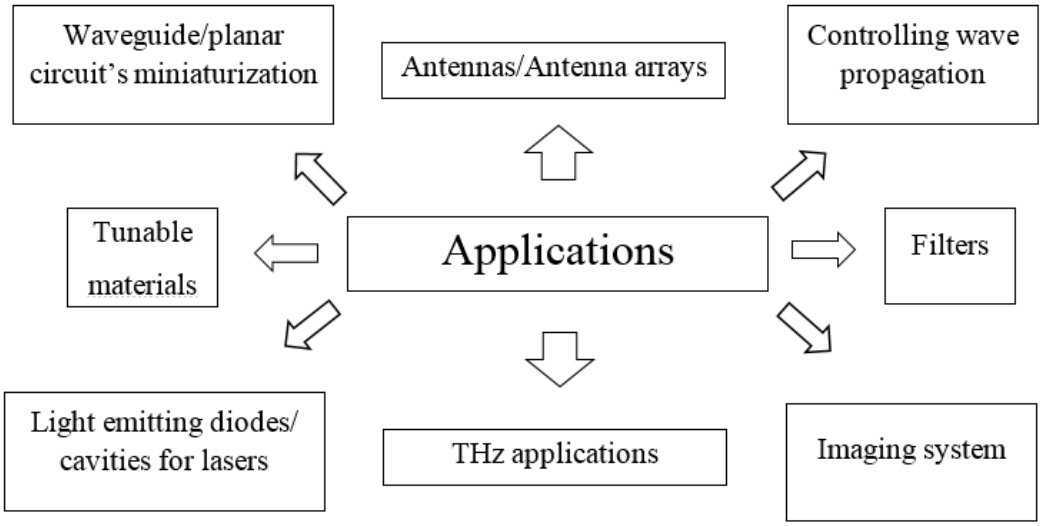


Fig. 2.13. Application areas of metamaterials.

As far as antenna application of metamaterials are concerned, these materials have been used for directivity enhancement, size reduction, multiband operation, broadband operation, creating circular polarization, mutual coupling reduction in arrays etc. (Fig. 2.14) [34][35][37].

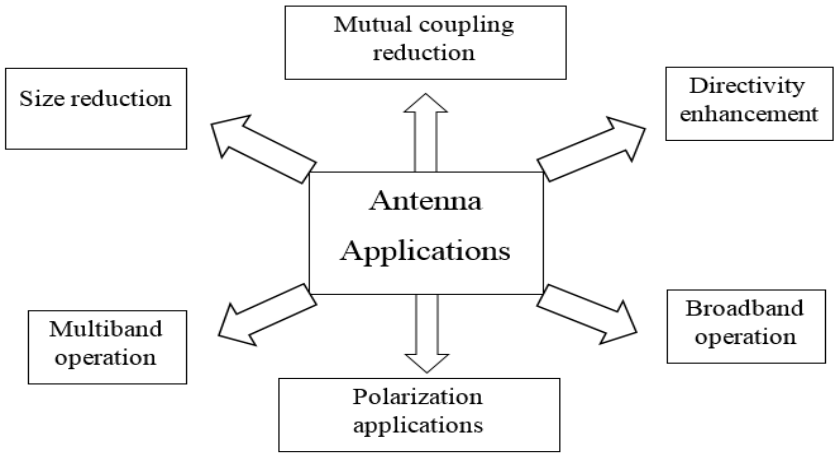


Fig. 2.14. Application areas of metamaterials in antennas.

## 2.6 Concluding Remarks:

The literature survey reveals many interesting properties and applications of electromagnetic metamaterials. Although the macroscopic behaviour of these materials have been studied and the related applications have been reported, but a microscopic analysis of these periodic structures when used in conjunction with radiating structures is still missing from the literature. Furthermore, the design aspects of these metamaterials have not been attempted vigorously. In this thesis, our aim is to bridge these gaps and to use these metamaterials for performance enhancement of planar antennas.

# 3.

# CSRR Loaded Patch Antenna: Analytical Formulation

## 3.1 Introduction

Performance enhancement of patch antennas using metamaterials is one of the major focussed areas among antenna community, in the recent decade [38-40]. These artificial fabricated materials that are based on periodic or quasi-periodic structures have been used for patch antenna miniaturization, multi-banding, and broad-banding purposes. The most widely used planar structures for creation of resonant metamaterials are split-ring resonator (SRR) and its dual, the complementary SRR (CSRR), as shown in Fig. 3.1. SRRs have been found to provide negative permeability whereas CSRRs provide negative permittivity [34, 41]. The use of CSRRs for miniaturization of patch antennas has been reported in the literature [42-45]. Through these work, lately it has been agreed upon that, it is not the metamaterial effect that cause the miniaturization but rather the placement of the CSRR slots and their dimensions that result in *LC* loading of the patch resulting in miniaturization. Therefore, even a single CSRR when properly placed underneath the patch results in significant miniaturization. In line with this argument, these reported works use either a single or a couple of CSRR unit cells to achieve performance enhancement of the antenna in the form of size reduction. The equivalent circuit models of these structures are provided where the associated lumped element values are extracted with the help of commercially available electromagnetic simulators.

At this point it should be noted that, even from metamaterial point of view, periodicity of the CSRRs on the ground plane of the antenna is not a necessity, as long as the largest cell is much smaller than the guided wavelength for electromagnetic homogeneity [46]. But at the same time, as long as the effective medium condition is satisfied, there is no constraint on the minimum number of unit cell of CSRRs required for metamaterials operation. So the array of

CSRRs below the radiating patch is a convenience. This fact can be suitably used to get maximum miniaturization in the antenna by using an array of CSRR instead of one or couple of CSRRs. Furthermore, from bandwidth point of view, it is more in case of the miniaturized antenna loaded by an array of CSRR with certain periodicity. This is because of the fact that the stop band bandwidth increases for a periodic CSRR when compared with a single CSRR. Therefore, reduced size with enhanced bandwidth patch antennas can be conceived by using periodic CSRRs in the ground plane of the antenna.

Presence of number of unit cell CSRRs makes the structure bit complex to be handled analytically. The aim of this work is to develop an analytical formulation to get a first-hand calculation of the resonant frequency of CSRR loaded patch antennas. This will also help in designing miniaturized but enhanced bandwidth antenna structures. The validity of the developed formulation is cross checked with the commercially available simulators as well as with experimental results.

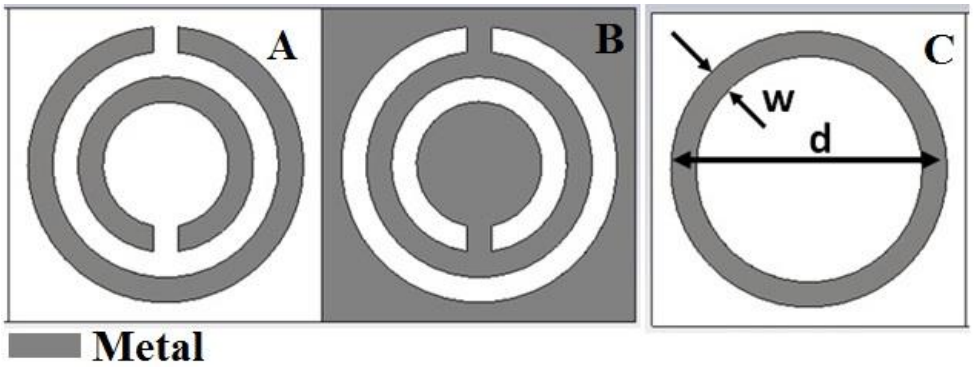


Fig. 3.1. Schematic of SRR and CSRR.

## 3.2 Compact Printed Antennas: A Brief Review

The increased demand for small size wireless devices has been forcing the antenna engineers to design compact antennas with broad bandwidth to accommodate multiple functions in the device. The classic properties of printed antennas like low profile, ease of fabrication, conformable to planar and nonplanar surfaces, simple and inexpensive to manufacturing are the added advantages. Over the years, differnet techniques have been used to reduce the overall size of the planar antennas, such as (i) use of high dielectric constant substrates (ii) introduction of resonant slots in the patch (iii) folding asingle layer patch into a double layer (iv) use of shorting pin and (v) Quater wave patch approach [47 - 51].

Metamaterials have also been used for designing reduced size printed antennas [52 - 57]. These are artificial materials which shows the properties that are usually absent in naturally occurring materials. Miniaturization of microstrip patch antennas using ε-negative metamaterial was reported in 2008 [52]. In this communication the authors have used complimentary split ring resonator in the ground plane of the antenna to obtain the size reduction. Use of μ-negative metamaterial has been reported in [53-54]. In [54], the authors have used multiple split ring resonators for μ-negative metamaterial. In thatwork, the authors have used many SRRs underneath the substrate to create an environment of -ve μ. In addition to this, metamaterial based transmission line zeroth order resonant antenna can be seen in [46, 55]. Authors in [46] have used printed circuit based metamaterial transmission lines. This is basically a travelling wave antenna. Some researchers have used the split ring resonator itself as antenna [56]. Anelectrically small metamaterial inspired patch antenna, called spired split ring resonator antenna, reported in [57], use a half split ring resonator as radiator.

## 3.3 Complimentary Split Ring Resonators (CSRRs)

Electromagnetic metamaterials can be classified as: (i) single -ve (-ve permittivity or -ve permeability) metamaterials, (ii) double negative metamaterials (-ve permittivity and permeability) and (iii) EBG (Electronic band gap) metamaterials. This section briefly describes the structure and characteristics of complimentary split ring resonators (CSRR), which exhibit negative permittivity behavior. Pendry [58-59] proposed rodded structure to realize negative permittivity and split ring resonator (SRR) to realize negative permeability. A printed circuit version of this rodded structure which can give negative permittivity is complimentary split ring resonator or CSRR. This structure is proposed by number of researchers [60].

CSRR is excited by an axial time varying electric field, whereas SRR is excited by an axial magnetic field. Basically CSRR is a negative blue print of SRR. SRR consists of an inner ring and outer ring which are separated by a distance. They themselves have a small cut. These cuts in the inner ring and outer ring are placed diametrically opposite to each other. Both the SRR and CSRR can be modeled as a *LC* resonator [61]. Their equivalent LC model of SRR and CSRR is shown in figures 3.2 and 3.3 respectively.

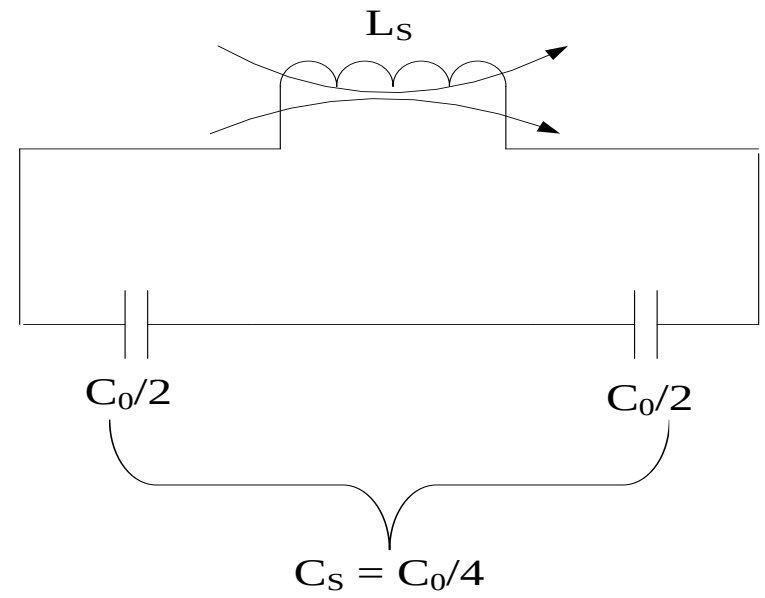


Fig. 3.2. Equivalent circuit model of aSRR.

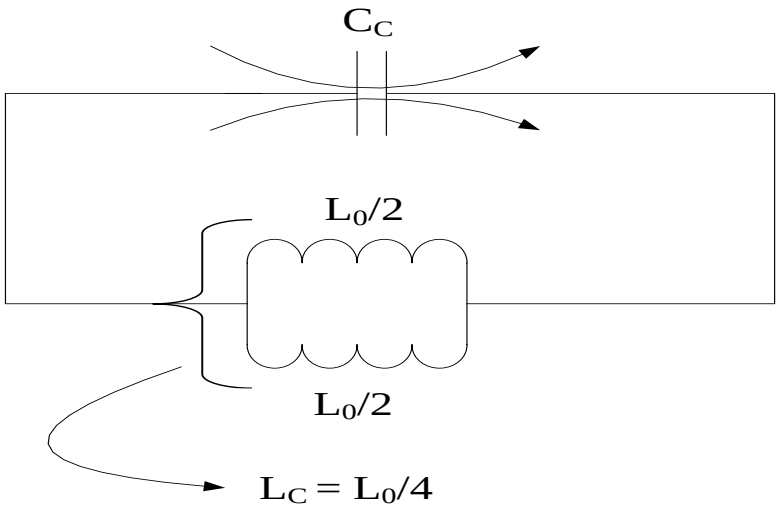


Fig. 3.3. Equivalent circuit model of a CSRR.

In figure 3.3, $C_C$ and $L_C$ are the equivalent capacitance and equivalent inductance of CSRR unit cell. Resonant frequency of this CSRR unit cell is a function of the radius of inner and outer ring slots, gap between the ring slots, thickness of the ring slots, dielectric constant of the substrate on which it is printed and the thickness of the substrate. When CSRR is printedon the other side of a microstrip line, it rejects a particular frequency depending on its dimensions. In other words, it acts as band stop filter. When a single unit cell of the CSRR is used, this stop band bandwidth is narrow. With the use of an array of CSRRs, this stop band

bandwidth increases manifold. Figures3.4 and 3.5shows the S-parameter plots of a microstrip line backed by a single CSRR and a linear array of four CSRRs, respectively. These CSRRs are printed on a substrate having dielectric constant 3.0 and with thickness of 0.5mm. Dimension of CSRRs used in this simulation are:

outer radius of outer circle = 2.0mm

outer radius of inner circle = 1.6mm.

thickness of the ring slots = 0.2mm

separation between the ring slots = 0.2mm.

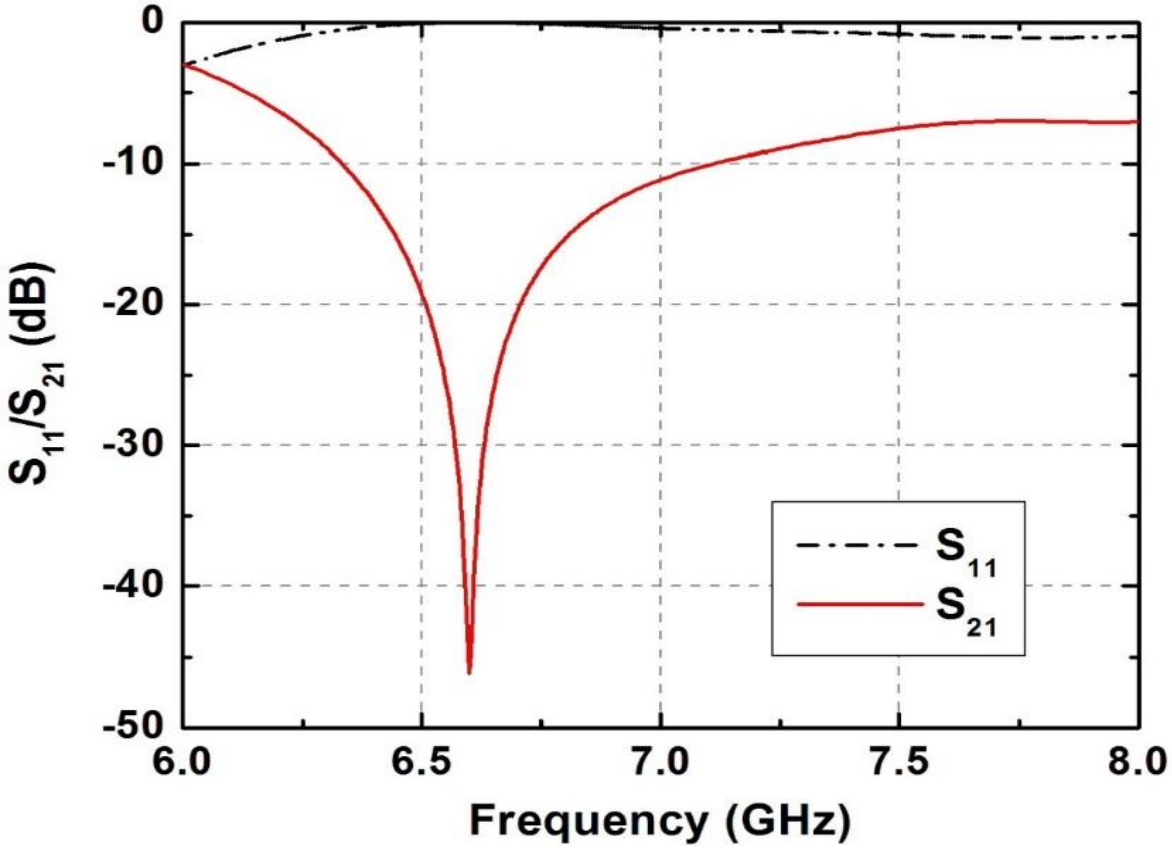


Fig. 3.4. S-parameters of a microstrip line backed by a single CSRR.

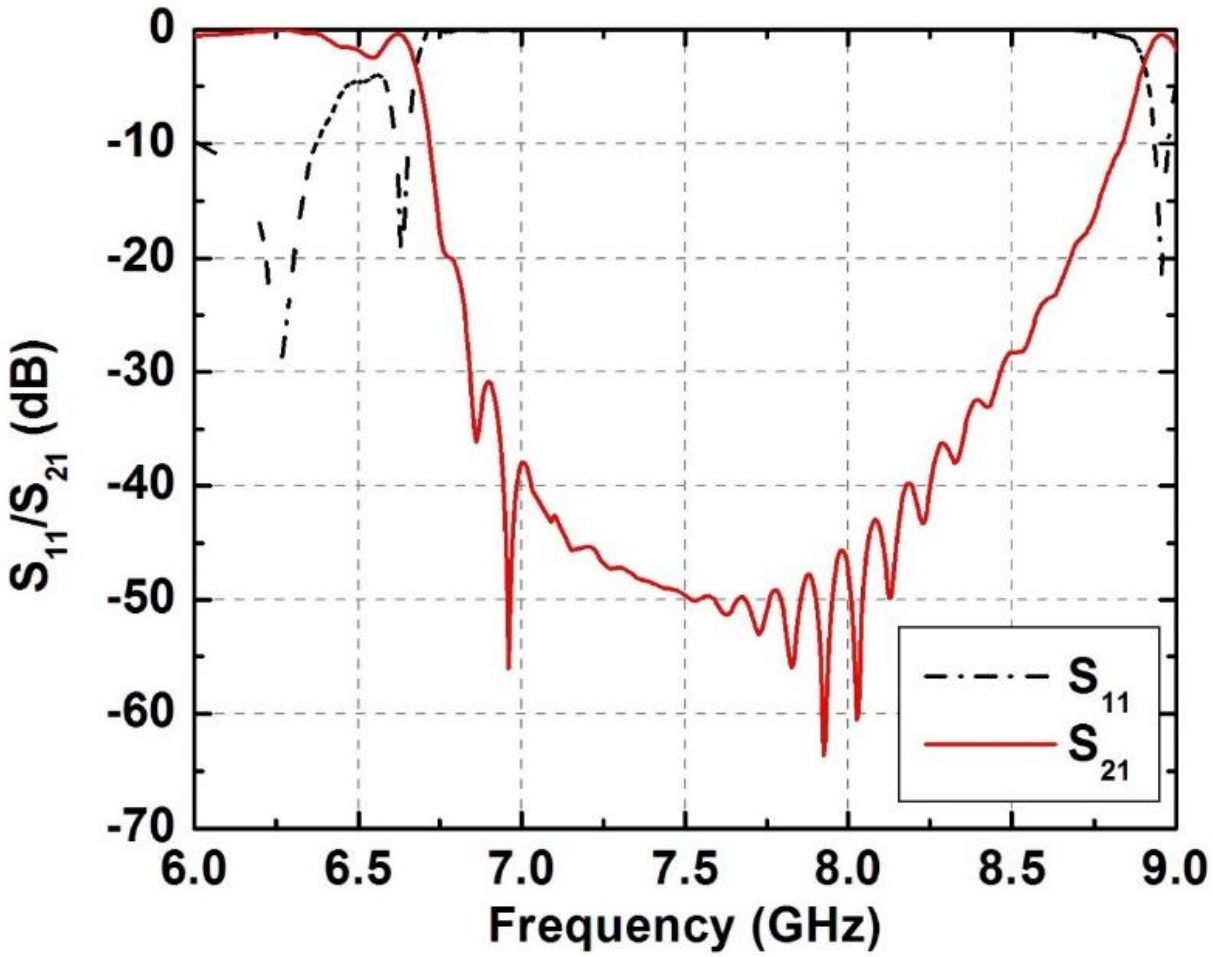


Fig. 3.5. S-parameter of a microstrip line backed by a linear array of four CSRRs.

Usually the CSRRs are placed in systems where the electric field is very strong. As they are negative blue print of SRR, so their working principle can be best understood by the application of Babinet's principle. Babinet's principle states that in a complimentary structure illuminated by complimentary field causes a complimentary scattering with its reflectance and transmittance interchanged. The origin of resonance in CSRRs can be explained with the help of two principles, namely (i) plasmon polariton resonance in dielectric nanostructure embedded into metal and (ii) Fabry–Perot resonance of guided waves propagating perpendicular to the structure. Detailed discussion regarding this resonance phenomenon can be found in [62]. In this type of microstrip structures, the type of losses that occur are conductor loss, substrate loss and radiation loss. For antenna applications, the radiation loss is important.

Radiation loss is given by [65]

$$P_r = 60(k_0 h)^2 F(\varepsilon_{eff}) \quad (3.1)$$

where $k_0$ is the free space wave number, $h$ substrate thickness and $F(\varepsilon_{eff})$ is the form factor for microstrip line.

Form factor $F(\varepsilon_{eff})$ is given by

$$F(\varepsilon_{eff}) = 1 - \frac{\varepsilon-1}{2\sqrt{\varepsilon}} \log \frac{\sqrt{\varepsilon}+1}{\sqrt{\varepsilon}-1} \quad (3.2)$$

For the microstrip structure with four CSRR unit cells on the ground plane with a dielectric of $\varepsilon_r$ of 3.0 and substrate thickness of 0.5 mm, the radiation loss comes out to be 0.18 watt.

## 3.4 Analytical Formulation of CSRR Loaded Patch Antenna

The rectangular patch antenna structure with array of CSRRs printed on its ground plane is shown in Fig. 3.6. The periodically etched CSRR structure alters the dispersion characteristics of the substrate. Different methods of extracting the circuit equivalent parameters of SRR structure have been discussed in [63]. All these methods predict almost same value of the electrical parameters (*L* and *C*) of the SRR structure within 5% of difference in the resonant frequency. The equivalent inductance and capacitance of a unit cell SRR is given by [64-65].

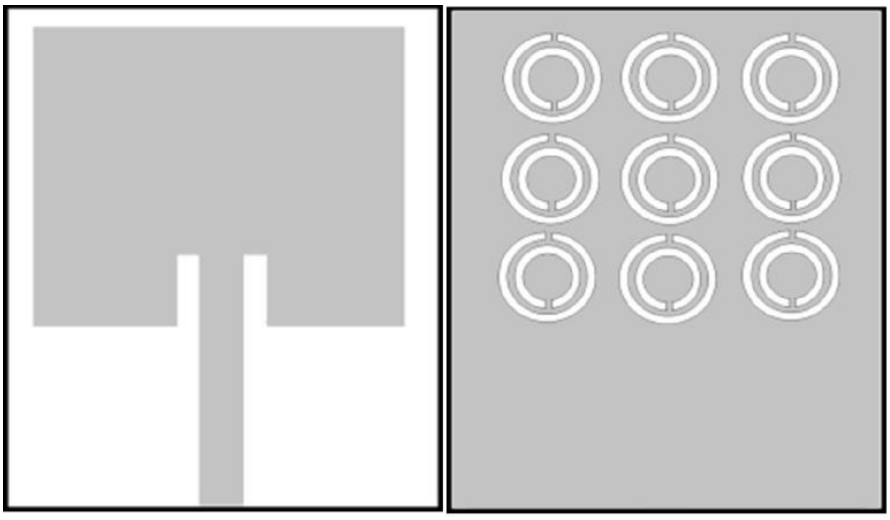

Fig. 3.6. Front and back view of CSRR loaded patch antenna.

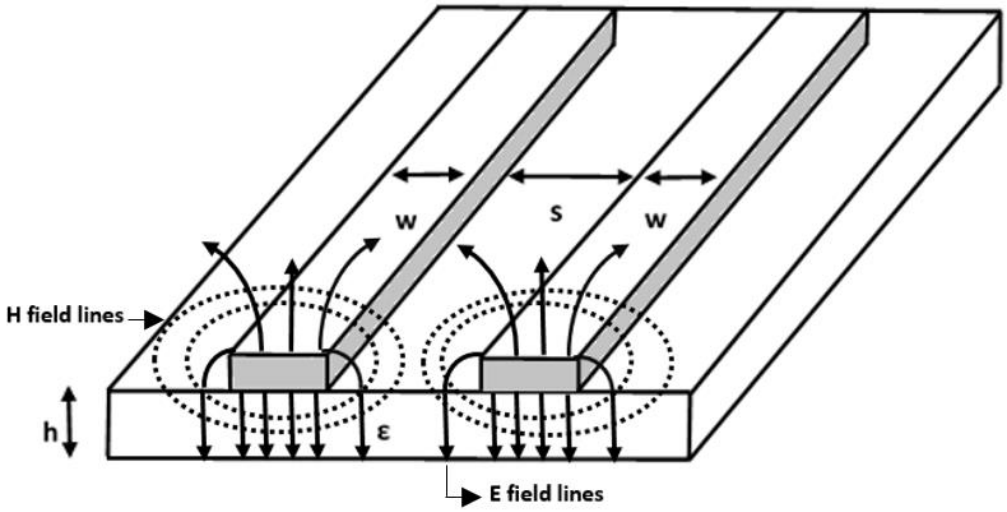


Fig. 3.7. Schematic of coplanar strip transmission line.

$$L_s = \frac{\mu d}{2}\left[\ln\left(\frac{d}{w}\right) + 0.9 + 0.2\left(\frac{w}{d}\right)\right] \tag{3.3}$$

$$C_s = \frac{C_0}{4} = \frac{\pi d\beta}{4\omega Z_0} = \frac{\pi d\sqrt{\varepsilon_e}}{4cZ_0} \tag{3.4}$$

where *w*, *d* are the width, and average diameter of the SRR rings as shown in Fig. 3.1(C). $\varepsilon_e$ is the effective dielectric constant and $Z_0$ is the characteristics impedance of equivalent coplanar strip transmission line (Fig. 3.7), given by [61]

$$Z_0 = \frac{120\pi}{\sqrt{\varepsilon_e}}\frac{K(k)}{K(k')} \tag{3.5}$$

where $$\frac{K(k)}{K(k')} = \begin{cases} \left[\frac{1}{\pi}\ln\left(2\frac{1+\sqrt{k'}}{1-\sqrt{k'}}\right)\right]^{-1} \text{ for } 0 \le k \le 0.7 \\ \frac{1}{\pi}\ln\left(2\frac{1+\sqrt{k}}{1-\sqrt{k}}\right) \text{ for } 0.7 \le k \le 1 \end{cases}$$

and $$k' = \sqrt{1-k^2}, k = s/(s+2w)$$

Following [66], the circuit equivalent parameters of unit cell of CSRR would be $L_c = (C_0/16)(\mu_0/\varepsilon_0)$ and $C_c = 4L_s(\varepsilon_0/\mu_0)$.

The equivalent circuit of periodically etched CSRR array structure is shown in Fig. 3.8. In the previous attempted works, where the authors have used a couple of CSRR unit cells, the effect of mutual coupling was not taken into consideration. Once the CSRRs are in array, in addition to their individual circuit parameters values, the coupling parameters will also play a major role in determining the resonant frequency of the array of CSRR resonators. Theoretical and experimental evidence of electrical coupling between these unit cells is reported in [66] where it has been shown that the wave propagation through this chain of CSRRs is basically an electroinductive wave and hence the inter-resonator coupling will be capacitive. Therefore the mutual capacitance between the adjacent unit cells has to be taken into account in order to calculate the resonance of the CSRR array. This mutual capacitance is shown in Fig. 3.8 and denoted as $C_M$.

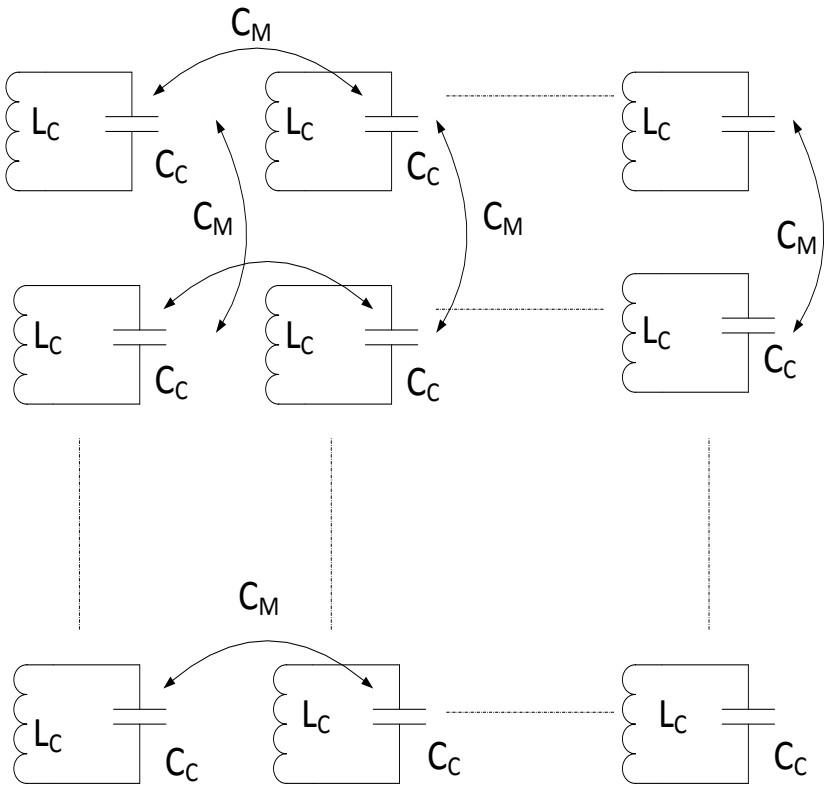


Fig. 3.8. Equivalent LC circuit model of CSRR array.

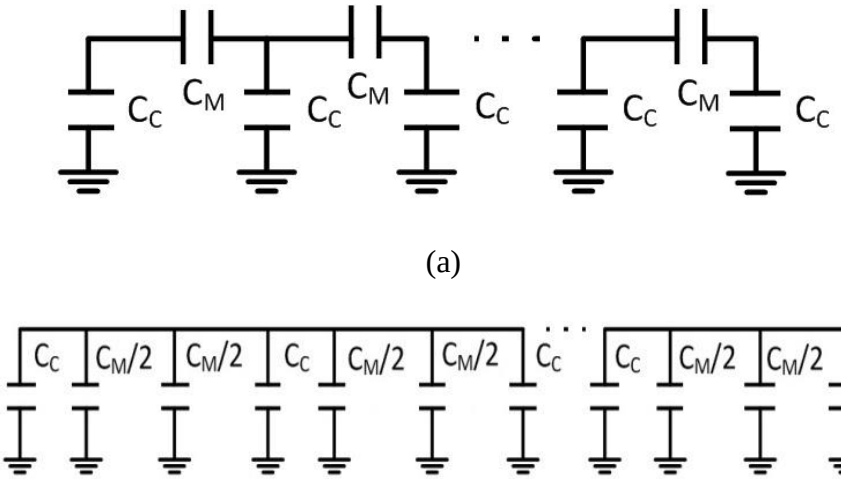


Fig. 3.9. Equivalent circuit of a row of CSRRs with mutual coupling for calculation of capacitance: (a) Step 1 (b) Step 2.

For an m×n size array of CSRRs, the equivalent capacitance of each row of CSRR can now be found from the circuit shown in Fig. 3.9 (a), which can be represented in a modified form as shown in the circuit in Fig. 3.9 (b). From this circuit the equivalent capacitance of each row can be written as: $C_{row} = \mathrm{n}C_c + 2\,(\mathrm{n}-1)\frac{C_M}{2}$. The capacitance of the entire array of CSRRs can now have a value of

$$C_{\mathrm{meta}} = \frac{\mathrm{n}C_c+(\mathrm{n}-1)C_M}{\mathrm{m}} + \frac{C_M}{\mathrm{m}-1} \tag{3.6}$$

The value of the mutual capacitance $C_M$ depend on separation between the elements, type of the elements (whether rectangular or circular) and dimensions of the elements [67]. The value of this parameter was calculated according to the method described in [66, 68]. As per this method, equivalent circuit parameters of a chain of SRRs that resonates at the same frequency as that of CSRR was found out. Then Babinet's principle was applied and these equivalent circuit parameters of SRR was used to calculate the value of $C_M$, given by the relation $C_M = KM$, where $M$ is the mutual inductance of SRR chain and $K$ (= 4ε/μ) is a constant. ε and μ are the substrate permittivity and permeability respectively. In this calculation, the following two assumptions were made: (i) the centre of the radiating patch and the CSRR array must be aligned at the same point and (ii) all the CSRRs should be confined within the area covered by the radiating patch. It was found that an array of circular shape CSRRs gives an average value of $C_M$ equal to 0.3 pF for a range of inter-resonator

spacing of 0.3mm. to 0.6mm. In case of rectangular shape CSRRs, this value is more because of larger area of closeness between consecutive elements.

As there is no coupling exists between the inductors, the inductance of each row of CSRRs can be represented by the equivalent circuit diagram shown in Fig. 3.10 with a inductance value of$L_{row} = L_c/\mathrm{n}$.

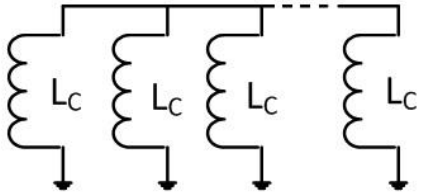


Fig. 3.10. Equivalent circuit of a row of CSRRs for calculation of overall inductance.

The equivalent inductance of the entire array of CSRRs can now have a value of

$$L_{\mathrm{meta}} = \frac{\mathrm{m}L_c}{\mathrm{n}} \tag{3.7}$$

For an inset fed patch antenna, the equivalent capacitance and inductance that gives rise to the resonant frequency ($\omega = 2\pi f$) are given by [69]:

$$C_{\mathrm{ant}} = \frac{(\varepsilon_e \varepsilon_0 lW)}{2h}\left[\cos\left(\frac{\pi y_0}{l}\right)\right]^2 \tag{3.8}$$

$$L_{\mathrm{ant}} = \frac{1}{\omega^2 C_{\mathrm{ant}}} \tag{3.9}$$

where ($l \times W$) is the size of the patch, $h$ is the height of the substrate, and $y_0$ is the location of the feed point from the edge. Here it may be noted that the equivalent resistance of the patch antenna and the CSRR array has not been considered in the *LC* equivalent circuit model of the resonators, because it does not play any role as far as the calculation of resonant frequency is concerned.

The patch antenna (represented by $L_{\mathrm{ant}}$, $C_{\mathrm{ant}}$) loaded with the CSRR array (represented $L_{\mathrm{meta}}$, $C_{\mathrm{meta}}$) resonates at a lower frequency, lower than that of only the patch, resulting in miniaturization of the antenna. In this case, the CSRRs are excited by the orthogonal electric field of the radiating patch antenna. Therefore, the coupling of this array with the patch is capacitive and this coupling is carried out through $C_{\mathrm{ant}}$. Hence the equivalent circuit of CSRR

backed patch antenna can be represented as shown in Fig. 3.11, where $L_{\text{trans.line}}$ is the inductance of the feed line and not been considered in the calculation of the resonant frequency. Here it may be emphasized that, ideally when the resonant frequency of the patch matches with that of the CSRR unit cell, then the metamaterial effect can be observed. But in practice, where size reduction is the main objective, CSRR unit cell resonant frequency can be within 10% range that of the patch. Under this condition, the resonant frequency of the CSRR array backed patch antenna can be given by $f_{\text{ana}} = 1/2\pi\sqrt{LC}$ where $L = (L_{\text{meta}} + L_{\text{ant}})$ and $C = [C_{\text{meta}}C_{\text{ant}}/(C_{\text{meta}}+C_{\text{ant}})]$.

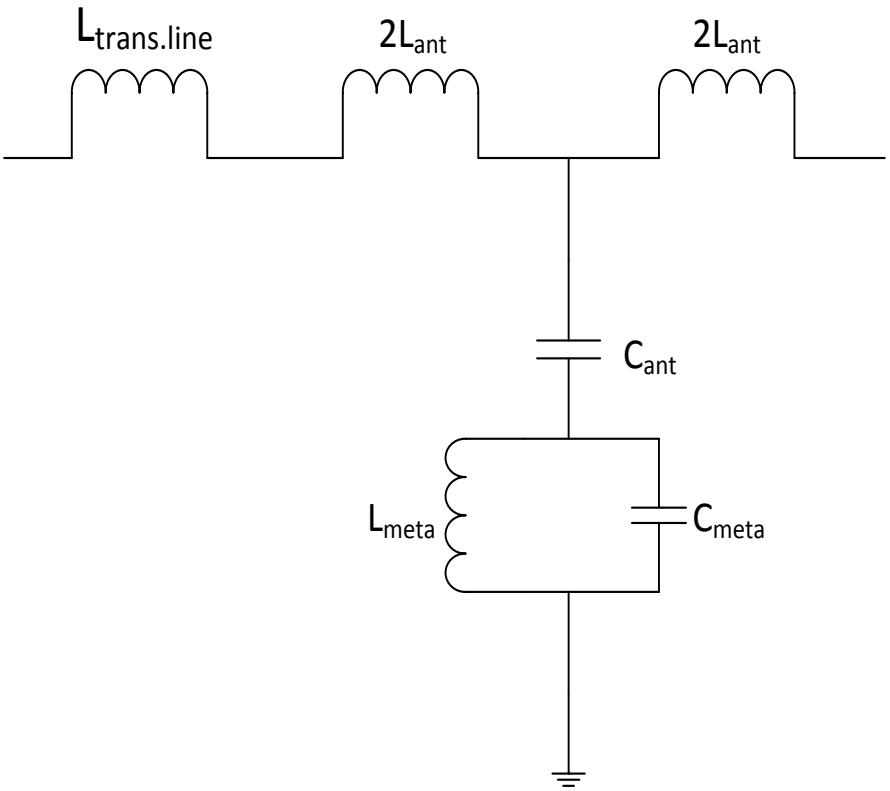


Fig. 3.11. Equivalent circuit of CSRR backed microstrip antenna.

## 3.5 Results and Discussion

In order to validate the developed analytical formulation, number of antennas were simulated using CST Microwave Studio v12 simulator, with varying antenna as well as CSRR parameters. In all the antenna structures that are analyzed, (i) the centre of the CSRR

array was matching with the centre of the radiating patch and (ii) the resonant frequency of unit cell CSRR was chosen within 10% range that of the patch only. Table I compares simulated frequency ($f_{sim}$) with that obtained from the developed analytical formulation ($f_{ana}$), for some typical cases. In addition to the closeness of these two results, the size reduction of the CSRR loaded antenna can also be marked by comparing with the values of $f_{ant}$. Although a number of laboratory prototypes of the CSRR loaded antennas were fabricated and the $S_{11}$ was measured using an Agilent PNA series network analyzer, two typical result (last two rows of Table I: 23.8×19.1 mm$^2$, and 18.2×12.8 mm$^2$) are shown in Fig. 3.12 and Fig. 3.13 respectively. The agreement between the experimental, simulated and the developed analytical formulation can be marked from this Figure and Table 3.1. Microstrip antenna dimensions were calculated based on closed form formula which is based on transmission line model [122] **.

**Table 3.1: Comparison of the resonant frequency of CSRR backed microstrip antennas**

| **Antenna $W\times l\times h$ (mm), $\varepsilon_r$** | **CSRR Array size (m×n)** | **CSRR* $r_i$, $r_o$, $w$, $s$, $p$ (mm)** | **$f_{ant}$ GHz** | **$f_{sim}$ GHz** | **$f_{ana}$ GHz** |
|---|---|---|---|---|---|
| 31.07× 24.2× 1.6, 3.85 | 3×3 | 1.6, 3.6, 0.9, 0.2, 0.5 | 3.1 | 2.61 | 2.57 |
| 16.0×20.0×1.6, 3.0 | 5×3 | 1.5, 4.0, 1.0, 0.5, 0.3 | 4.31 | 2.96 | 3.16 |
| 15.48×12.6×0.49, 2.43 | 5×5 | 1.4, 2.0, 0.2, 0.2, 0.4 | 7.35 | 5.5 | 5.20 |
| 25.8×19.2×2.2, 5.6 | 3×3 | 1.6, 2.5, 0.3, 0.3, 0.5 | 3.2 | 3.01 | 2.80 |
| 9.85×7.73×0.5, 2.33 | 3×3 | 0.4, 1.5, 0.3, 0.5, 0.6 | 12.1 | 8.96 | 9.04 |
| 23.8×19.1×1.57, 2.2 | 3×3 | 1.5, 3.0, 0.5, 0.5, 0.5 | 5.0 | 4.44 | 4.38 |
| 18.2×12.8×1.5 4.4 | 3×3 | 2.5,1.5, 0.5,0.5,0.4 | 5.3 | 4.0 | 4.22 |

*$r_i$, $r_o$, $p$: inner and outer radius of the CSRR and separation distance between CSRRs.

** See appendix I.

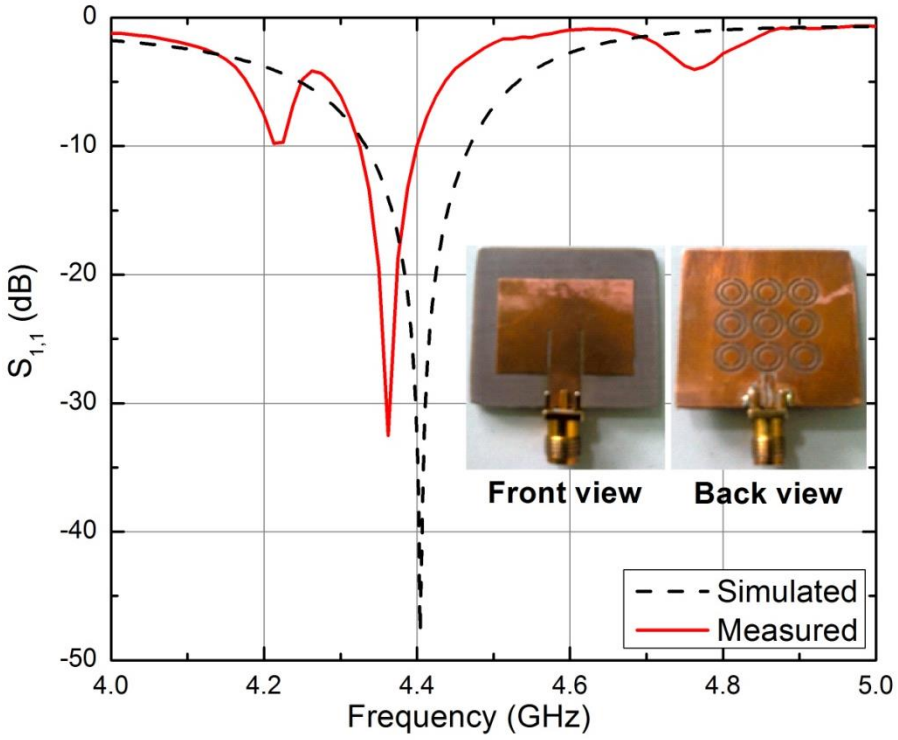


Fig. 3.12. Comparison with experimental results (for 23.8×19.1 $mm^2$ patch).

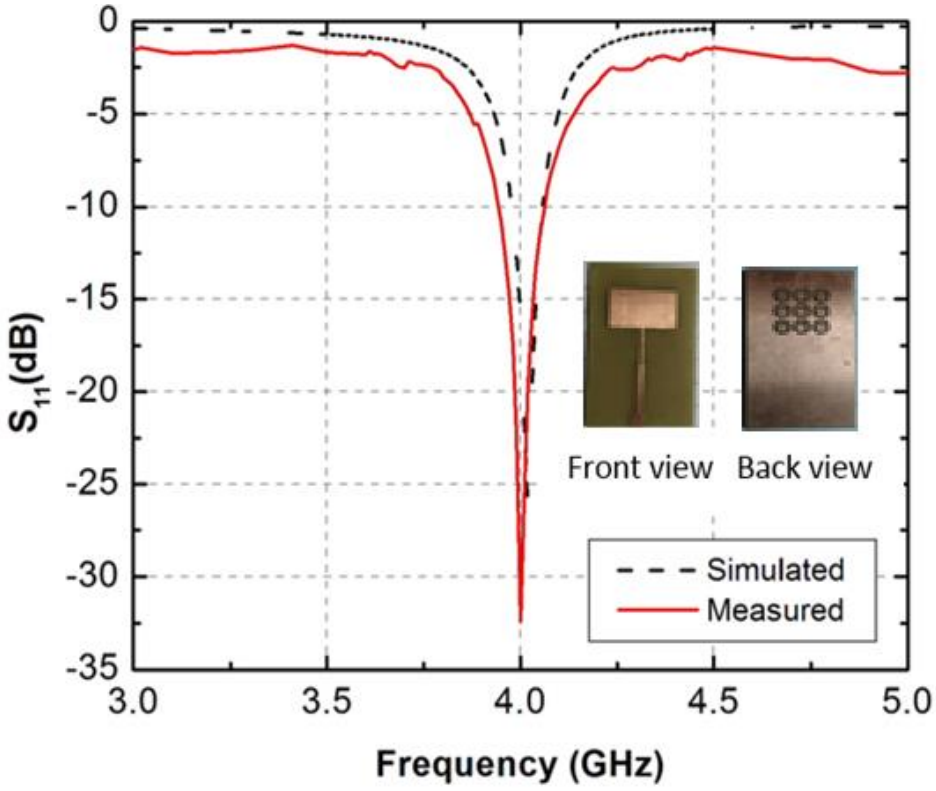


Fig. 3.13. Comparison with experimental result (for 18.2×12.8 $mm^2$ patch).

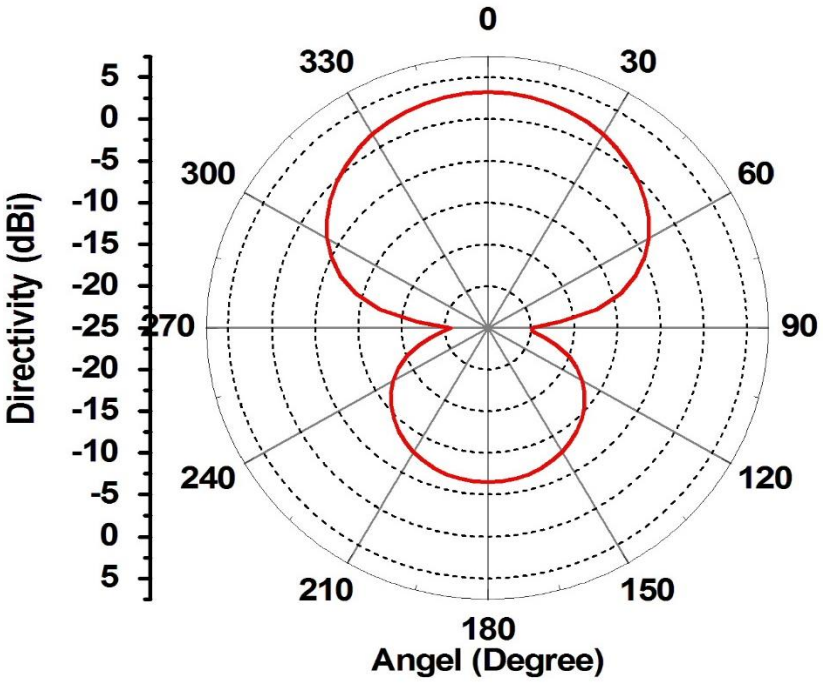


Fig. 3.14. E plane radiation pattern (for 18.2×12.8 mm$^2$ patch).

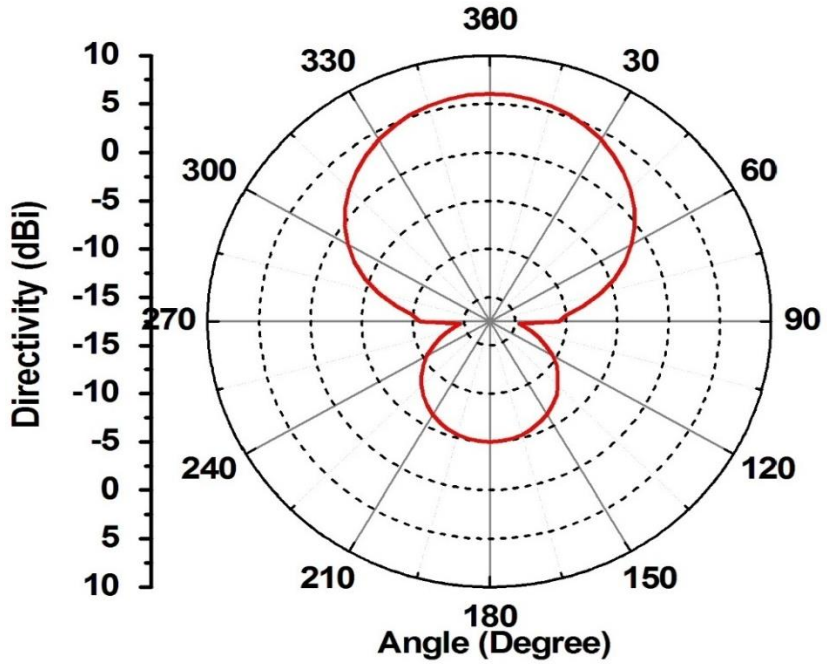


Fig. 3.15. E plane radiation pattern (for 23.8×19.1 mm$^2$ patch).

**Table 3.2: Results for varied CSRR array size**

| CSRR array size | $f_{sim}$ GHz | $f_{ana}$ GHz | *%age Bandwidth* |
|---|---|---|---|
| 1×3 | 2.83 | 2.44 | 1.35 |
| 2×2 | 2.79 | 2.53 | 1.40 |
| 2×3 | 2.68 | 2.60 | 1.52 |
| 3×3 | 2.61 | 2.57 | 1.70 |
| 5×5 | 2.52 | 2.54 | 1.78 |

In order to see the effect of periodicity of the CSRR array, keeping the patch size same (first row of Table 3.1: 31.07×24.2 $mm^2$), the CSRR array size was varied and the results are shown in Table 3.2. A couple of things can be noted from this table: (i) with the increase in size of the array, the results from the developed formulation gradually approach the simulation results, and (ii) the percentage bandwidth of the overall structure gradually increases with the increase in the array size. In summary, the developed formulation can be helpful for analysis of compact, broadband patch antennas at desired centre frequencies. Furthermore, the developed analytical model can be inserted in the loop of any optimization algorithm for designing these compact broadband patch antennas, that is, to determine the dimensions of the CSRRs as well as the patch.

## 3.6 Concluding Remarks

In this chapter, we presented an equivalent circuit based closed form formulation of the resonant frequency of CSRR backed patch antenna. The formulation developed can be used in fixing the radiator and CSRR dimensions for the design of compact microstrip antenna structures with enhanced bandwidth. Although in this work we have taken circular split ring resonators, the method can be extended for analysis of other metamaterial loaded patch antennas and also for the analysis of metasurfaces.

# 4.

# Design Optimization of Metamaterial based Compact Patch Antennas: A Machine Learning Approach

## 4.1. Introduction

In the previous chapter analysis of CSRR backed microstrip antenna was attempted and a closed-form formula for the resonant frequency was found out. In this chapter, the design aspect of metamaterial based compact patch antennas is considered. During design of these antennas, the task is to fix all the design parameters of the radiating patch as well as the metamaterial structure, so that the antenna will resonate at a fixed desired frequency. Because of the complicated structure of the metamaterials, the designer has to play with a lot of design parameters to fix the resonant frequency of the metamaterial based antenna, making the task a time consuming and cumbersome one. In order to alleviate that and to develop a fast and flexible design approach for these antennas, in this chapter a machine learning approach has been used. The design task was converted to an optimization problem and solved using Particle Swarm Optimization (PSO). In order to make the process faster, the cost-function of the PSO was evaluated with the help of a trained Neural Network (NN). Although the same CSRR array backed microstrip antenna was taken as the candidate antenna for demonstrating the effectiveness of the developed machine learning based methodology, the same can be extended for the design of other metamaterial based antennas.

## 4.2. Machine Learning Techniques

Machine learning based techniques are basically a class of optimization tools whose functioning principle originates from biological systems. These optimizers are usually

preferred in large scale applications where traditional optimizers encounter difficulties. Some of the other acronyms used for these tools are soft-computing techniques, biologically inspired computational techniques etc. The tools available under this name are artificial neural network or simple neural network (ANN or NN), Fuzzy logic (FZ), Rough sets (RS), Genetic algorithm (GA), Particle swarm optimization (PSO), Ant colony optimization (ACO) and Bacteria Foraging optimization (BFO) etc. The list is expanding to include other tools that are hitting the literature recently. Each one of these techniques has its own capabilities, advantages and drawbacks. Applications of these techniques can be found in every branch of engineering. Microwave engineering is no exception and applications can be found since 1990s. As on today application of soft-computing techniques specifically in antenna engineering is plenty in number including books [70-73], journal special issues [74-75], review articles[76-77] and number of research papers devoted to this topic.

In the present work, the task of design of metamaterial based patch antennas is converted to an optimization problem and solved using PSO, because of the simple reason that, PSO is easy to implement compared to other machine learning approaches. In order to make the iterative process faster, the cost function of the PSO was evaluated with the help of a trained NN. A brief description of these two tools is described in the below subsections.

### 4.2.1. Neural Networks

As the name indicates the calculation paradigm of a NN is based on an idealized model of a biologically neuron (structural constituent of brain). In its most general form, it is a machine that is designed to model the way in which the brain performs a particular task or functions of interest. It is a massively parallel distributed processor that has a natural propensity for storing experimental knowledge and making it available for use [76]. It resembles the brain in two respects:

a) knowledge is acquired by the network through a learning process
b) inter-neuron connection strengths are used to store the knowledge

Since its inception the neuron computing is constantly being exploited for several different applications. Some of the typical applications of NN that left an impression of its achievements are: 1) Text to speech transformation 2) picture data compression 3) recognition of handwriting 4) industrial inspection 5) steering of autonomous vehicles 6) explosive detector 7) adaptive robot screening 8) signature examiner etc. These applications

of neural computing are due to its three important virtues (a) leaning (b) generalization and (c) robustness against noise. These appealing features also make NNs a good candidate for overcoming some of the difficulties in microwave modelling and optimization problems [77].

One of the interesting properties of the NNs is its ability to learn from its environment, and to improve its performance through learning. The improvement in performance takes place with time in accordance to some prescribed measure. Learning, in the context of NNs, is defined as change in connection weight values that result in the capture of information that can be recalled later. Figure 4.1 shows a diagrammatical representation of NN learning process.

Data is an important constituent for NN. The network has to adapt itself to input and corresponding output data pattern, generated by an environment. It may be noted that the dimensionality of the input pattern is not necessarily the same as the output pattern (i.e. number of input is not necessarily the same as the number of output neurons). The inputs must represent the features of the environment in a parameterized form. Sometimes the data are pre-processed in order to draw the featured and a post-processing is applied at the output. Usually the generated data are divided into two sets. One set of data (training set) is used to train the network and the other set (test set) is used to test whether the network has been trained effectively or not. Obviously the test data set is different from the training data set.

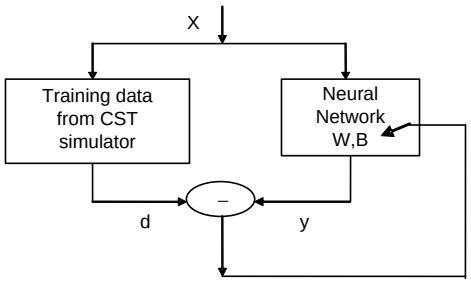


Figure 4.1 Neural network learning process.

Mostly, multi-layered feedforward NNs trained in the backpropagation mode are in use for antenna applications [77] **. These are best suited for solving mapping formulation type of problem. Although the details of this training algorithms can be found elsewhere in the literature [78], in brief this can be summarized as follows:

1. Initialize weights.

** See appendix II

2. Repeat for each pair in the training set
   2.1 Apply the input vectors (x)
   2.2 Calculate the output vectors (y)
   2.3 Calculate the error at the output layer (d)
   2.4 Adjust weights layer by layer to minimize error until performance is satisfactory

NNs have some inherent qualities like [94]

1. Processing takes place in parallel instead of in serial mode, making it suitable for solving complex problems.

2. They can learn either in supervised mode, where the network is provided with the correct response, or in an unsupervised mode, where the network self organizes and extracts patterns from the data presented to it.

3. A three layer network can perform any continuous non-linear mapping from input to outputs, making it easy compared to other conventional pattern matching or statistical methods.

4. Hardware implementation of these systems is possible using the VLSI technology.

NNs can be exploited to solve problems related to pattern classification, optimization, self-organization and associative memory. From the present research perspective, we have used the NN to form a black box model between the design parameters of the metamaterial with its analysis parameter (resonant frequency).

### 4.2.2. Particle Swarm Optimization

As the name indicates, PSO is basically an optimization technique based on evolutionary strategy. It is inspired by the social behaviour of a flock of birds and insects. This optimization technique was originally proposed by Kennedy and Eberhart [95]. This and the other optimization methods are becoming popular in solving engineering problems, because classical optimization have some major demerits like (i) they are time consuming (ii) they fail to deal with complex problems involving several parameters (iii) they are local search methods and involve the derivative techniques and (iv) in several cases they are

computationally unstable or less efficient. Simple and powerful machine learning based optimization techniques that are available in the form of GA, PSO, BFO, ACO are stochastic in nature and are global optimizer. They are less prone to converge to a week local optimum than traditional methods. In the present work we have opted for PSO because it is simple and easy to apply. The purpose of the optimizer in the context of the present work is to replace the trial and error method of adjusting different parameters of the metamaterial, during the simulation, by a systematic approach.

The application of PSO starts with the initial choice of bunch of random solutions called *population*, within the permissible range of each parameter to be optimized. Depending on the number of such parameters (say N), the PSO searches for the solution in the N-dimensional solution space. The optimality of the solution is measured by the value of fitness function (or cost function). Fitness function which depends on the user's requirements, tags the value of all N parameters that represent a possible solution in the solution space and returns a single umber representing the goodness of that particular solution**.

Having defined the solution space and a fitness function, the task is to set the value of optimization parameters and run the PSO programme. The particle positions and velocities for each particle in the population are changed according to the following two equations [80][81]

$$v_{iN} = wv_{iN} + c_1 rand()(p_{iN} - x_{iN}) + c_2 rand()(p_{gi} - x_{iN}) \quad (4.1)$$

$$x_{iN} = x_{iN} + v_{iN} \quad (4.2)$$

Where $c_1$ and $c_2$ are positive constants. $c_1$ is the factor which determines how much the particle is influenced by the memory of its best location and $c_2$ is a factor which determines how the particle is influenced by the rest of the swarm. *rand* () is a random number in the range of [0,1], to stochastically vary the relative pull of best positions of particles. $x_i = (x_{i1}, x_{i2}, \ldots, x_{iN})$ represents the current position vector of the $i^{th}$ particle of the population in the N-dimensional solution space and $p_i = (p_{i1}, p_{i2}, \ldots, p_{iN})$ represents the best previous position vector (the position giving the best fitness value is called *personal best* or *pBest*) of the $i^{th}$ particle. The symbol *g* represents the rate of the position changes (velocity) for $i^{th}$ particle. After finding the two best values, the particle updates its velocity and position using equation 4.1 and 4.2. A flow chart for the classical PSO is shown in figure 4.2.

** See appendix III.

In order to force particles to search inside the solution space of interest during the optimization procedure, four boundary conditions have been reported in the literature for PSO algorithm, viz. (i) absorbing boundary (ii) reflecting boundary (iii) damping boundary and (iv) invisible boundary [97]. The detailed algorithm for the PSO is discussed elaborately elsewhere in the literature [77]. Although modified and faster version of the PSO are available [98] in the literature, in this work classical one is used because our aim is to show the feasibility of this technique for the problem at hand.

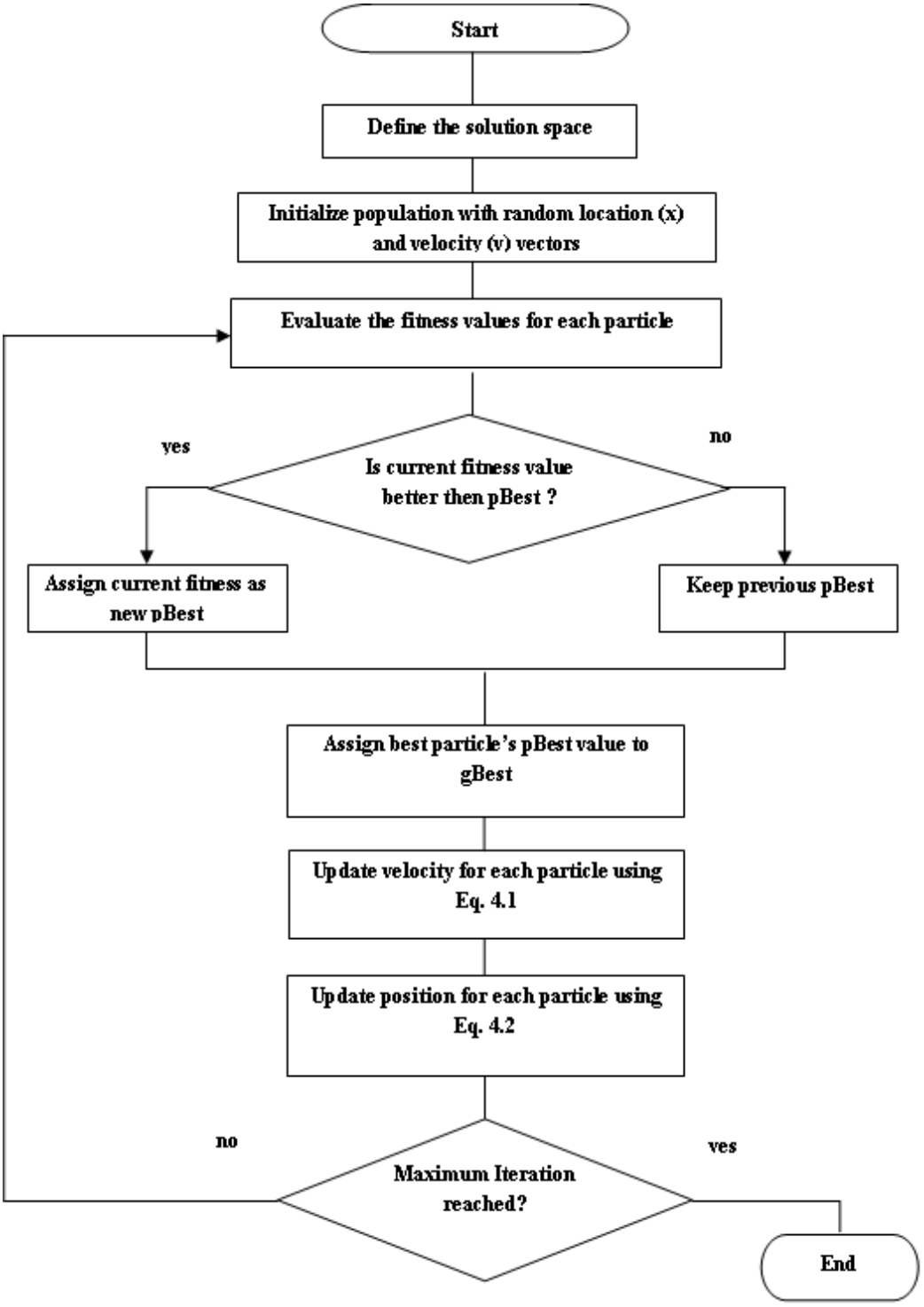


Figure 4.2 Flow chart of PSO algorithm

## 4.3. Design Methodology

The problem statement for the design of metamaterial based compact antenna is: given the resonant frequency of the patch antenna and the user intended resonant frequency of the metamaterial based compact patch antenna (that means, same patch with a lower

resonant frequency), then to find out the dimensions of the metamaterial. The candidate antenna taken to validate the developed machine learning based design procedure is the same antenna taken for analysis purpose, that is, a CSRR array backed microstrip antenna. The developed design methodology is shown in figure 4.3 diagrammatically. It's basically a two-step method.

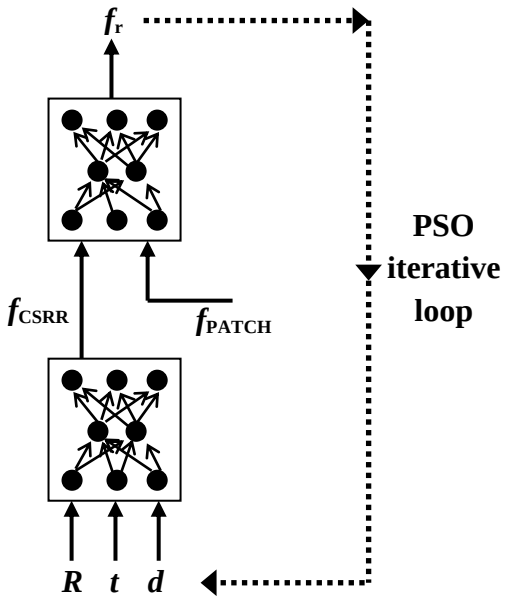


Fig. 4.3 Machine learning based design strategy of compact patch antennas.

In the first step, two trained neural networks were developed. The first neural network forms a mapping between the design parameters (*R*: external radius, *t*: thickness of the rings and *d*: separation between the rings) of a unit cell CSRR with its resonant frequency. The second neural network forms a mapping between the input parameters consisting of the CSRR resonant frequency and the patch resonant frequency with a single output parameter of resonant frequency of the CSRR array backed patch antenna. These two neural networks are embedded inside the iterative loop of the PSO as shown in figure 4.3. The main reason of developing two different trained neural networks is to reduce the number of training data set required for training of these networks.

### 4.3.1. NN Implementation

Multilayer perceptrons trained in the backpropagation mode [71] is used for the design of the neural networks. The characteristics of the two networks are given in Table 4.1.

**Table 4.1: Characteristics of the trained neural networks**

| Characteristics | NN1 | NN2 |
|---|---|---|
| **Size** | 3×11×1 | 2×5×1 |
| **Input parameters** | *R*: external radius (1mm - 4.5mm)<br><br>*t*: thickness of the rings (0.1mm - 1.0mm)<br><br>*d*: separation between the rings (0.1mm-0.5mm) | $f_{CSRR}$: CSRR unit cell resonant frequency<br><br>$f_{PATCH}$: patch resonant frequency |
| **Output parameters** | $f_{CSRR}$: CSRR unit cell resonant frequency | $f_r$: resonant frequency of the CSRR array backed patch antenna |
| **Training data set size** | 200 | 100 |
| **Training data source** | CST Micworave Studio (v12) simulated data | CST Micworave Studio (v12) simulated data |
| **Neuron transfer functions** | Sigmoidal: for hidden layer neurons<br><br>Linear: for output layer neurons | Sigmoidal: for hidden layer neurons<br><br>Linear: for output layer neurons |

At this point it should be mentioned that the characteristics of the dielectric (dielectric constant and the height of the substrate)was not taken as the variable parameter, because of the reason that it is not always possible to have dielectrics commercially available with the characteristic values given by the optimizer. After proper training of the neural network, updated weights and biases were stored for further use. These updated weights and biases can be used in place of simulator to obtain the resonant frequency of CSRR.

### 4.3.2. PSO implementation

The most time consuming part of the PSO process is the evaluation of the cost function. In order to circumvent the same we have used the trained NNs for evaluation of the cost function. The input to the PSO is the required resonant frequency and the outputs are the design dimensions of the CSRR structural parameters (*R*, *t* and *d*). Dielectric permittivity was not treated as a variable in the optimization process because of the simple reason that the optimized $\varepsilon_r$ produced by the optimizer may or may not available commercially. In the

present analysis, CSRRs were printed on a substrate with $\varepsilon_r$ = 3.85 and $h$ = 1.6 mm. Cost function used for optimization is

$$F = (F_r - f_r) \times (F_{\text{CSRR}} - f_{\text{PATCH}})^2 \tag{4.3}$$

Where $F_r$ is the desired frequency and $f_r$ is the instantaneous frequency produced by the PSO iterations. Parameters of the PSO optimization are given in the table 4.2. Dimension $N_d$ is decided by the number of structural parameters of CSRR (*R*, *d* and *t*). There is no hard and fast rule for selection of $N_P$ in PSO.

**Table 4.2: PSO parameters**

| PSO parameter | Value | Use |
|---|---|---|
| $c_1$ | 1.4 | Constant to determine $p_{best}$ |
| $c_2$ | 1.4 | Constant to determine $g_{best}$ |
| $N_P$ | 30 | Number of particle |
| $N_d$ | 3 | Number of dimension |
| $W_{max}$ | 0.9 | Maximum inertial weight |
| $W_{min}$ | 0.4 | Minimum inertial weight |

## 4.4. Results and Discussion

With the range of the values taken in the present work, for the design parameters of the CSRR, the developed machine learning based design module is applicable to work in 1 – 5 GHz range. Furthermore, for all the structures considered in this work, an array of CSRR of size 3×3 with its centre exactly matching with the centre of the patch is assumed. Number of antenna structures was designed using the developed machine learning based module. The result for two typical structures is presented in this thesis.

In the first design the resonant frequency of the radiating patch was 3 GHz and the desired frequency of the metamaterial based patch antenna was 2.6 GHz. For the second design the resonant frequency of the patch is 3.5 GHz and that of metamaterial based patch is 2.85 GHz. The design dimensions of CSRR unit cells obtained for these two structures, with the help of developed formulation is tabulated in Table 4.3.

**Table 4.3: Design dimensions of CSRR unit cells obtained using the developed formulation for two typical cases**

| Resonant frequency (GHz) | Outer radius (*R*) (mm) | Thickness of rings (*t*) (mm) | Separation of rings (*d*) (mm) |
|---|---|---|---|
| 3 | 3.58 | 0.6 | 0.19 |
| 3.6 | 3.4 | 0.9 | 0.3 |

### 4.4.1. Effective Parameter Retrieval of Metamaterials

Once the optimized parameters are found out using the machine learning approach it is necessary to validate the resonant frequency of the metamaterial units. Simulation study of S-parameters is one of the ways through which we can validate the resonant frequency of the metamaterials. But in case of electromagnetic metamaterials cross validation of negative properties of permittivity or permeability (in case of single negative metamaterial) or both (in case of double negative metamaterial) for specified frequency band is not possible through S-parameter simulation. Analytical method is the other alternative way to find out frequency range in which these artificial structures show negative properties. If the structure is complex, then analytical methods also become either very lengthy or extensively calculative. Effective parameter extraction of the metamaterial is another suitable alternate to analytical methods.

Many parameter retrieval approaches have been described in the literature [99-101]. In the present work we have used Ziolkowski's method [102], which is basically an extension of Nicolson-Ross-Weir approach. In this method effective parameters of electromagnetic metamaterials can be found out through S-parameters obtained through any commercially available simulator. The brief formulation is discussed below:

$$V_1 = S_{21} + S_{11} \tag{4.4}$$

$$V_2 = S_{21} - S_{11} \tag{4.5}$$

Where $S_{11}$ and $S_{21}$ are S-parameters of the metamaterial.

$$X = \frac{1+V_1V_2}{V_1+V_2} \tag{4.6}$$

$$Y = \frac{1-V_1V_2}{V_1-V_2} \tag{4.7}$$

$$Z = X \pm \sqrt{X^2 - 1} \tag{4.8}$$

where $Z$ is the transmission coefficient term.

$$\Gamma = Y \pm \sqrt{Y^2 - 1} \tag{4.9}$$

where $\Gamma$ is the reflection coefficient term.

$$k = \frac{1}{jd}\frac{(1-V_1)(1+\Gamma)}{1-\Gamma V_1} \tag{4.10}$$

where $k$ is the complex wave number term and $d$ is the thickness of the slab.

$$\mu_r = \frac{2}{jk_0 d}\left(\frac{1-V_2}{1+V_2}\right) \tag{4.11}$$

$\mu_r$ is the effective relative permeability.

$$\varepsilon_r = \left(\frac{k}{k_0}\right)^2 \frac{1}{\mu_r} \tag{4.12}$$

$\varepsilon_r$ is the effective relative permittivity.

$$n = \sqrt{\varepsilon_r \mu_r} \tag{4.13}$$

$n$ is the reflection coefficient of the medium.

Fig. 4.4 and Fig. 4.5 shows the return loss and insertion loss plots for the two typical unit cell CSRRs respectively.

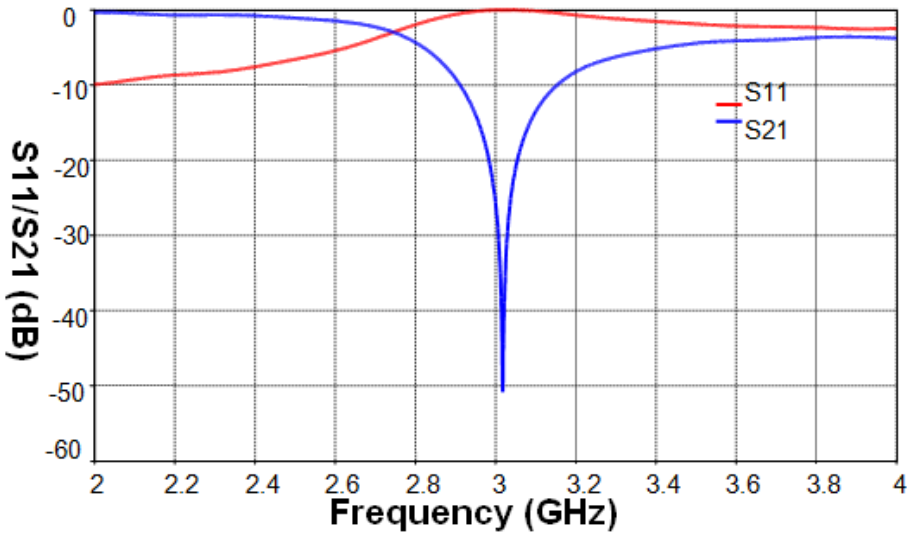


Fig. 4.4. S parameters of CSRR at 3GHz.

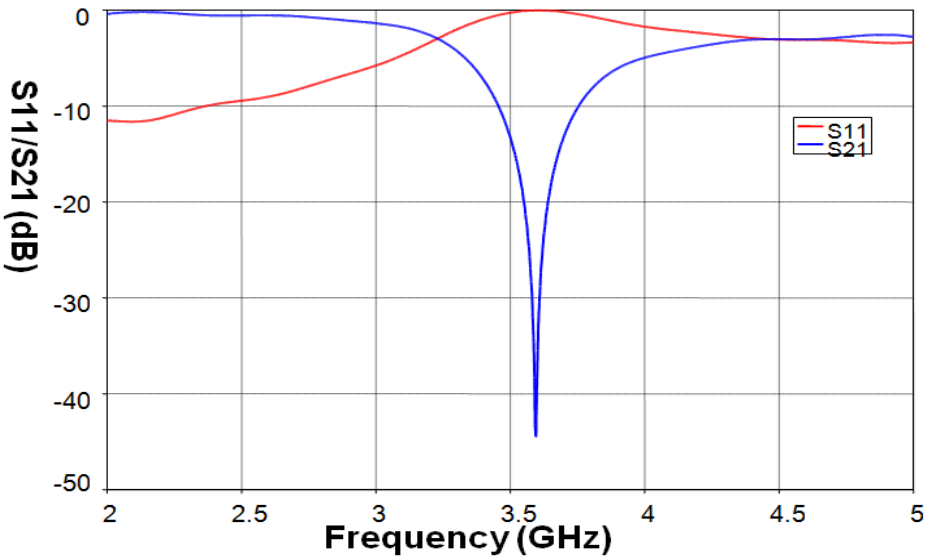


Fig. 4.5. S parameters of CSRR at 3.6GHz.

Fig. 4.6(a), 4.6(b) and 4.7(a), 4.7(b) shows the plots of extracted parameters for CSRRs at 3 and 3.6 GHz respectively. These plots show the capability of the developed artificial materials for creation of an effective negative-$\varepsilon$ medium at resonance.

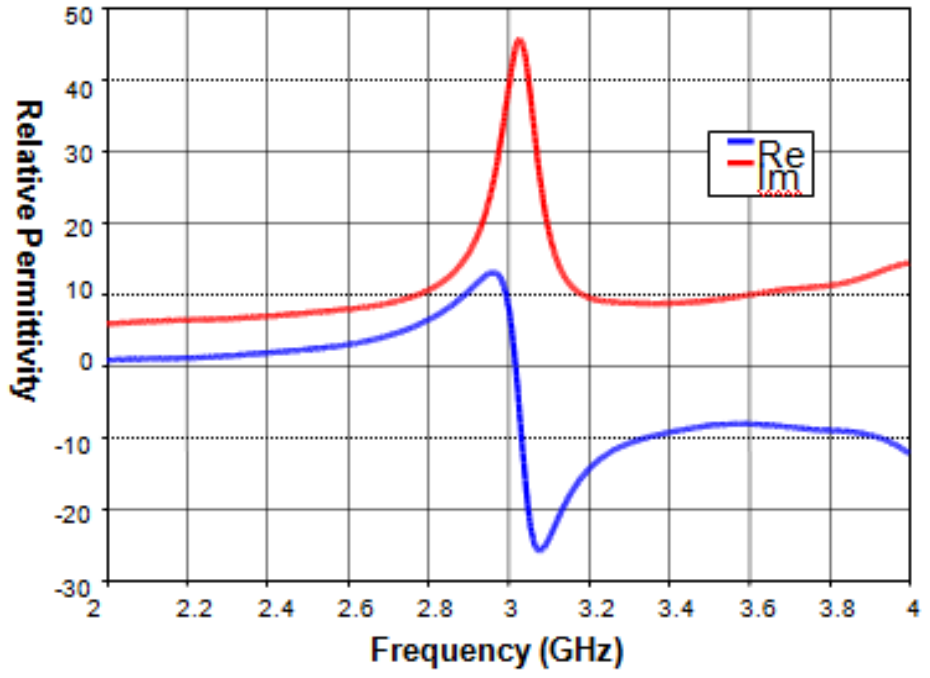


Fig. 4.6(a) Extracted relative permittivity of CSRR resonating at 3.0 GHz.

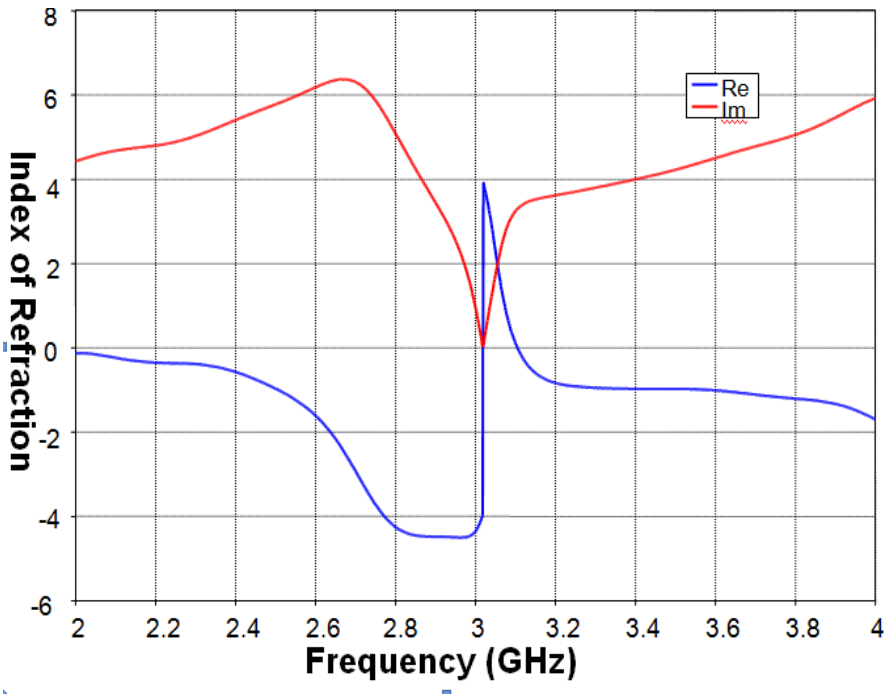


Fig. 4.6(b) Extracted index of refractionof CSRR resonating at 3.0 GHz.

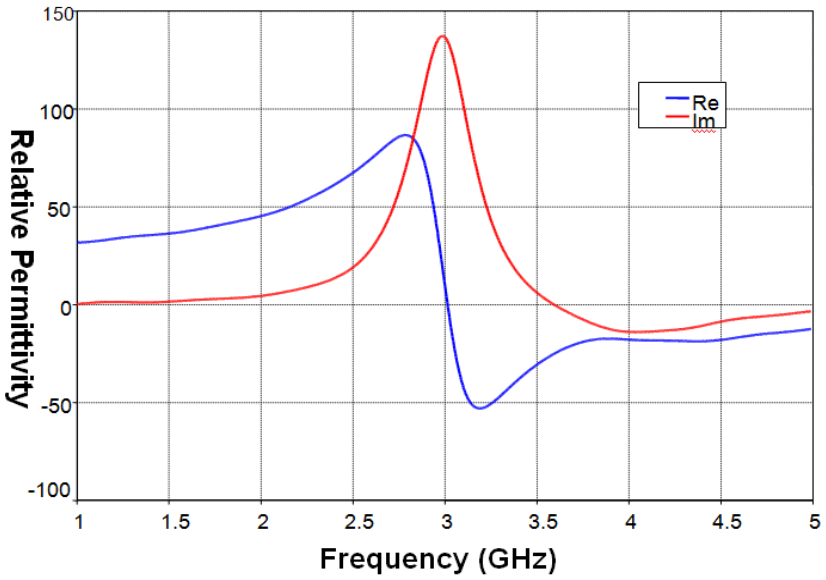


Fig. 4.7(a) Extracted relative permittivity of CSRR resonating at 3.6 GHz

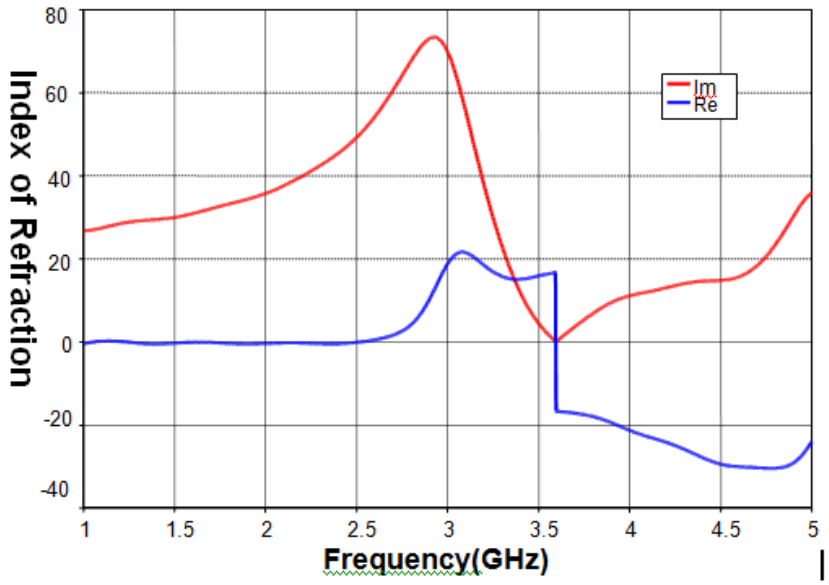


Fig. 4.7(b) Extracted index of refraction of CSRR resonating at 3.6 GHz.

### 4.4.2. Loading of Patch Antenna with CSRR

After verifying the effective medium parameters of the designed CSRRs, a 3×3 array of these were incorporated on the patch antenna for its miniaturization. Experimental verification of this fact has been demonstrated in [52, 45]. For the first case, an inset fed rectangular patch antenna of size (31 mm. × 26 mm.) was designed to resonate at 3 GHz and CSRR array was printed on its ground plane. As shown in Fig. 4.8, now the combined structure is resonating at 2.6 GHz. For the second case the antenna was designed at 3.5 GHz. The CSRR incorporated patch antenna resonant frequency now shifts to 2.85 GHz, as shown in Fig. 4.9.

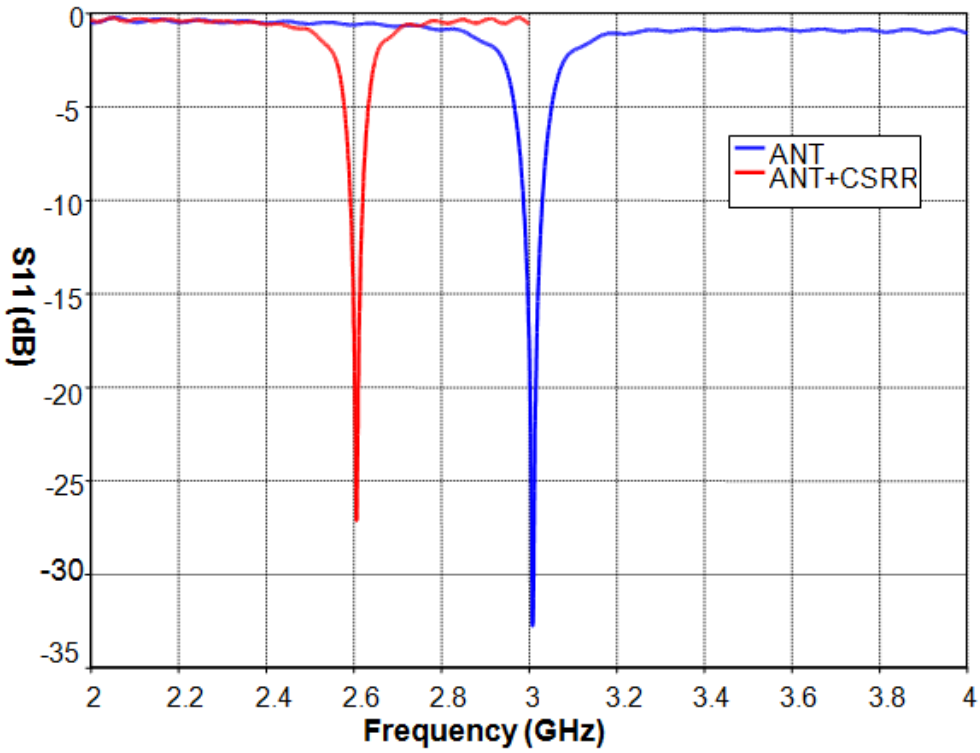


Fig. 4.8 Resonant characteristics of CSRR incorporated patch antenna in comparison with that of only patch resonating at 3GHz.

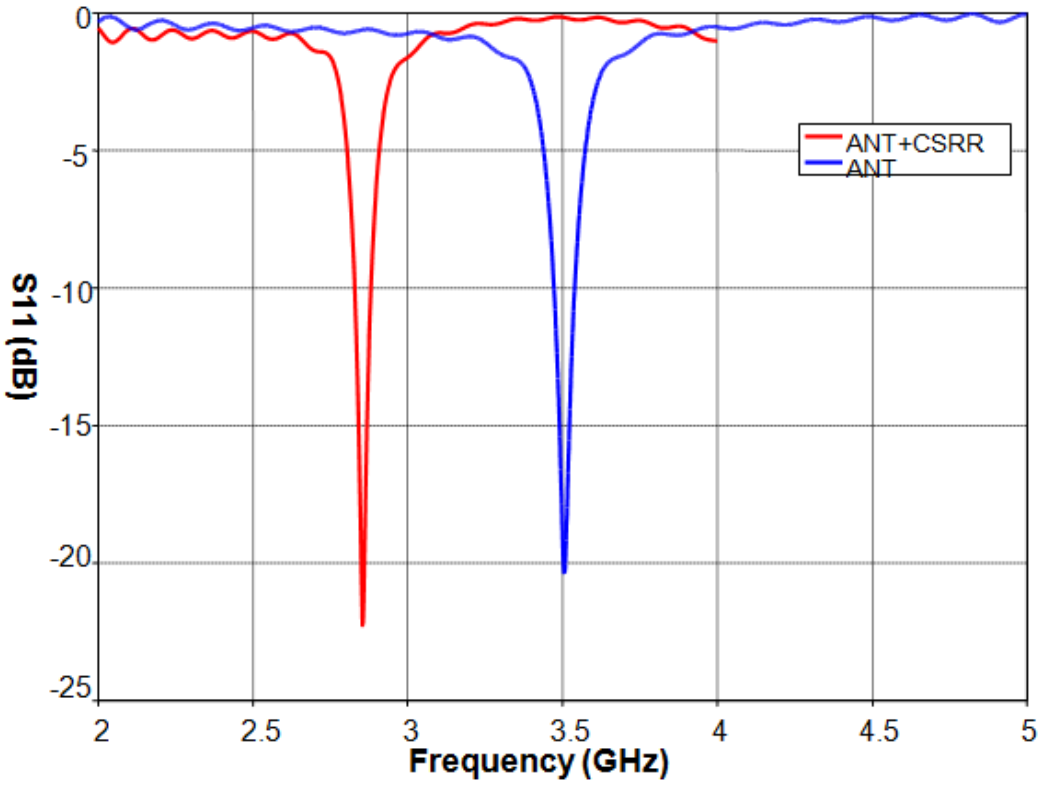


Fig. 4.9 Resonant characteristics of CSRR incorporated patch antenna in comparison with that of only patch resonating at 3.6 GHz.

## 4.5. Concluding Remarks

In this chapter, a fast and flexible procedure for designing a CSRR backed patch antenna is presented. Utilization of ANN and PSO techniques together, allowed the procedure to eliminate lengthy optimization process of CSRR to resonate at a user defined frequency.

The task was approached as an optimization problem and solved using PSO, whose cost function was evaluated with the help of a trained neural network. This completely bypasses the trial-error based approach of designing metamaterial structures during simulation and hence drastically reduces the design time. Since the response time of the NNs is very fast the entire optimization process takes only a few seconds whereas manual optimization may take several minutes altogether. Few typical structures were designed to investigate the miniaturization behaviour of the antenna. Although developed for a specific metamaterial structure, the same methodology can be extended for design of other electromagnetic metamaterials.

# 5.

# CSRR Based Multiband Microstrip Antenna

## 5.1 Introduction

The design of multiband antennas is one of the major areas of research among antenna engineers to meet the constant unconventional demands of communication engineers. Miniaturization is an added challenge. In this direction, use of metamaterials, in the form of array of split ring resonators (SRRs) or CSRRs (complementary SRRs) are one of those techniques used for performance enhancement of microstrip antennas along with the usage of CRLH transmission line [103-108]. But lately it has been agreed upon that it is not the metamaterial effect that cause this but rather the placement of the CSRR slots and their dimensions that result in *LC* loading of the patch resulting in miniaturization. Therefore, a single CSRR when properly placed underneath the patch results in significant miniaturization. Taking advantage of this fact, this chapter demonstrates the design of a miniaturized multiband antenna with CSRR loading. Although the problem looks simple, it has been found that the implementation is not straightforward. For this reason, we have outlined the simple design guidelines for such antennas. Using these guidelines, few typical tri-band antennasare designed and the results are cross checked experimentally.

## 5.2 Existing Metamaterial based Multiband Antennas

One of the methods of achieving metamaterial loaded printed multiband antenna is to load the antenna with resonant metamaterial particles [109]. In [110], the authors have used SRRs to load an antipodal printed monopole. By loading the antenna with SRR they have achieved dual band operation. By examining the current distribution, it has been shown, in this paper, is that the first frequency is due to the fundamental mode of the monopole and the second mode is due to the presence of the SRR. Another self diplexed SRR loaded monopole is described in [111]. In this case SRRs are printed around the patch to achieve dual band as

well as triple band operation. It is also proved that, as the number of SRRs is increased, the number of frequency bands is also increased. In [112], open complimentary split ring resonators (OCSRR) have been used to achieve multiband. In this communication also, the first band is due to the fundamental mode of the monopole and the second frequency of operation is due to the resonance of OCSRR. Triple band has also been achieved by adding another OCSRR to the monopole. A dual band CPW fed patch antenna is reported in [113]. This monopole consists of a thin strip of inductor and an interdigital capacitor. This reactive loading of the monopole is inspired by transmission line metamaterial which is related to the concept of zero index of refraction. Using this technique two frequency bands of operation has been achieved. A tri-band metamaterial inspired antenna is reported in [114]. There, the authors have used modified S shaped resonator (MSR) in the vicinity of printed monopole. These MSRs are directly connected to the monopole. A different concept of metamaterial enhanced multiband antenna is presented in [115]. These are mostly monopole antennas where researchers have used metamaterial to achieve multiband operation in the antenna. A multilayer metamaterial inspired antenna is reported in [116]. Another way to achieve multiband in metamaterial enhanced antenna is to incorporate composite right hand / left hand (CRLH) transmission line. CRLH transmission line has different resonant modes. They may have positive as well as negative resonance modes. Even $0^{th}$ order resonance is also possible. Conventionally $0^{th}$ order resonance is used for size reduction of antennas and other modes are used for multiband operation. In [117], Itoh et. al., have reported a CRLH transmission line based leaky wave antenna. They have used different modes of CRLH transmission line for multiband operation. The modes used in that work are -1, 0 and +1. A similar structure is reported in [118]. An EBG based multilayer antenna is reported in [119]. In that, the simple substrate of patch antenna is replaced by EBG loaded substrate. The three modes of operation include one monopole radiation pattern in n=0 mode and two patch like radiation pattern n = -1 and n = +1. Furthermore, the last two modes which have patch like radiation pattern can be tuned by dimensional parameters of EBG. For n = +1 mode, circular polarization is obtained and for n = 0 linear polarization. Two other multiband patch antennas have been reported in [120-121]. Both these works are also based on CRLH transmission line. In this work also, authors have utilized different modes of operation of CRLH transmission lines.

## 5.3 Background Theory

In the context of microstrip antennas, generally an array of CSRRs is employed in the ground plane of the antenna. These CSRRs are excited by the electric field of the patch, which is orthogonal to the CSRR cells [61]. The miniaturization of the overall antenna structure comes from the process of presence of the CSRR array, which is an *LC* resonant tank circuit, near the patch, which is basically a parallel *RLC* resonator. The resonant frequency of the CSRR loaded antenna down shifts from the resonant frequency of the antenna without CSRR loading. At this point it should be noted that, from metamaterial point of view, in order to have electromagnetic homogeneity, periodicity of CSRRs is not a mandatory requirement. Furthermore, for metamaterial operation, there is no restriction on the minimum number of CSRR unit cells on the ground plane, if it satisfies the effective medium condition. This means that, for having a continuous medium behavior, a single CSRR unit is enough, if placed at suitable position with proper orientation on the ground plane. So the array of CSRRs below the radiating patch is a convenience.

Therefore in order to make a multiband microstrip antenna, it can be loaded with CSRRs of different sizes. But it has been found, through simulations that, placing that many number of CSRR unit cells of required dimensions doesn't give the desired performance. Because of the confinement of number of CSRR unit cells in a limited space, mutual coupling between them play a major role and distorts the resonance behavior of the radiating structure. Furthermore, placement of the unit cell CSRRs is another important factor that affects the resonant frequencies.

## 5.4 Design Guidelines

Although these design guidelines doesn't lead to a unique ground plane antenna structure, but certainly help in reaching to a structure that satisfies the desired specifications. These guidelines are:

(i) At first, based on the available space in the system, design the patch antenna, using to the closed-form formulas available [122]. In the present work, we have restricted the focus on rectangular microstrip antennas. Calculate the resonant frequency of this antenna. Inset feed design was carried out based on the transmission line formulae [122]**.

** See appendix I

(ii) Use the above calculated resonant frequency and the desired frequencies of the multiband antenna to decide the resonant frequency of each individual CSRR unit cell, according to the analysis described in chapter-3. Hence decide the equivalent $L$ and $C$ values of the individual CSRRs.

(iii) Use individual resonant frequency information to find the design dimensions of the individual CSRR unit cells, as per the formulas available in [61,63, 64,65].

(iv) Place these CSRR unit cells towards the radiating edges of the antenna, on the ground plane, with all the cells aligned in the same direction.

(v) Place another unit cell (tuning CSRR) that covers almost the entire central space available on the ground plane, aligned in the same direction.

(vi) Adjust the position and orientation of a single cell until getting the desired response.

## 5.5 Example Problem and the Results

The aim was to design an antenna for simultaneous operation in WLAN (5.24 GHz) and fixed satellite service (FSS) uplink/downlink (6.28, 7.28 GHz) applications. Depending on the availability of space, a microstripline fed rectangular microstrip antenna was designed ($l \times w$ = 14.4 × 17.4 mm$^2$, $h$ = 0.508 mm, and $\varepsilon_r$ = 2.2) to operate at 6.8 GHz. Three CSRR unit cells corresponding to three working frequencies of the multiband antenna and one tuning CSRR, whose characteristics are shown in Fig. 5.1 and dimensions are given in Table 5.1, were placed on the ground plane, as per the design guidelines. The frequency response of the antenna with different stages of placement of the unit cell CSRRs, according to the design guidelines, is shown in Fig. 5.2.

From the first stage it can be marked that, even though three CSRR unit cells whose dimension are suitable to produce the required working frequencies of the antenna, according to the circuit theory principle, but it is not showing the desired response. With the placement of the tuning CSRR (second stage) gives the indication of the three resonant frequencies of the antenna. In the third stage, position of only one unit cell is varied to make all the three frequencies prominent. In the final stage, the orientation of that unit cell is changed to give a final refinement of the resonance pattern.

**Table 5.1: CSRR unit cell dimensions**

| CSRRs<br><br>(thickness and separation of rings is 0.5 mm.) | Inner radius (mm.) | Outer radius (mm.) |
|---|---|---|
| CSRR1 (for 5.24 GHz) | 1.0 | 2.5 |
| CSRR2 (for 6.28 GHz) | 0.7 | 2.2 |
| CSRR3 (for 7.28 GHz) | 0.5 | 2.0 |
| CSRR4 (tuning CSRR) | 1.5 | 3.0 |

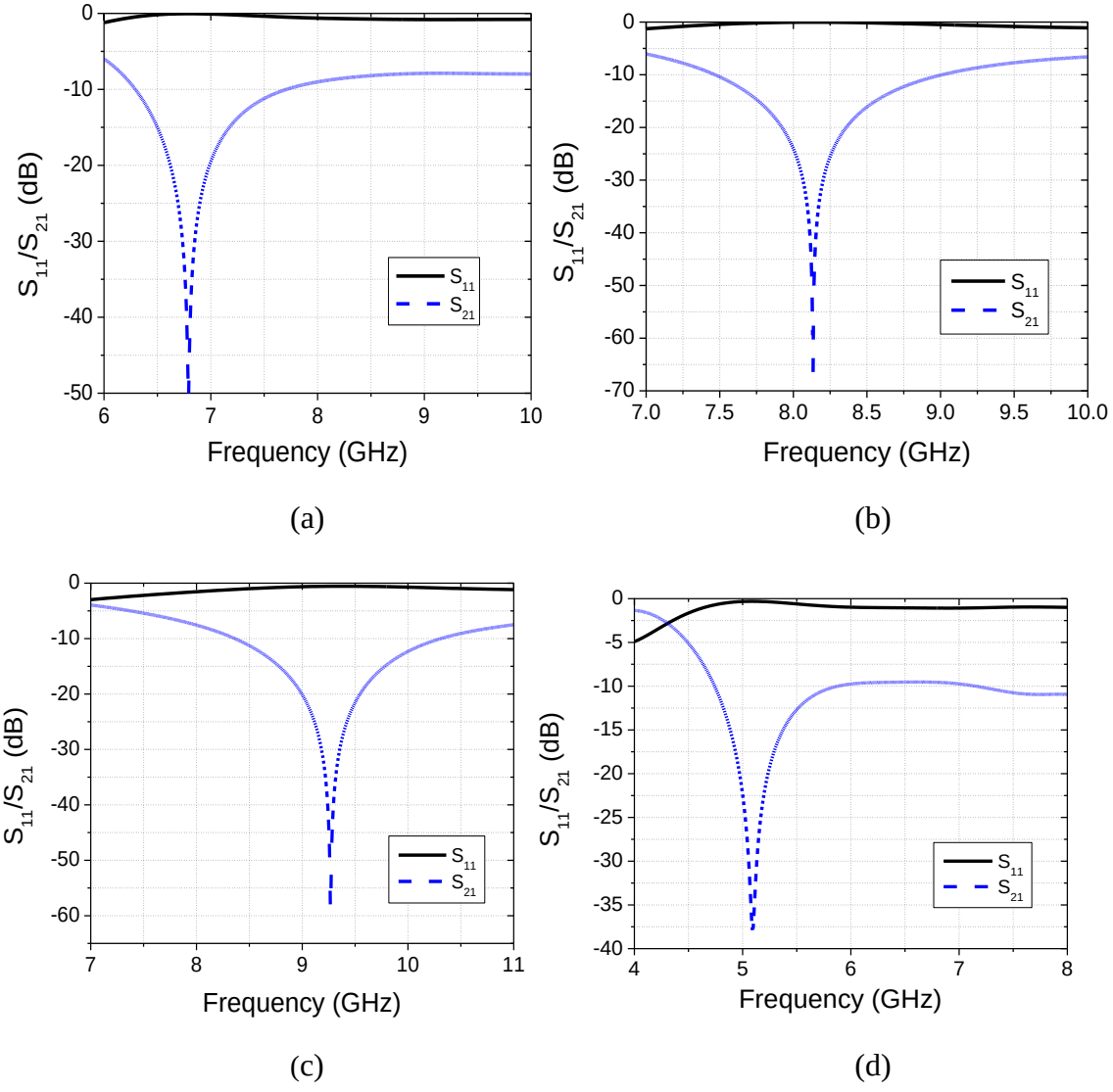


**Fig. 5.1** $S_{11}$ and $S_{21}$ of CSRR unit cells. a: CSRR1, b: CSRR2, c: CSRR3, d: CSRR4

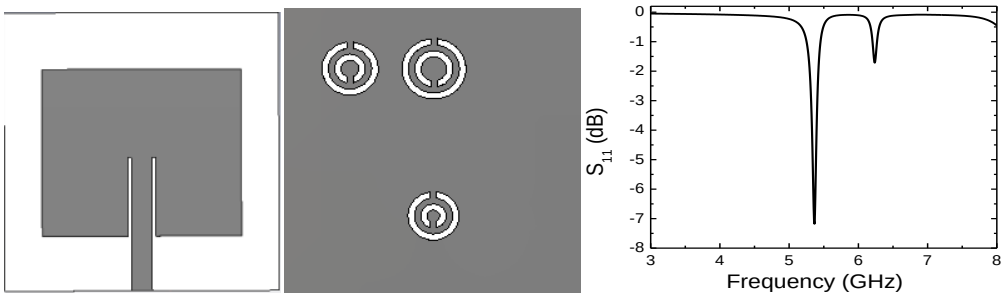


First stage

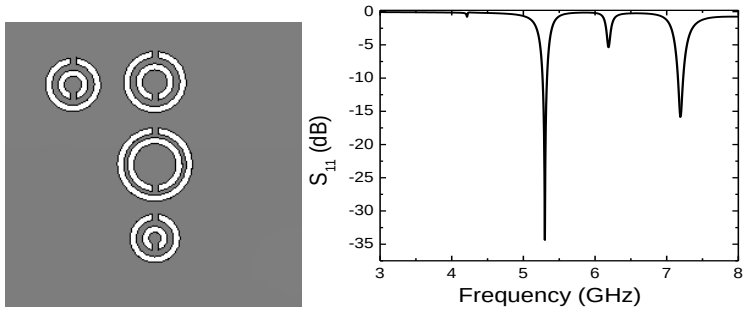


Second stage

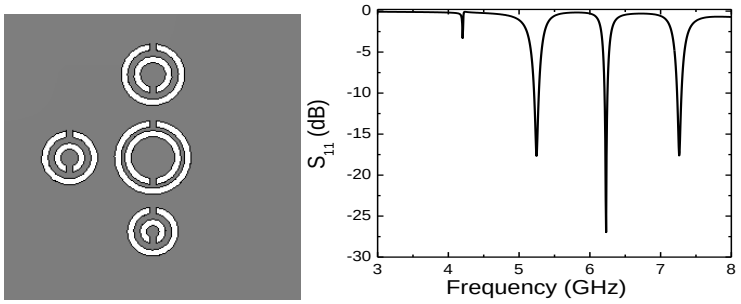


Third stage

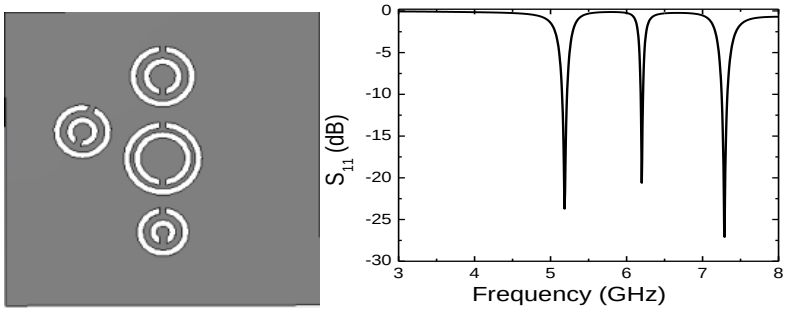


Final stage

**Fig. 5.2** Different stages of positions of the CSRR unit cells on the ground plane of the antenna placed according to the design guidelines, along with their $S_{11}$ response. First stage also shows the front view of the antenna.

CST Microwave studio v12 was used to design, simulate and analyze the proposed multiband antenna. The proposed final structure was fabricated and the $S_{11}$-parameters were measured using an Agilent PNA series network analyzer to cross verify the simulated results. Fig. 5.3 also shows the comparison of the simulated with the measured scattering parameters along with the photograph of the fabricated antenna in the inset. The slight variation between the measured and simulated resonant frequencies of the antenna is because of the less fineness of CSRR unit cells fabricated with the existing facilities. The simulated 3-D radiation pattern of the antenna at these three frequencies is also shown in Fig. 5.3. The directivities of at these three frequencies are 2.8dBi, 1.5dBi, and 3.8dBi respectively.

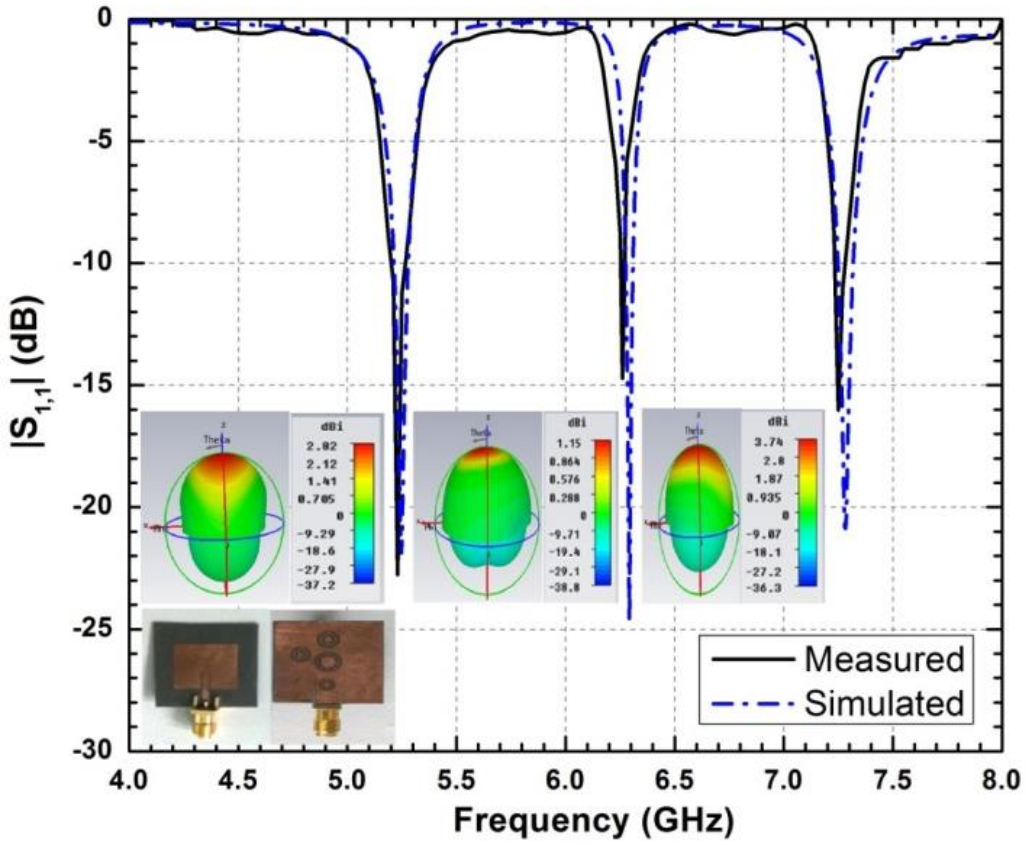


**Fig. 5.3** Comparison of simulated $S_{11}$ with the measured results. The 3D patterns and the fabricated antenna photograph is shown in the inset.

Fig. 5.4 shows the current distribution on the CSRR unit cells at the three operating frequencies of the antenna. The contribution of individual unit cells can be marked clearly from these current distributions. Although the tuning CSRR does not show its individual resonance, but it participates in all three resonant frequencies of the antenna.

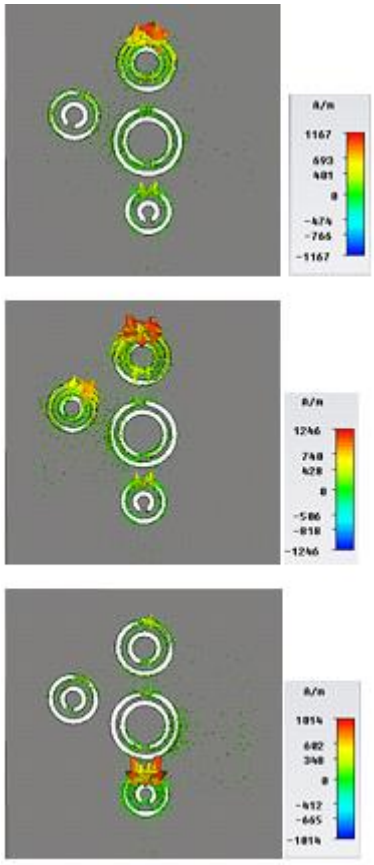

**Fig. 5.4** Current distribution on the CSRR unit cells at 5.24, 6.28 and 7.28 GHz respectively.

Another example problem was taken to reconfirm the design methodology. In this example a simple patch is taken ($l \times w$ = 13.5× 18.2 mm$^2$, $h$ = 1.5 mm, and $\varepsilon_r$ = 4.4) which resonates at 5 GHz. Dimensions of four CSRR unit cells (Including tuning CSRR ) etched in the ground plane of the patch are given in Table 5.2. This CSRR backed patch antenna resonates at 3.4GHz, 4.3GHz and 7.2GHz frequencies respectively. Fig. 5.5 shows a comparison of simulated and measured scattering parameter along with the photograph of fabricated antenna in the inset. Radiation pattern of the antenna at these three frequencies are also shown in fig. 5.5. Directivities at these three frequencies are 1.63dBi, 1.12dBi and 0.5dBi respectively.

**Table 5.2: CSRR unit cell dimensions**

| CSRRs<br><br>(thickness and separation of rings is 0.5 mm.) | Inner radius (mm.) | Outer radius (mm.) |
|---|---|---|
| CSRR1 (for 3.4 GHz) | 1.5 | 2.5 |
| CSRR2 (for 4.3 GHz) | 1.2 | 2.2 |
| CSRR3 (for 7.2 GHz) | 1.0 | 2.0 |
| CSRR4 (tuning CSRR) | 2.5 | 3.5 |

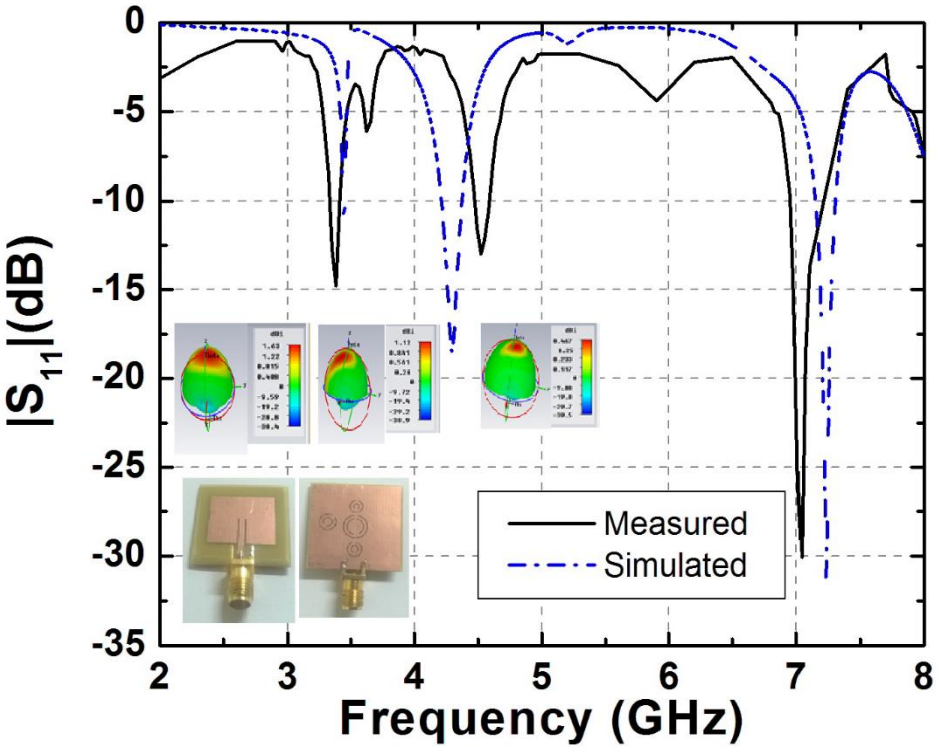


**Fig. 5.5** Comparison of simulated $S_{11}$ with the measured results. The 3D patterns and the fabricated antenna photograph is shown in the inset.

Fig. 5.6 shows the current distribution on the CSRR unit cells at the three operating frequencies. As in the earlier case the contribution of individual CSRR's for different frequency can be understood from the current distribution plots. Participation of tuning CSRR in all the three resonant frequencies can also be seen from the plots.

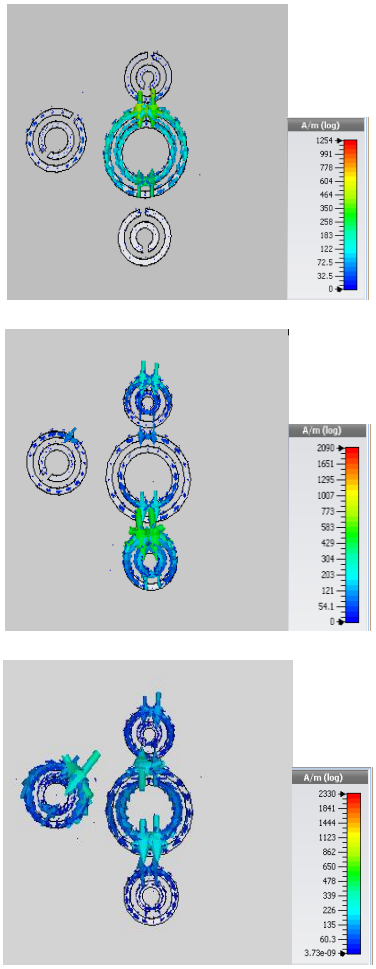


**Fig. 5.6** Current distribution on the CSRR unit cells at 3.4, 4.3 and 7.2 GHz respectively.

## 5.6 Concluding Remarks

This chapter explains the design process of miniaturized multiband microstrip antennas with CSRR loading. Design guidelines are provided to design similar structures at other multiple frequencies. From the simulated and measured results of the designed typical antenna, it is observed that the guidelines can be used to design antennas with compact dimension, higher isolation between bands, good radiation pattern characteristics and with stable gain.

# 6.

# Directivity Enhancement using Metamaterials

## 6.1 Introduction

As the HPBW of a microstrip antenna is a broad one, efforts have been made to make the antenna pattern more directive. Different methods of enhancing the directivity of microstrip patch antennas have been reported in the literature. Among these, the common techniques are use of stacked patches [123][124], use of superstrate [125-127], use of photonic band gap structures [128] etc. Another class of alternative approach is to use metamaterial to increase the directivity of microstrip patch antennas. Collimation properties of metamaterial has been demonstrated in many literatures [129-130]. In [129] authors have proved that the radiated beam passing through a metamaterial medium will be directed very close to normal drawn at the interface of the medium if the refractive index of the medium is close to zero. Hence they can be used for directivity and gain enhancement. In the present work, we have used near *epsilon* zero metamaterial superstrate to enhance the directivity of the antenna. This near epsilon zero metamaterial was proposed by Pendry in late 1990s. The physical concept behind this technique is the formation of Fabry–Parrot cavity. This Fabry-Parrot cavity is formed between the antenna ground plane and the superstrate layer.

Some literatures are available to increase the directivity of patch antennas using *mu* zero metamaterial, EBG material, wire mesh structure etc. Rodded metamaterial structure has a plasma frequency which is usually very high. But the dielectric enhanced metamaterial structure has got a comparatively low plasma frequency. This kind of metamaterial structure can be used for lower frequency band of operation. When the higher dielectric constant materials are used, the plasma frequency further reduces to a lower value. Pendry's formula suggests that, to bring down the plasma frequency the radius of metallic wire structure should be very small. But the structure proposed in this work has metallic rods inserted into the dielectric and has considerably larger diameter as compared to conventional smaller

dimensional wires. A comparative study of plasma frequency with the separation of rods has also been carried out in this chapter.

## 6.2 Near Epsilon-zero Metamaterial and Principle of Directivity Enhancement

In this section we explain the principle of directivity enhancement using metamaterial. Let us consider a point source inside a slab of near zero index material surrounded by a homogeneous isotropic materials as shown in the figure6.1.

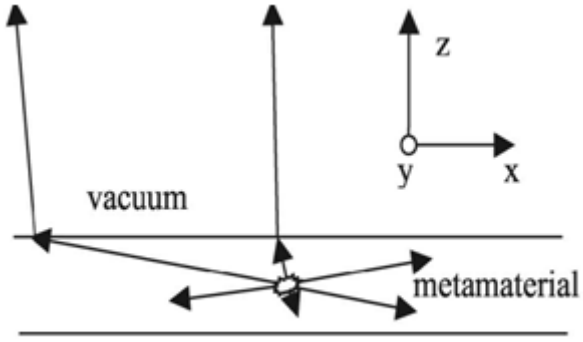


Fig. 6.1 A schematic of directivity enhancement using metamaterial superstrate

Consider an incident ray on an interface with grazing incidence that comes from a source inside the slab of metamterials. The Snell-Decarte's law [1] implies that with near zero index the ray in the media above the slab will be refracted in a direction very close to the normal (lower is the optical index, closer is the direction towards the normal).Then almost all the rays will travel in the same direction around the normal. Hence almost all the rays will be directed perpendicular to the surface, thereby increasing its directivity [131].

A near zero index metamaterial may be *epsilon* zero metamaterial or *mu* zero metamaterial. In the present work, we have concentrated on *epsilon* negative metamaterials. The concept that wire media can behave as plasma medium was first known in the year 1950. One of the methods to obtain *epsilon* negative metamaterial effect is to have metallic wires used in an array. This structure shows negative permittivity for a frequency band and many researchers have used this to achieve *epsilon* negative metamaterials [131-136]. Unusual properties of wire media were investigated by many researchers [137-139].It means that the dispersion relation of the propagation modes in this structure shaped like plasmas of electron gas. Theoretical and experimental work has shown that such arrays of continuous wires are

characterized by a plasma frequency. Pendry[8] showed that the effective relative permittivity of this wired medium can be expressed in terms plasma frequency and the frequency of operation of the medium as

$$\varepsilon_{eff} = 1 - \frac{\omega_p^2}{\omega^2} \tag{6.1}$$

where $\omega_p$ is the angular plasma frequency and $\omega$ is angular frequency of operation. The first consequence of this microwave plasma frequency is that the equivalent permittivity is negative when the operating frequency is below the plasma frequency. That is, the optical index is exactly zero or very close to zero when the frequency of operation is exactly the plasma frequency or frequency of operation very near to plasma frequency. When the permittivity is exactly zero or very near to zero then we will have refractive index also to be exactly zero or very near to zero.This property of the material helps in enhancement of directivity.

Sarychev [140], Markos [137], Belov [141], Pendry [8] and Maslovski [142] have reported empirical formulae for the plasma frequency of rodded media. The most widely used Pendry's formula for plasma frequency of such a rodded media is given by

$$\omega_p^2 = \frac{n_{eff} e^2}{\varepsilon_0 m_{eff}} \tag{6.2}$$

where $m_{eff}$ is the effective mass of electrons in the wire which makes the media. This, in turn is given by

$$m_{eff} = \frac{\mu_0 \pi r^2 e^2 n}{2\pi} ln\left(\frac{a}{r}\right) \tag{6.3}$$

where $n$ is the density of the electrons in the wire, $r$ is the radius of the wire, $a$ is the separation of the wires, and $n_{eff}$ is the density of the active electrons in the structures as a whole. $n_{eff}$ is given by

$$n_{eff} = n\frac{\pi r^2}{a^2} \tag{6.4}$$

where $n$ is the density of electrons in the wires. Plasma frequency can also be represented by

$$\omega_p^2 = \frac{2\pi c_0^2}{a^2 ln\left(\frac{a}{r}\right)} \tag{6.5}$$

This formula holds good when the wires are very thin. It is clear from the formula that plasma frequency decreases with the wire radius.Preferably the wire radius is in micrometres. It has two disadvantages, firstly thin wires are costly and not easily available and secondly

supporting this type of structures is very tough. But when the wires are thick (typically of the order ofmm.) and their radius is comparatively equivalent to that of the separation distance, then the equation modifies to [8]

$$\omega_p^2 = \frac{2\pi c_0^2}{a^2} \tag{6.6}$$

Still the plasma frequency of this wired media is quite high. So if we want to increase the directivity of antenna using this metameterial then the antenna size becomes very small. That itself is a big drawback. Here we propose a structure where we introduce metal wires inside a dielectric slab which shows reduction of plasma frequencyof the medium.

As velocity of light is modifiedin a dielectric medium hence after inserting the rods inside the dielectric the expression of plasma frequency is modified as

$$\omega_P = \frac{1}{1.1}\sqrt{\frac{2\pi c_0^2}{\varepsilon_r a^2}} \tag{6.7}$$

where $\varepsilon_r$ is the relative permittivity of the medium. In this case, as the separation of the wires are not approximately equal to that of the wire radius hence a correction factor has been added in eqn. (6.7). This correction factor is based on the discussions made in [22]. It is also clear from the equation that as the relative permittivity is increased, the plasma frequency becomes lower. We have simulated a number of cases by increasing the dielectric constant of the medium and the plasma frequency is reduced by many folds.

There are two methods to find out the plasma frequency of an artificial medium through simulation and these are eigenmode solver method and scattering parameter method [143]. In the present research, we have used the scattering matrix method to find out the plasma frequency of the medium. In [143] authors have used only transmission parameters to find the plasma frequency, but in the present work we have taken into account the returnloss parameters to clearly identify the plasma frequency. A number of cases have been investigated and are tabulated in table 6.1.

**Table 6.1: Plasma frequency of rodded media**

| No. | Separation of metallic rods (mm) | Rod diameter (mm) | Dielectric const. of medium | Plasma frequency without dielectric (GHz) | Plasma frequency with dielectric (Simulated) (GHz) | Plasma frequency with dielectric (analytical) (GHz) |
|---|---|---|---|---|---|---|
| 1 | 5.0 | 0.5 | 3.0 | 21.46 | 13.2 | 12.92 |
| 2 | 4.0 | 0.9 | 3.3 | 22.0 | 12.98 | 12.84 |
| 3 | 5.0 | 0.5 | 4.5 | 21.46 | 10.19 | 10.4 |
| 4 | 5.0 | 0.5 | 6.0 | 21.46 | 8.81 | 8.88 |
| 5 | 4.0 | 1.0 | 3.0 | 26.67 | 10.84 | 11.09 |
| 6 | 4.0 | 1.0 | 6.0 | 26.67 | 8.37 | 8.6 |
| 7 | 3.0 | 1.5 | 9.2 | 26.67 | 6.37 | 6.57 |

We have experimentally validated this phenomenon. Perspex with dielectric constant of 3.3 was chosen as dielectric material.Experiments were conducted for different separation distances of rods and various substrate heights of Perspex.In this thesis one typical result is presented. Copper rods of diameter of 0.9 mm were inserted inside the substrate with separation distance of 4.0mm. S-parameters of this structure were measured using a VNA. For cross verification, the same structure was also simulated using CST Microwave Studio v12. Photograph of fabricatedrodded media structure and measurement set up is shown in fig. 6.2, fig. 6.3 and fig 6.4.

Fig. 6.2 Fabricated rodded metamaterial structure

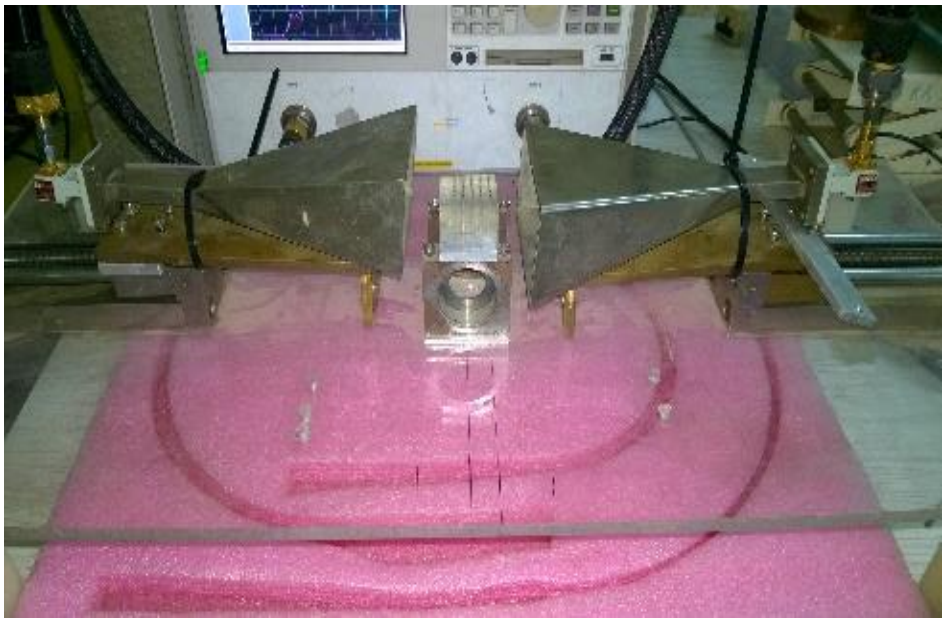

Fig. 6.3 Actual set up of measurement

Fig. 6.4 Measurement set up with absorbing materials

Plots of simulated and measured S-parameters are shown in fig.6.5 and fig. 6.6 respectively.A study was also carried out to observe the trend of plasma frequency with the change of dielectric constant of the medium and the separation of rods. It was observed that with the reduction in the dielectric constant of the medium and the separation of the rods, the plasma frequency also reduces.Plot of plasma frequency vs. dielectric constant and plasma frequency vs. rod separation distance is shown in fig. 6.7 and fig. 6.8 respectively.

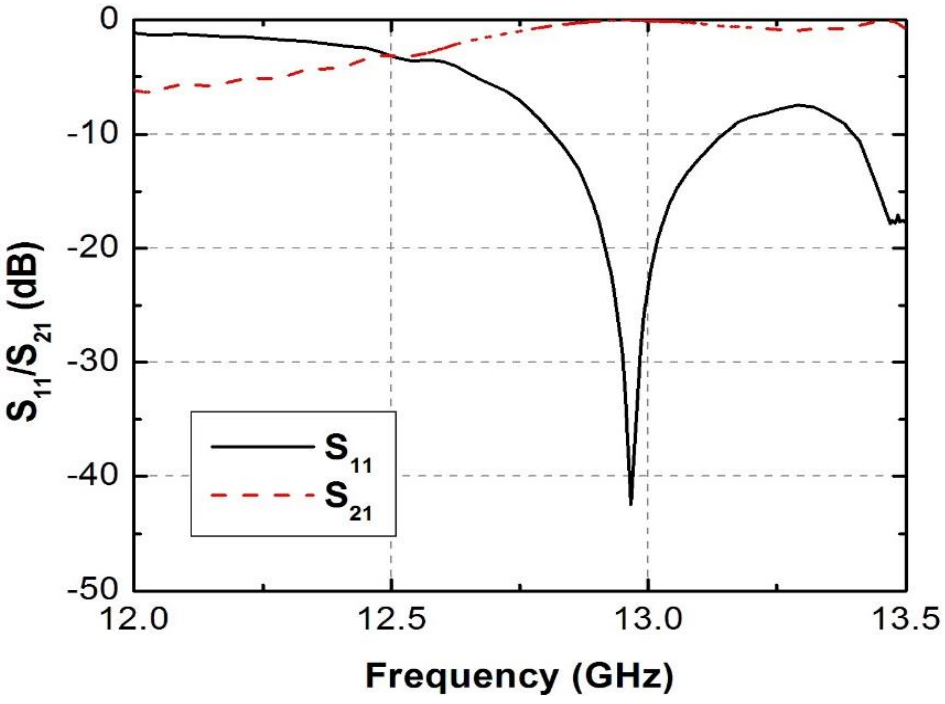


Fig. 6.5 Simulated S parameter of rodded media

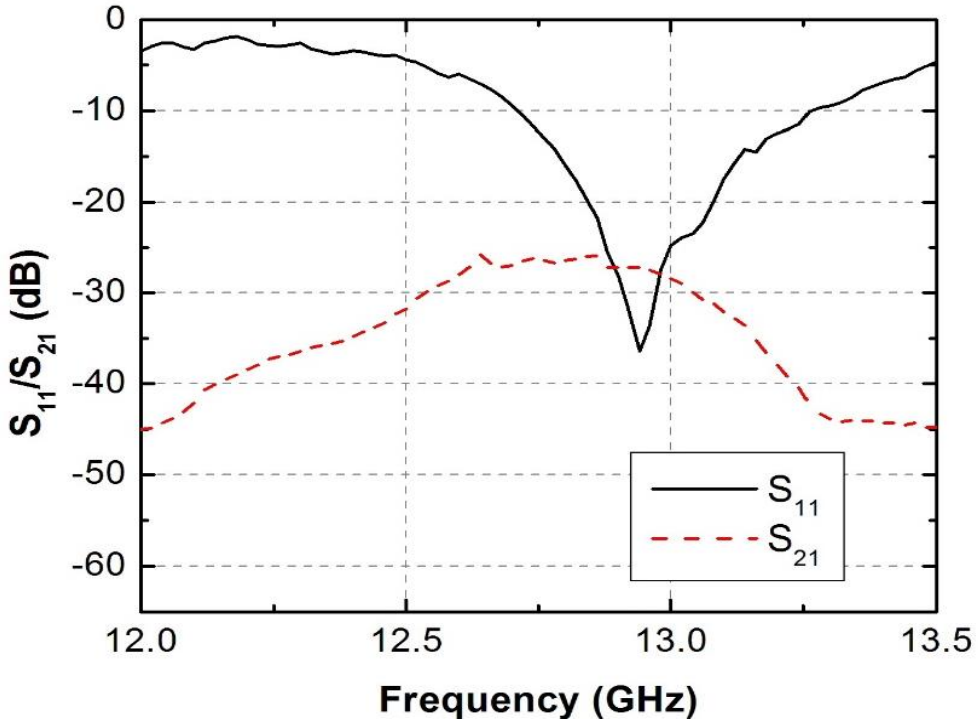


Fig. 6.6 Measured S parameter of rodded media

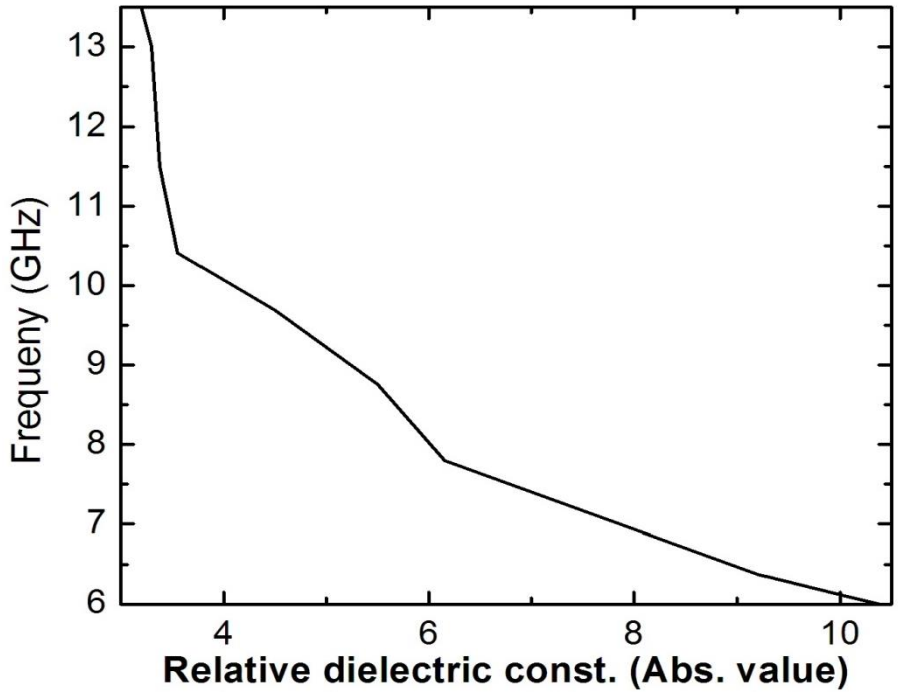


Fig. 6.7 Plot of plasma frequency vs. dielectric constant

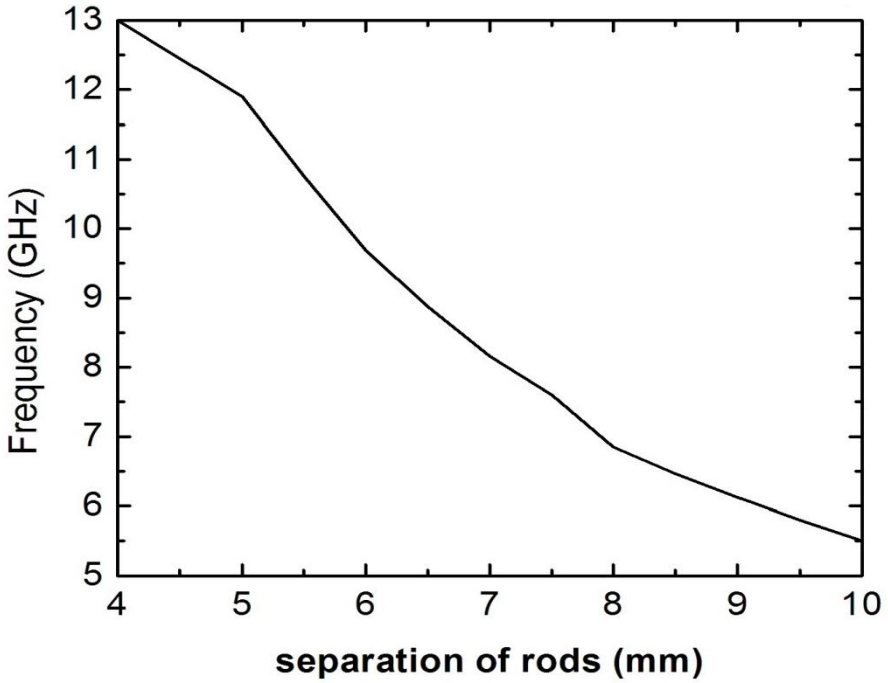


. Fig. 6.8 Plot of plasma frequency vs. separation of rods

## 6.3 Antenna Configuration and Formulation

Designed and optimized superstrate in the form of dielectric cover was placed above the antenna. The configuration of the whole structure with multiple layers superstrate is shown in the fig. 6.9.

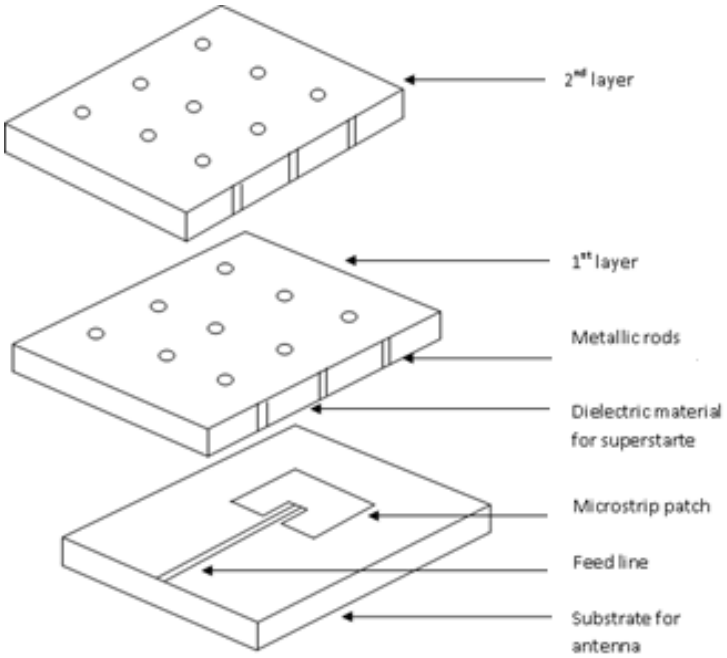


Fig. 6.9 Schematic of antenna with two layers of supersaturate

A cavity is formed in between the ground plane of the antenna and the first layer of superstrate which acts as a partially reflective surface (PRS) [144-145]. This type of cavity is known as Fabry-Parrot cavity resonator. A schematic of Fabry-Parrot cavity is shown in fig. 6.10. This PRS was considered as a homogeneous medium and edge effects of the ground plane of the antenna and PRS were neglected.

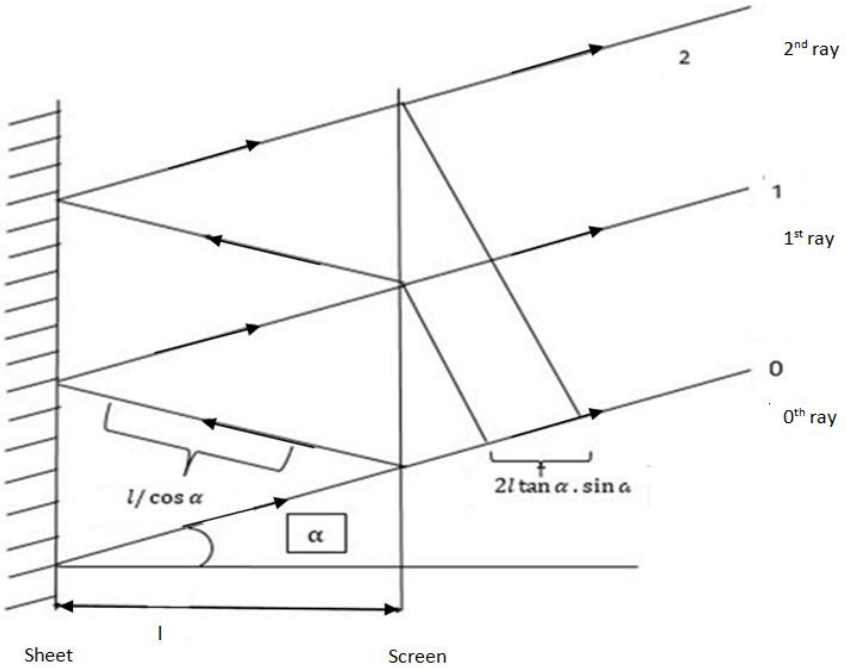


Fig. 6.10 Schematic of Fabry-Parrot cavity resonator between antenna ground plane and superstrate

As shown in the diagram, directed ray which is designated as 0th ray has an amplitude proportional to $\sqrt{1-p^2}$. The first reflected ray, designated as 1st ray, has an amplitude proportional to $p\sqrt{1-p^2}$. Proceeding in similar manner, the nth ray will have an amplitude proportional to $p^n\sqrt{1-p^2}$. As there are many reflections between antenna ground plane and the PRS, electric field intensity in the Fraunhofer zone is the vector sum of all the rays. If we consider the screen to be infinitely long then total electric field intensity will be given by

$$E = \sum_{n=0}^{\infty} f(\alpha) E_0 p^n \sqrt{1-p^2} e^{j\Theta_n} \tag{6.8}$$

where $f(\alpha)$ is the elemental pattern originating from a point, $p$ is the complex reflection coefficient of the sheet. $\Theta_n$ is the phase angle formed by phase variations of direct and

reflected rays formed by perfectly reflecting ground plane and the PRS. Phase difference between any two rays is given by

$$\Theta_n = n\phi = n\left[-\frac{4}{\pi} l \cos\alpha - \pi + \psi\right] \tag{6.9}$$

where ψ is the phase angle of complex reflection coefficient and *l* is the distance between sheet and the screen. The complex power pattern is given by

$$S = \frac{1-p^2}{1+p^2-2p\cos\left(\psi-\pi-\frac{4}{\pi}l\cos\alpha\right)} f^2(\alpha) \tag{6.10}$$

Maximum power in the direction of α=0 is obtained when

$$\psi - \pi - \frac{4}{\pi} l = 0 \tag{6.11}$$

In this condition the power pattern is modified as

$$S = \frac{1-p^2}{1+p^2-2p\cos\left(\psi-\pi-\frac{4}{\pi}l\right)} f^2(0) \tag{6.12}$$

Hence the equation determining the resonance distance of the PRS is given by

$$l_r = \left(\frac{\Psi_0}{360} - 0.5\right)\frac{\lambda}{2} + N\frac{\lambda}{2} \tag{6.13}$$

Here $\Psi_0$ is expressed in degrees and N = 0,1,2,3, etc.

From the above formulae it is clear that if we know the phase angle we can easily determine the resonant distance between the patch antenna and the PRS which basically acts as a Fabry-Parrot cavity resonator.It was found that, as the number of layers increased the directivity of the antenna increases to a certain limit. The distance of each layer is different fromthe other. Thickness of different superstrate layers are kept constant. In addition to the first layer if we add second layer, then there is enhancement of directivity. We can further add another layer (third layer) to increase the directivity to the next level. If one goes on adding further superstrate layers to this antenna it merely increases the directivity. It reaches to a saturated value, beyond which it is not possible to increase the directivity by simply adding layers. Another limitation is, as we go on increasing number of layers, inter layer spacing becomes less. A point will reach where two subsequent layers will overlap. Also after the addition of three layers as there is no significant directivity enhancement, hence this scheme is also not very much cost effective.

## 6.4 Design Methodology and Simulated Results

In the first step, an epsilon zero metamaterialwhich resonates at a particular frequency and to be used as the superstrate was designed. Then a simple rectangular patch antenna which also resonates at the same frequency was designed. Designed and optimized near epsilon zero metamaterial was used as the superstrate and placed over the antenna. Distance of the superstrate from the ground plane ws calculated from the formulae described in the previous section. Then the other layers were added to increase the directivity up to a significant amount. To demonstrate the phenomenon of directivity enhancement, we have taken a number of cases in different frequency bands. This is tabulated in table 6.2.

**Table 6.2. Directivity of patch antenna with different layer of superstrate**

| Sl. No. | Frequency of operation (GHz) | Directivity of simple patch (dBi) | Directivity of patch with one layer of superstrate (dBi) | Directivity of patch with two layers of superstrate (dBi) | Directivity of patch with three layers of superstrate (dBi) |
|---|---|---|---|---|---|
| 1 | 6.81 | 7.61 | 8.2 | 11.9 | 14.1 |
| 2 | 12.42 | 7.5 | 8.1 | 10.9 | --- |
| 3 | 19.72 | 9.4 | 10.2 | 11.2 | 13.1 |

In first case, a rectangular microstrip antenna resonating at 6.81 GHz was designed. 3D radiation pattern of this antenna, having a directivity of 7.55dBi, is shown in fig 6.11. A near epsilon zero (rodded media) metamaterial, which shows its plasma frequency at 6.81 GHz, was also designed.This rodded media was used as superstrate layer over the antenna. Extracted real part of permittivity and imaginary part of permittivity are very close to zero at this frequency. Plots of extracted real part and imaginary part of permittivity of this rodded media is shown in fig. 6.12 and fig. 6.13. The dimension of the superstrate layer is 15mm × 15mm. Metallic rods are separated by a distance of 5.0mm from each other and the diameter of the rods are 0.5mm. The dielectric constant of this superstrate was 10.

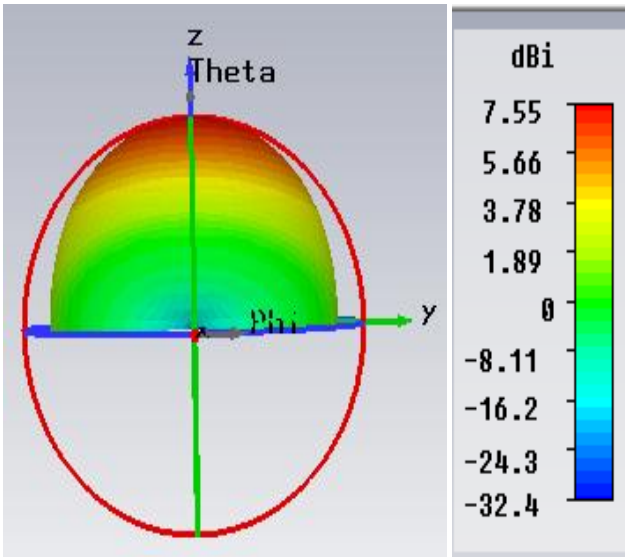


Fig. 6.11 3D radiation pattern of only patch

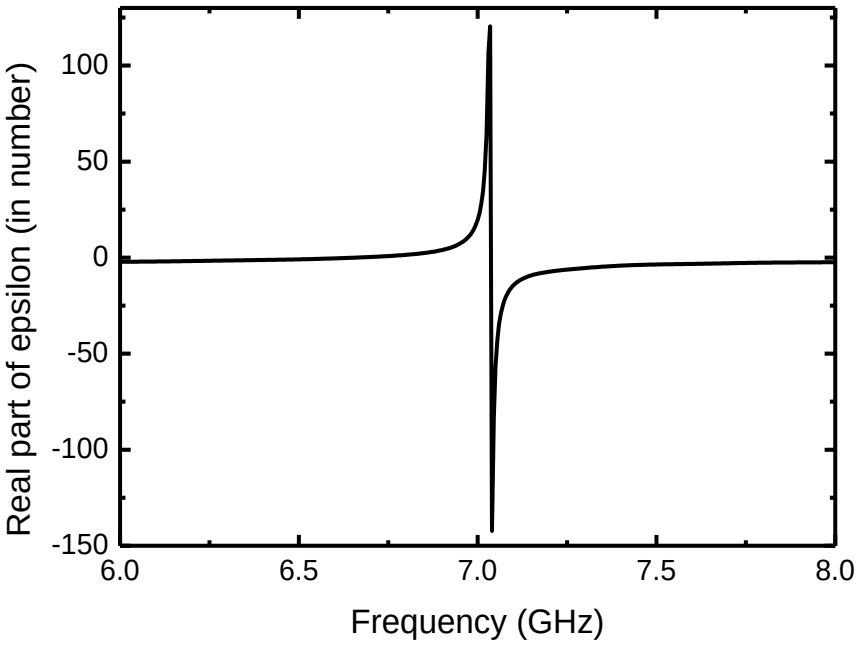


Fig. 6.12 Real part of extracted permittivity of rodded media

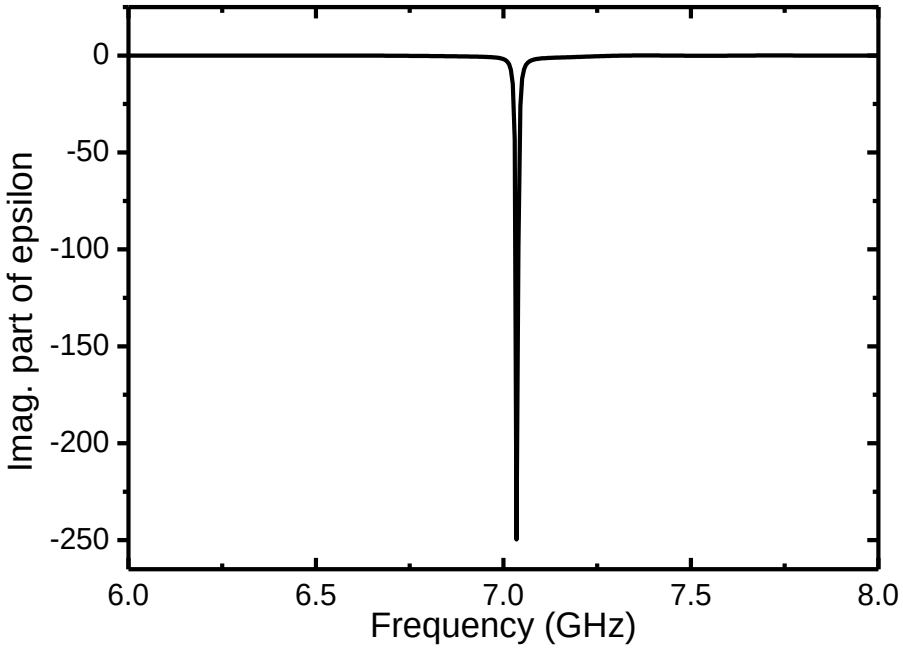


Fig. 6.13 Imaginary part of extracted permittivity of rodded media

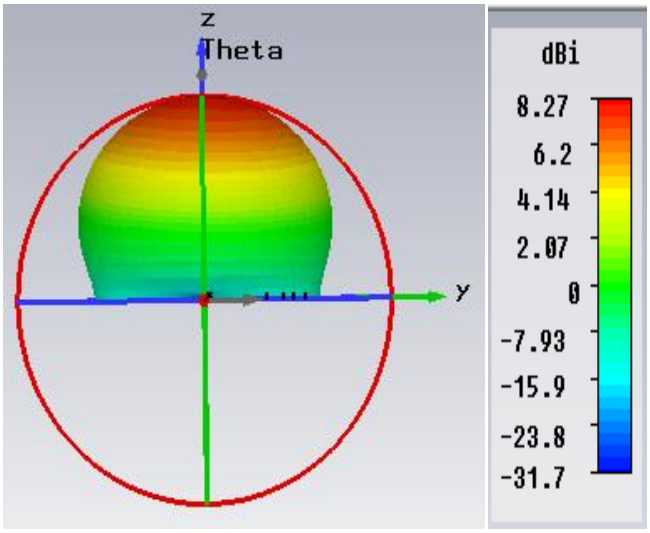


Fig. 6.14 3D radiation pattern of antenna with singlelayer of superstrate.

The superstrate was placed above the antenna at a distance of 5.0 mm. The calculated distance using the empirical formula was 4.8 mm. The 3D radiation pattern of the antenna after adding the layer of superstrate is shown in fig. 6.14. With single layer of superstrate, directivity of the antenna system was found to be 8.2 dBi. A comparison of E-plane radiation pattern of the antenna with single layer of superstrate with that of the simple antenna is shown in fig. 6.15.

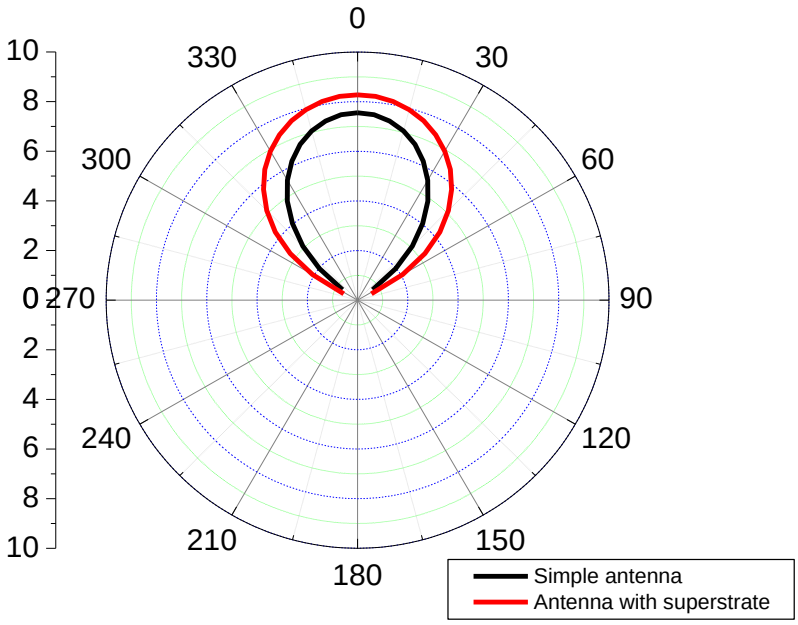


Fig. 6.15 Comparison of E plane radiation pattern of simple antennawith that of antenna with single layer of superstrate

Then another layer of superstrate was added to enhance the directivity further. 3D radiation pattern of antenna after adding two layers of superstrate is shown in fig. 6.16.Now the directivity was found to be 11.9 dBi. A comparison of E-plane of a simple antenna with that of the antenna with two layers of superstrate is shown in fig. 6.17. A comparison of S-parameter of simple antenna and antenna with two layers of superstrate is shown in fig. 6.18. 3D radiation pattern of the antenna with three layers of superstrate is shown in fig. 6.19.

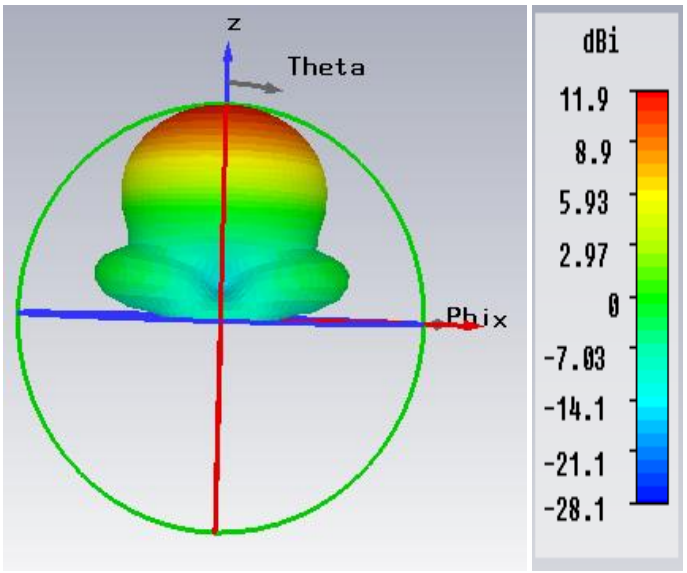


Fig. 6.16 3D radiation pattern of antenna with twolayers of superstrate

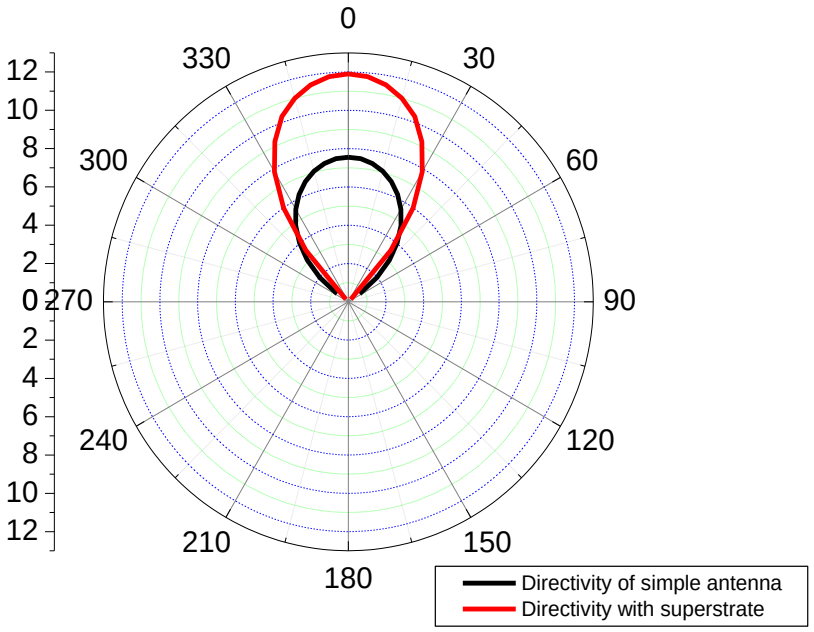


Fig. 6.17 Comparison of E-plane radiation pattern simple antennawith that of antenna with two layers of superstrate

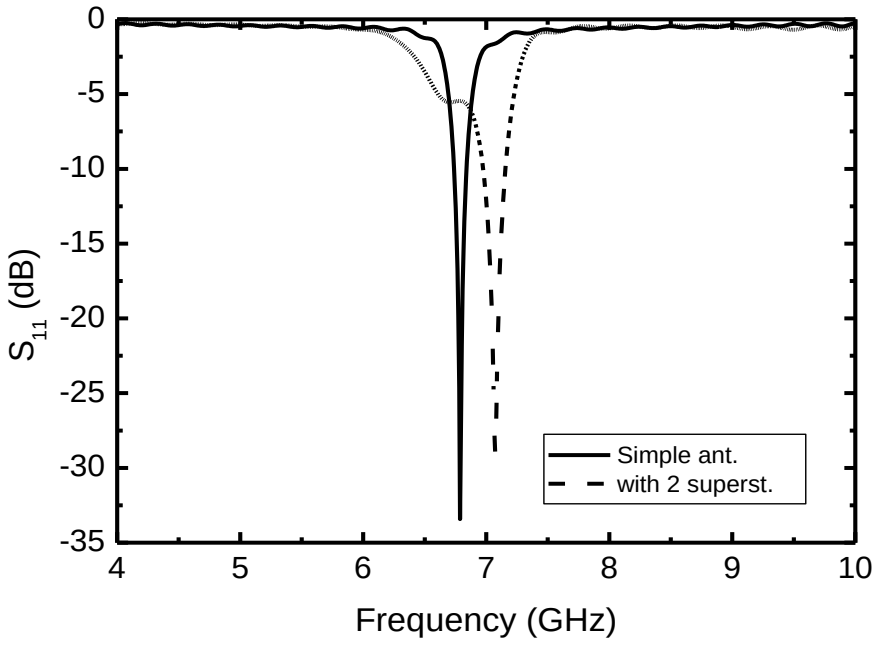


Fig. 6.18 Comparison of $S_{11}$ of simple antenna with that of antenna with double layer of superstrate

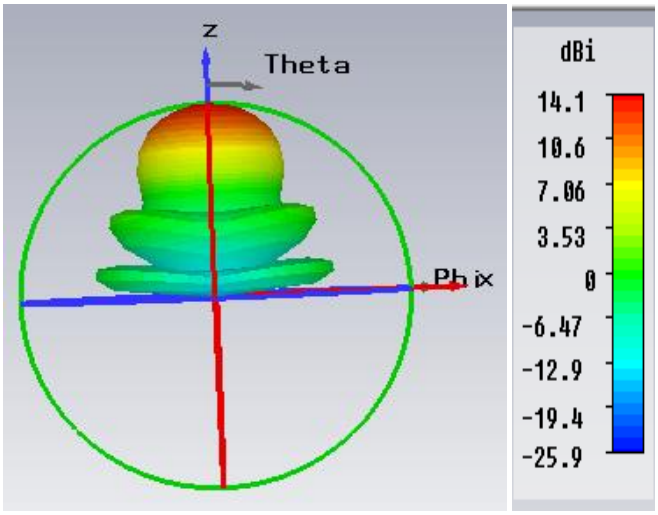


Fig. 6.19 3D radiation pattern of antenna with three layers of superstrate

In other test cases tabulated in Table 6.2, there is significant enhancement of directivity after addition of superstrate layers over the antenna surface. Data from Table 6.2 also signifies that this technique is applicable for all frequency bands.

## 6.5 Concluding Remarks

A simple near epsilon zero metamaterial which consists of an array of metallic rods inserted in a dielectric medium was discussed and analysed in this chapter. Plasma frequency of this near epsilon zero metamaterial is comparatively low. This kind structure is very easy to fabricate compared to conventional wire mesh structure. Parametric analysis showed that the plasma frequency of this near zero metamaterial decreases with increase in dielectric constant of the medium. At the same time as the separation of the dielectric rod separation increase the plasma frequency decreases. Also in case of conventional structure of wire mesh, the diameter of the wires should be very small (preferably in μm) to bring down the plasma frequency of the structure. Use of this kind of near zero metamaterial structure as superstrate to enhance the directivity of patch antenna was demonstrated. Simulation results showed that using two or three layers of superstrate there is a significant increase in directivity. As the superstrate is a solid dielectric structure, so supporting a single layer or multiple layers over the patch antenna is very easy. After using three layers of superstrate even the directivity can be enhanced by a margin of 7dBi.

# 7.

# Conclusion and Future Scope of Work

## 7.1 Conclusion

Analysis and design of metamaterial based patch antennas have been done in this thesis with special emphasis on antenna performance enhancement. The work started with a comprehensive review of metamaterial based microstrip antennas. It was found that, most of the work available in the literatures are structures designed using commercially available em-simulators and the corresponding measured results. A proper analysis of metamaterial based patch antennas was missing from the literature. Therefore, an attempt was made in this thesis to develop an analytical model of a CSRR array backed patch antenna. Mutual coupling factor was considered at proper places and a closed form formula for the resonant frequency of this radiating structure was found out. The result of this analytical formulation has been cross verified with the experimental results for some typical antenna structures.

In order to reduce the computation time of design of these complicated structures, machine learning approaches have been used. With the help of ANN and PSO, a fast and flexible design module for these varieties of antennas has been developed.

Different sizes of CSRR metamaterial structures have been used to design simple multiband patch antennas and its design guidelines are outlined. Another form of metamaterials has been used for directivity enhancement of patch antennas.

Overall the thesis gives a new direction of handling metamaterial based planar antennas analytically. The developed analysis procedure gives the designer an insight into the effect of presence of a periodic structure near the radiating surface. Because a lot of focus has now been given to the metasurface based planar antennas, the developed analytical process can be extended to the analysis of those complicated structures. Compared to analysis, the real challenge lies in the design of these metamaterial based planar antennas. The work done in this thesis gives a simple and new direction of designing metamaterial based planar

antennas. Furthermore, the performance enhancement of planar antennas using metamaterials has been experimentally verified.

## 7.2 Future Scope of Work

Although a few types of metamaterial structures has been analysed in this research, the same can be extended for other varieties of metamaterials.

Efforts should be made to develop methods of analysis and design of metasurfaces and metasurface based antennas in the same line as developed in this thesis.

The developed formulations of this thesis can be incorporated in the existing commercially available em-simulators to enhance their capabilities.

# Appendix-I

## Formula for fixing the design dimensions of rectangular microstrip antenna:

Transmission line based closed form formulae were used to fix the design dimensions of the rectangular microstrip antennas. The process starts with the choice of the PCB sheet $(\varepsilon_r, h)$ for specific operating frequency $f_r$ of the antenna.

Width *w* of patch can be calculated using the following formula:

$$w = \frac{1}{2f_r\sqrt{\mu_0\varepsilon_0}}\sqrt{\frac{2}{\varepsilon_r + 1}}$$

Then the effective dielectric constant $\varepsilon_{reff}$ can be calculated using

$$\varepsilon_{reff} = \frac{\varepsilon_r + 1}{2} + \frac{\varepsilon_r - 1}{2}\left[1 + 12\frac{h}{w}\right]^{-\frac{1}{2}}$$

The extended incremental length of the patch can be calculated using

$$\frac{\Delta L}{h} = 0.412\frac{\left(\varepsilon_{reff} + 0.3\right)\left(\frac{w}{h} + 0.264\right)}{\left(\varepsilon_{reff} - 0.258\right)\left(\frac{w}{h} + 0.8\right)}$$

Then the actual length *L* of the patch is

$$L = \frac{\lambda}{2} - 2\Delta L$$

where $\lambda$ is the free space wavelength corresponding to $f_r$

In order to fix the dimensions of the inset feed for a 50Ω feed line, the following formulae were used.

The Characteristics impedance of a microstrip line is given by

$$Z_C = \frac{60}{\sqrt{\varepsilon_{reff}}} \ln\left[\frac{8h}{W_0} + \frac{W_0}{4h}\right] \qquad when\ \frac{W_0}{h} \leq 1$$

$$Z_C = \frac{120\pi}{\sqrt{\varepsilon_{reff}}\left[\frac{W_0}{h} + 1.393 + 0.667 \ln\left(\frac{W_0}{h} + 1.444\right)\right]}\ when\ \frac{W_0}{h} > 1$$

The Input resistance for the inset feed is approximately given by

$$R_{in}(y = y_0) = \frac{1}{2(G_1 + G_{12})}\left[\cos\left(\frac{\pi}{L_0} y_0\right)\right]^2 = R_{in}(y = 0)\left[\cos\left(\frac{\pi}{L_0} y_0\right)\right]^2$$

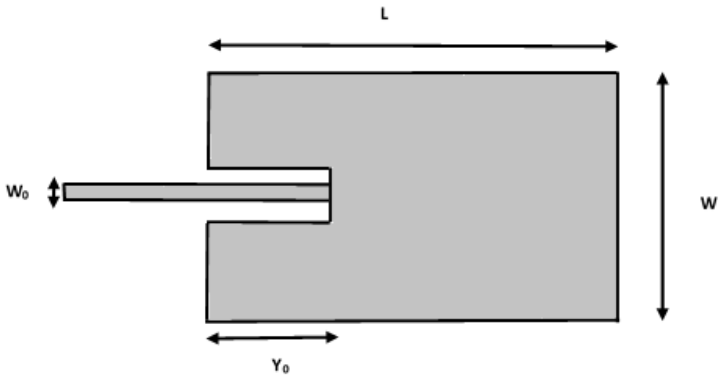


Inset fed microstrip antenna

# Appendix – II

## Error backpropagation training algorithm:

Given *p* training pairs of data set (input and the corresponding output)

$$\{z_1, d_1, z_2, d_2, \dots\dots, z_p, d_p\},$$

where $z_i$ is of dimension $(l \times l)$, $d_i$ is of dimension $(K \times l)$, and $i = 1,2, \dots\dots, p$. Note that the $I^{th}$ component of each $z_i$ is of value -1, since input vectors have been augmented. Size $J - 1$ of the hidden layer having outputs *y* is selected. Note that the $J^{th}$ component of *y* is of value -1, since hidden layer outputs have also been augmented; *y* is $(J \times 1)$ and 0 is $(K \times 1)$.

Step 1: $\eta < 0$, $E_{max}$ chosen.

Weights *W* and *V* are initialized at small random values; *W* is$(K \times J)$, *V* is$(J \times I)$.

$$q \leftarrow 1, p \leftarrow 1, E \leftarrow 0$$

Step 2: Training step starts here

Input is presented and the layers outputs computed as

$$z \leftarrow z_p, \qquad d \leftarrow d_p$$

$$y_j \leftarrow f(v_z^t z), \quad for\ j = \ 1,2, \dots\dots, J$$

where $v_j$, a column vector, is the $j^{th}$ row of *V*, and

$$o_k \leftarrow f(w_k^t y), \quad for\ k = \ 1,2, \dots\dots, K$$

where $w_k$, a column vector, is the $j^{th}$ row of *W*.

Step 3: Error value is computed:

$$E \leftarrow \frac{1}{2}(d_k - o_k)^2 + E, \qquad for\ k = \ 1,2, \dots\dots, K$$

Step 4: Error signal vectors $\delta_0$ and $\delta_y$ both layers are computed. Vector $\delta_0$is$(K \times 1)$, $\delta_y$ is $(J \times 1)$.

The error signal terms of the output layer in this step are

$$\delta_{ok} = \frac{1}{2}(d_k - o_k)(1 - o_k^2), for\ k = \ 1,2, \dots \dots \dots, K$$

The error signal terms of the hidden layer in this step are

$$\delta_{yj} = \frac{1}{2}\left(1 - y_j^2\right) \sum_{k=1}^{K} \delta_{ok} w_{kj}, for\ j = \ 1,2, \dots \dots \dots, J$$

Step 5: Output layer weights are adjusted:

$$w_{kj} \leftarrow \ w_{kj} + \ \eta \delta_{ok} y_j, for\ k = \ 1,2, \dots \dots \dots, K \text{ and } j = \ 1,2, \dots \dots \dots, J$$

Step 6: Hidden layer weights are adjusted:

$$v_{ji} \leftarrow \ v_{ji} + \ \eta \delta_{yj} z_i, for\ j = \ 1,2, \dots \dots \dots, J \text{ and } i = \ 1,2, \dots \dots \dots, I$$

Step 7: If $p \ < P$ then $p \ \leftarrow p + 1$ and $q \ \leftarrow \ q + 1$ go to step 2; otherwise go to step 8

Step 8: The training cycle is completed

For $E \ < E_{max}$, terminate the training session. Output weights *W*, *V*, $q$ and *E*

If $E \ > E_{max}$, then q ← 0 , $p \leftarrow 1$, and initiate the new training cycle by going to Step 2.

# Appendix – III

## PSO Algorithm:

Formally the algorithm can be described as below:

- Define the solution space

  In this step the parameters to be optimized by PSO are defined. Each parameter is provided with a range for searching the optimal solution. So the minimum and maximum value for each dimension is specified to define the solution space of the problem.
- Define a fitness function

  Fitness function relates the physical problem to the optimization algorithm. It takes the value of all *N* parameters that represents a possible solution of the problem and measures the goodness of that particular solution. The fitness function should exhibit a functional dependence with each parameters being optimized.
- Random initialization of swarm positions and velocities

  Let the initial position and velocity of each particle in the swarm (a population of particles) are $X_i = (x_{i1}, x_{i2}, \dots\dots\dots\dots x_{iN})$ and $V_i = (v_{i1}, v_{i2}, \dots\dots\dots\dots v_{iN})$ (where $N$ is the number of design parameters of the optimization problem), respectively. In the first run, the initial positions of the each particle is designed as the best positions encountered by the each individual and is represented as $P_i = (p_{i1}, p_{i2}, \dots\dots\dots\dots p_{iN})$. The global best position of all particles is selected from these initial positions by evaluating the fitness function at each solution space and is represented by $P_g = (p_{g1}, p_{g2}, \dots\dots\dots\dots p_{gN})$.
- Update the particle velocity

  The velocity of each particle is updated according to the individual best position and the global best position of the swarm

  The velocity is updated in each time step using the relation:

  $$v_{id}(t+1) = wv_{id}(t) + c_1 r_1(p_{id} - x_{id}) + c_2 r_2(p_{id} - x_{id}) \qquad (1)$$

  where $c_1$(cognitive constant) and $c_2$(social constant) are two positive constants, $r_1$ and $r_2$ are two random numbers with uniform distribution in the interval [0,1]. The parameter $w$ is the inertial weight that correlates the particles current velocity to its

previous velocity. The convergence of PSO depends on the values of *w*in each iteration. The values $c_1$ and $c_2$ are considered to be equal in most PSO literature to balance movement of particles in both cognitive and social components. Equation (1)describes the flying trajectory of a population particle. This equation consists of three parts. The first part is the momentum part implying that the velocity can't be changed abruptly. The second part is the cognitive part which represents the learning from its own flying experience. The third part is the "social" part i.e. learning from flying experience of the group. The velocity of each particle is restricted by the maximum velocity vector $V_{max}$ on each dimension.

- Update the position

  In this step, the position of each particle is updated and the particle moves to a new location. The velocity determined from equation 1 is applied for a given time step and the new position is obtained by

  $$x_{id} = x_{id} + \Delta \times v_{id} \quad (2)$$

- Fitness function evaluation:

  The updated positions of the particles are used to evaluate the fitness function$f(X_i)$. This fitness value of each particle is compared with the previously obtained best fitness value of the corresponding particle.

  If $f(X_i) < f(P_i)$ then $P_i = X_i$

  Similarly the global best position $P_g$ is updated, if the best particle in the current swarm has lower $f(X)$ then$f(P_g)$.

- Termination criteria:

  The velocities of the particles are updated in each time step and the particles change their locations towards its personal towards its personal best and global best positions. The process is continued till a specified number of iterations or a minimum error criterion is attained.

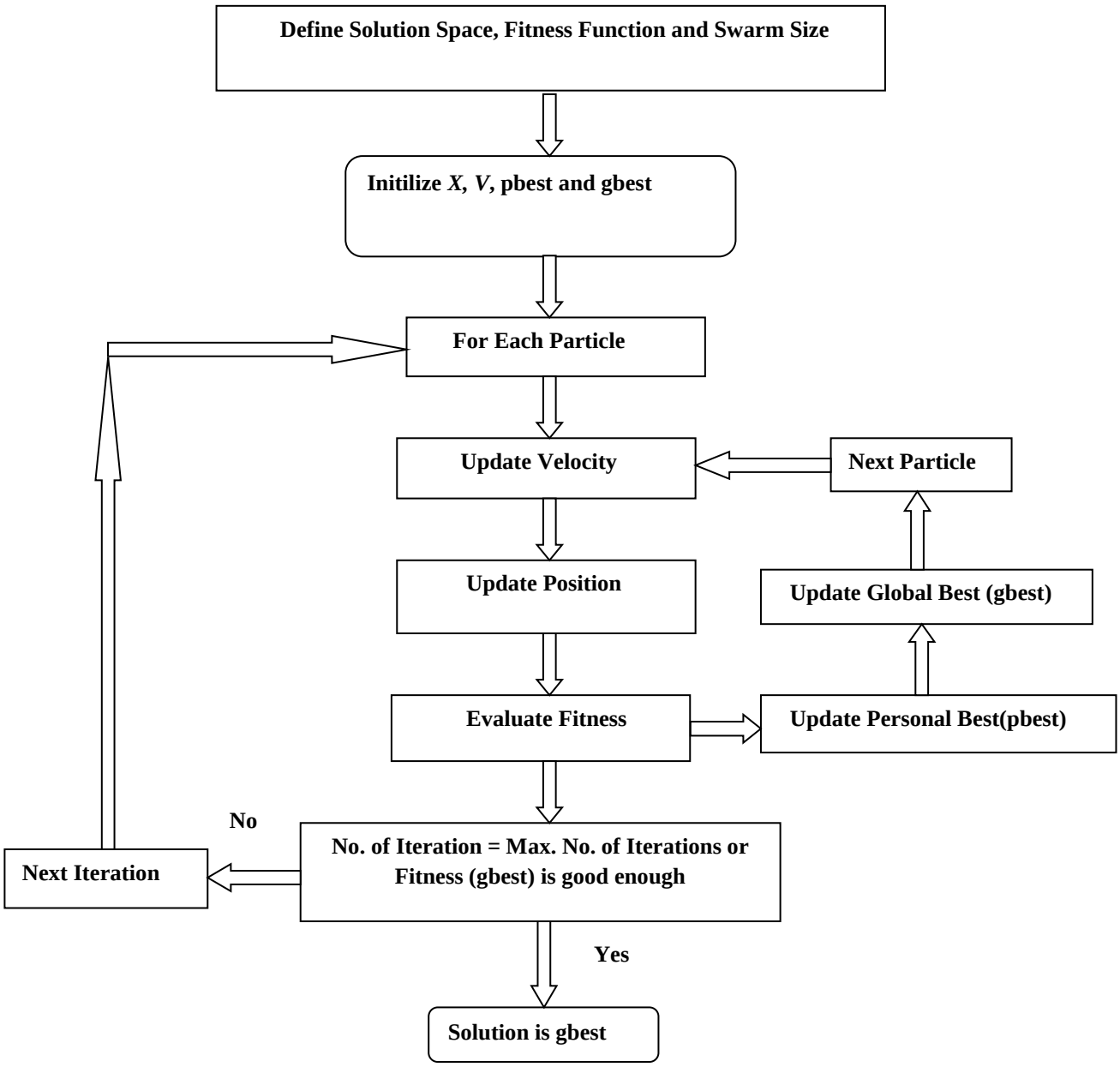


Flow chart of PSO algorithm

# References


[1] C. Caloz and T. Itoh. Electromagnetic Metamaterials: Transmission Line Theory and Microwave Applications. New York: Wiley and IEEE Press, 2005.

[2] L.I. Mandelstam, Complete Works, vol. 5 (USSR Academy of Sciences, Moscow, 1950), Lectures given on 26 February 1940 and on 5 May 1944.

[3] G. D. Malyuzhinets, A note on the radiation principle, *Zhurnal Technicheskoi Fiziki* 21, 940-942 (1951).

[4] D. V. Sivukhin, The energy of electromagnetic waves in dispersive media. *Opt. Spektrosk* **3**, 308–312 (1957).

[5] R.G.E. Hutter: Beam and wave electronics in microwave tubes. Van Nostrand Reinhold, Princeton, NJ, 220-230 (1960)

[6] R. Silin, V. P. Sazonov: Slow wave structures. Moscow, Soviet Radio (1966) (in Russian).

[7] V.G. Veselago, "Electrodynamics of substances with simultaneously negative values of ε and μ," *Soviet Physics Uspekhi*, vol. 10, pp. 509-514, 1968.

[8] J. B. Pendry, A. J. Holden, W. J. Stewart and I. Youngs, "Extremely low frequency plasmons in metallic mesostructures," *Physics Review Letters*, vol. 76, pp. 4773-4776, 1996.

[9] J. B. Pendry, A. J. Holden, D. J. Robbins and W. J. Stewart, "Magnetism from conductors and enhanced nonlinear phenomena*," IEEE Transactions on Microwave Theory and Techniques*, vol. 47, pp. 2075-2084, 1999.

[10] D. R. Smith, Willie J. Padilla, D. C. Vier, S. C. Nemat-Nasser, and S. Schultz, "Composite medium with simultaneously negative permeability and permittivity," *Physical Review Letters*, Vol. 84, pp. 4184-4187, 2001.

[11] T. J. Cui, J. A Kong "Time domain electromagnetic energy in a frequency dispersive left handed media," *Physical Review Letters*, B-70, November, 2004.

[12] T. J. Cui, Q. Cheng, W. B. Lu, Q. Jiang and A. J. Koy, " Localization of electromagnetic energy using a left handed medium slab," *Physical Review Letters*, B-71, January, 2005

[13] J. Huangfu, L. X. Ran, H. S. Chen, X. M. Zhag, K. S. Grzegorczyk and J. A. Kong, "Experimental confirmation of negative refractive index of a metamaterial composed of omega like metallic patterns," *Applied Physics Letters* 84, pp. 1537-1539, 2004.

[14] D. R. Smith, J. J. Mock, A. F. Starr and D. Schuring, "Gradient index metamaterials," *Physical Review Letters*, B-71, March, 2005.

[15] J. B. Pendry, "Negative refraction makes a perfect lens," *Physical Review Letters*, vol.85, pp. 3966–3969, 2000.

[16] N. Fang, and X. Zhang, "Imaging properties of a metamaterial superlens," *Applied Physics Letters*, vol. 82, pp. 161–163, 2003.

[17] D. R. Smith, "Limitations on sub diffraction imaging with a negative refractive index slab," *Applied Physics Letters*, vol. 82, pp. 1506–1508, 2003.

[18] I. A.Larkin and M. I. Stockman "Imperfect perfect lens," *Nano Letters*, vol. 5, pp. 339–343, 2005.

[19] Z. Liu, "Rapid growth of evanescent wave with a silver superlens," *Applied Physics Letters*, vol. 83, pp. 5184–5186, 2003.

[29] N. Fang., Z. Liu., T. J. Yen and X. Zhang, "Regenerating evanescent waves from a silver superlens," *Optical Express*, vol. 11, pp. 682–687, 2003.

[21] G.V. Eleftheriades, O. Siddiqui, and A.K. Iyer, "Transmission line models for negative refractive index media and associated implementations without excess resonators," *IEEE Microwave and Wireless Components Letters*, vol. 13, no. 2, pp. 51-53, Feb. 2003.

[22] A. Grbic, and G. V. Eleftheriades, "Negative refraction, growing evanescent waves and sub-diffraction imaging in loaded transmission-line metamaterials," *IEEE Transactions on Antennas and Propagation*, vol. 51, No. 12, pp. 2297-2305, December, 2003.

[23] C. Caloz, and T. Itoh, "Transmission line approach of left-handed (LH) materials and microstrip implementation of an artificial LH transmission line," *IEEE Transactions on Antennas and Propagation*, vol. 52, No. 5, pp. 1159-1166, May 2004.

[24] A. Lai, C. Caloz, and T. Itoh, "Composite right/left-handed transmission line metamaterals," *IEEE Microwave Magazine*, pp. 34-50, September 2004.

[25] A. Sanada, C. Caloz and T. Itoh, "Characteristics of the composite right/left-handed transmission lines," *IEEE Microwave and Wireless Components Letters*, vol. 14, no. 2, pp. 68-70, Feb. 2004.

[26] I. Lin, M. DeVincentis, C. Caloz, and T. Itoh, "Arbitrary dual-band components using composite right/left-handed transmission lines," *IEEE Transactions on Microwave Theory and Techniques*, vol. 52, pp. 1142–1149, Apr. 2004

[27] C. Caloz and T. Itoh, "A novel mixed conventional microstrip and composite right/left-handed backward-wave directional coupler with broadband and tight coupling characteristics," *IEEE Microwave Wireless Component Letters*, vol. 14, pp. 31–33, Jan. 2004

[28] C. Caloz, A. Sanada, and T. Itoh, "A novel composite right/lefthanded coupled-line directional coupler with arbitrary coupling level and broad bandwidth," *IEEE Transactions on Microwave Theory and Techniques*, vol. 52, pp. 980–992, Mar. 2004.

[29] S. Lim, C. Caloz, and T. Itoh, "A reflecto-directive system using a composite right/left-handed (CRLH) leaky-wave antenna and heterodyne mixing," *IEEE Microwave Wireless Component Letters,* vol. 14, pp. 183–185, April 2004.

[30] S. Lim, C. Caloz, and T. Itoh, "Metamaterial-based electronically controlled transmission line structure as a novel leaky-wave antenna with tunable radiation angle and beamwidth," *IEEE Transactions on Microwave Theory and Techniques*, vol. 53, no. 1, January 2005.

[31] K. D. Jang, J. H. Kim, D. H. Lee, and W. S. Park "Compact resonant antenna based on composite right/left handed transmission line with a magneto-dielectric material," *Microwave and Optical Technology Letters* , vol. 51, no. 8, August 2009.

[32] T. Yang, P.L. Chi and R. Xu "novel composite right/left-handed leaky-wave antennas based on the folded substrate-integrated-waveguide structures," *Progress In Electromagnetics Research C*, vol. 29, pp. 235–248, 2012.

[33] Y. Rahmat-Samii and H. Mosallaei. Electromagnetic BandGap Structures: Classification, Characterization and Applications. *11 International Conference on Antennas and Propagation*, vol. 2(no. 480):pp. 560-564, April 2001.

[34] N. Engheta and R. W. Ziolkowski. Electromagnetic Metamaterials: Physics and Engineering Exploration. Wiley and IEEE Press, 2006.

[35] B. A. Munk. Frequency Selective Surfaces: Theory and Design. John Wiley and Sons and IEEE Press, May 2000.

[36] Ricardo Marques, Ferran Martin and Mario Sorolla: Metamaterials with Negative Parameters Theory Design and Microwave application. Wiley, Inc., U.S.A, 2007.

[37] Y. Rahmat-Samii and H. Mosallaei. Electromagnetic BandGap Structures: Classification, Characterization and Applications. *11 International Conference on Antennas and Propagation*, vol. 2(no. 480):pp. 560-564, April 2001.

[38] D. Guha and Y. M. M. Antar (Editors): Microstrip and Printed Antennas: New Trends, Techniques and Applications, John Wiley & Sons, West Sussex, UK, 2011.

[39] R. W. Ziolkowski and A. Erentok, "Metamaterial-based efficient electrically small antennas," *IEEE Transactions on Antennas and Propagation,* vol. 54, no. 7, pp. 2113-2130, 2006.

[40] Y. Dong, T. Yang, and T. Itoh, "Substrate integrated waveguide loaded by complementary split-ring resonators and its applications to miniaturized waveguide filters," *IEEE Transactions on Microwave Theory and Techniques*, vol. 57, no. 9, pp. 2211-2223, 2009.

[41] T. J. Cui, D. Smith, R. Liu (Editors): Metamaterials Theory, Design, and Applications, Springer, 2010 .

[42] R. K. Baeel, G. Dadashzadehl, and F. G. Kharakhilil, "Using of CSRR and its Equivalent Circuit Model in Size Reduction of Microstrip Antenna," *Proceedings of Asia-Pacific Microwave Conference 2007*.

[43] X. Cheng, D. E. Senior, C. Kim, and Y.-K. Yoon, "A Compact Omnidirectional Self-Packaged Patch Antenna With Complementary Split-Ring Resonator Loading for Wireless Endoscope Applications," *IEEE Antennas and Wireless Propagation Letters*, vol. 10, pp. 1532- 1536, 2011.

[44] M. S. Sharawi, M. U. Khan, A. B. Numan, and D. N. Aloi, "A CSRR Loaded MIMO Antenna System for ISM Band Operation," *IEEE Transactions on Antennas and Propagation*, vol. 61, no. 8, pp. 772-785, February 2012.

[45] Y. Dong, H. Toyao, and T. Itoh, "Design and Characterization of Miniaturized Patch Antennas Loaded With Complementary Split-Ring Resonators," *IEEE Transactions on Antennas and Propagation*, vol. 60, no. 2, pp. 772-785, February 2012.

[46] C. Caloz, T. Itoh, and A. Rennings, "CRLH metamaterial leaky-wave and resonant antennas," *IEEE Antennas and Propagation Magazine*, vol. 50, no. 5, pp. 25-39, 2008.

[47] J. R. James and P.S. Hall, Handbook of Microstrip Antennas: IEE Peter Peregrinus Ltd, London, 1989.

[48] J. Huang, "Miniaturized UHF microstrip antenna for a Mars mission," *Antennas and Propagation Society International Symposium, 2001. IEEE*, Boston, MA, USA, 2001, pp. 486-489 vol.4.

[49] R. Chair, K. M. Luk. and K. F. Lee "Miniature multi-layer shorted patch antenna," *Electronics Letters*, vol. 36, pp. 3-4, January, 2000.

[50] R. Waterhouse, "Small microstrip patch antenna," *Electronics Letters*, vol. 31, no. 8, pp. 604-605, 13 Apr 1995.

[51] R Chair, K.F. Lee and K.M. Luk, "Bandwidth and cross polarization characteristics of quarter wave shorted patch antenna," *Microwave and Optical Technology Letters*, 1999, 22(2), pp. 101-103

[52] Y. Lee and Y. Hao, "Characterization of microstrip patch antennas on metamaterial substrates loaded with complimentary split ring resonators," *Microwave and Optical Technology Letters*, vol 50, no-8, August 2008, pp-2131-2135.

[53] A. Alu, F. Bilotti, N. Engheta, and L. Vegni, 2007. "Sub-wavelength compact, resonant patch antennas loaded with metamaterial," *IEEE Transactions on Antennas and Propagation*, vol. 55, no. 1, pp. 13–25.

[54] F. Bilotti, A. Alu and L. Vegni, 2008. "Design of miniaturized metamaterial patch antennas with μ-negative loading," *IEEE Transactions on Antennas and Propagation*, vol. 56, no. 6, pp. 1640 – 1647.

[55] A. B. Ochetan and G. Lojewski, "Metamaterial leaky-wave and resonant type antennas," *Electronics and Telecommunications (ISETC), 2010 9th International Symposium on*, Timisoara, 2010, pp. 57-60.

[56] O. E. Marbet, M. Aznabet, F. Falcone, H. Rmili, J. M. Floch, M. Drissi and M. Essaaidi "A compact split ring resonator antenna for wireless communication system," *Progress in Electromagnetic Research Letters*, vol. 3, pp. 201-207, 2013.

[57] Z. Duan and S. Qu "Electrically small antenna inspired by spired by split ring resonator," *Progress in Electromagnetic Research Letters*, vol. 7, pp. 47-57, 2009.

[58] J. B Pendry, A. J. Holden, W. J Stewart and I. Youngs, "Extremely low frequency Plasmon in metallic meso structures," *Physical Review Letters,* vol.76, June 1996, pp. 4773-4776.

[59] J. B. Pendry, A. J. Holden, W. J. Stewart and I. Youngs, " Magnetism from conductors and enhanced nonlinear phenomena," *IEEE Transaction on Microwave Theory and Techniques,* vol. 47, no. 11, Nov. 1999, pp. 2075-2084.

[60] F. Falcone, T. Lopestegi, J. D. Baena, F. Martin and M. Sorolla " Effective negative ε stopband microstrip lines based on complimentary split ring resonators," *IEEE Microwave and Wireless Component Letters*, vol. 14, no. 16, June 2004, pp. 280-282.

[61] J. D. Baena, J. Bonache, F. Martin, R. M. Sillero, F. Falcone, T. Lopetegi, M.A.G. Laso, J. Garcia-Garcia, I. Gill, M.F. Portillo and Mario Sorolla, "Equvalent circuit models for split ring resonators and complimentary split ring resonators coupled to planar transmission lines," *IEEE transaction on Microwave Theory and Techniques,* vol-53,no-4, April 2005,pp-1451-1461.

[62] C. Rocksthul, T. Zentgraf, P. T. Meyrath, H. Giessen and F. Lederer, "Resonances in complimentary metamaterials and nanoapertures," *Optics Express*, vol 16, no. 3, Feb. 2008, pp. 2080-2090.

[63] L. J. Rogla, J. Carbonell and V. E. Boria, "Study of equivalent circuits for open-ring and split-ring resonators in coplanar waveguide technology," *IET Microwave Antennas and Propagation*, vol. 1, no. 1, pp- 170-176, 2007.

[64] S. S. Mohan, "The design, modeling and optimization of on-chip inductor and transformer circuits," *Ph.D. Thesis*, Standford University, 1999.

[65] I. Bahl, P. Bhartia: Microwave Solid State Circuit Design, Hoboken, NJ, Wiley-Interscience 2003.

[66] M. Beruete, F. Falcone, M. J. Freier, Marques. R and J. D. Baena, "Electroinductive waves in chains of complimentary metamaterial elements," *Applied Physics Letters*, vol. 88, 2006.

[67] I. Gill, J. Bonache, M. Gill, J. G. Gracia, R. Marques and F. Martin, "Modeling complimentary split ring resonator (CSRR) left handed lines with inter resonator coupling," in *Proc. IEEE MELECON 2006*, Spain, May 16-19, pp. 225-228.

[68] M. J. Fereire, R. Marques, F. Medina, M. A. G. Laso and F. Martin "Planar magnetoinductive wave transducers: Theory and applications" *Applied Physics Letters*, vol. 85, 2004.

[69] I. J. Bahl, P. Bhartia: Microstrip Antennas, Artech House, Massachuaetts, 1980.

[70] N. C. Chauhan, M. V. Kartikeyan and A. Mittal, *Soft Computing Methods for Microwave and Millimeter- Wave Design Problems*, Springer, India, 2012.

[71] Q. J. Zhang and K. C. Gupta, Neural Network for RF and Microwave Design, Artech House, Norwood MA, 2000.

[72] C. Christodoulou and M. Georgiopolous, Application of Neural Networks in Electromagnetics, Artech House, Boston, 2001.

[73] Randy L Haput and Douglas H. Warner, Genetic Algorithims in Electromagnetics, John Wiley and Sons, Hobken, New Jersy, 2007.

[74] Q. J. Zhang and G. L. Creech [Guest Editors], "Specila issue on application of Artificial Neural Networks to RF and Microwave Design" *International Joournal of RF and Microwave Computer Aided Engineering*, vol. 12, no. 1, pp. 1-140, January 2002.

[75] Y Rahamat-Sammi and C. G. Christodoulou [Guest Editors], "Specila Issue on Synthesis and Optimization Techniques in Electromagnetics and Antewnna Design" *IEEE Transaction on Antenna and Propgation*, vol. 55, no. 3, pp. 518-522, March 2007.

[76] A Patnaik, D. E. Anagnostou, R. K. Mishra, C. G. Christodoulou and J. C. Lyke "Application of Neural Networks in Wireless Communications, *IEEE Antennas and Propagation Magazine*, vol. 45, no. 3, pp. 343-353, March 1997.

[77] N. Jin and Y. Rahamat-Sammi "Particle Swarm Optimization (PSO) for Antenna Designs in Engineering Electromagnetism*" Journal of Artificial Evolution and Applications*, vol. 2008, pp. 1-10, January 2008.

[78] X. Ding, V.K. Devabhaktuni, B. Chattaraj, M. Yagoub, M. Deo, J. Xu, and Q.J. Zhang, "Neural network approaches to electromagnetic based modeling of passive components and their applications to high-frequency and high-speed nonlinear circuit

optimization," *IEEE Transactions on Microwave Theory and Techniques*, vol. 52, pp. 436-449, January 2004.

[79] Q.J. Zhang, K.C. Gupta, and V.K. Devabhaktuni, "Artificial neural networks for RF and microwave design: From theory to practice," *IEEE Transactions on Microwave Theory and Techniques*, vol. 51, pp. 1339-1350, April 2003.

[80] D.Karaboga, K.Guney, S.Sagiroglu and M.Erler "Neural computation of resonant frequency of elect rica II y thin and thick rectangular m icrostri p antennas" *IEE Proc.-Microwave Antennas Propagation*., vol. 46, no. 2, April I999.

[81] Kerim Guney and Nurcan Sarikaya "A Hybrid Method Based on Combining Artificial Neural Network and Fuzzy Inference System for Simultaneous Computation of Resonant Frequencies of Rectangular, Circular, and Triangular Microstrip Antennas" *IEEE Transactions on Antennas and Propagation*, vol. 55, no. 3, March 2007.

[82] S. Baskar, A. Alphones and P. N. Suganthan, "Genetic algorithm based design of reconfigurable antenna array with discrete phase shifter" *Mirow. Opt. Technol. Lett.*, vol. 45, no. 6, pp. 461-465, June 2005.

[83] A. Alphones and V. Passoupathi, "Null steering in phased array by position perturbations: A genetic algorithm approach" *Proc. IEEE Int. symposium on phased array systems and technology*, Boston, MA, pp. 203-207, Oct 1996.

[84] Madhav V, Sarma N.V.S.N, "An Improved Genetic Algorithm with Clustering Techniques to Extend Network Lifetime in Homogeneous and Heterogeneous Wireless Sensor Networks**,"** *International journal of Advanced Research in Computer Science*, vol. 4, no. 8, May-June 2013, pp. 0976-5697.

[85] Vakula. D, Sarma N.V.S.N "Using Neural Networks for Fault Detection of Planar Antenna Arrays," *Progress in Electromagnetic Research letters (PIERS-L)*, vol. 14, 2010, pp 21 -30.

[86] S. Shailendra, R. Bhattacharjee, S. K. Bose, "A multipath variant of SCTP with optimized flow division extension" *Computer Communications*, vol. 67, pp. 56-65, Aug. 2015.

[87] A. Patnaik, D. E. Anagnostou, R. K. Mishra, C. G. Christodoulou and J. C. Lyke, "Neurocomputational Analysis of a Multiband Reconfigurable Planar Antenna", *IEEE Transactions on Antennas and Propagation*, vol. 53, pp: 3453 - 3458, Nov. 2005.

[88] A. Patnaik, D. E. Anagnostou, R. K. Mishra, C. G. Christodoulou and J. C. Lyke, "Applications of Neural Networks in Wireless Communications", *IEEE Antennas and Propagation Magazine*, vol.46, no. 3, pp. 130-137, June 2004.

[89] S. Shailendra, R. Bhattacharjee, S. K. Bose, "An implementation of Min-Max optimization for multipath SCTP through bandwidth estimation based resource pooling technique", *AEU - International Journal of Electronics and Communications,* vol. 67 (3), pp. 246-249, 2013.

[90] R. Ghatak, D.R. Poddar, R.K. Mishra " Design of Sierpinski gasket fractal microstrip antenna using real coded genetic algorithm " *IET Microw. Antennas Propag*., vol. 3, pp. 1133– 1140, 2009.

[91] S. Das and A. Chakraborty "A Novel Modeling Technique to Solve a Class of Rectangular Waveguide Based Circuits and Radiators**,"** *Progress in Electromagnetic Research,* vol. 61, pp. 231-252, 2006.

[92] Ghatak. R, Pal. M "Revisiting relations for modeling the input resistance of a rectangular microstrip antenna" *IEEE Antennas and Propagation Magazine*, vol. 57, pp. 114-116, 2015.

[93] S. Haykin, Neural Networks: A Comprehensive Foundation, IEEE Press/ IEEE Computer Socity Press, New York, 1994.

[94] A. Patnaik and R. K. Mishra "Artificial Neural Network Technique in Microwave Engineering" *IEEE Microwave Magazine*, vol. 1, no. 1, pp. 55-60, April 2000.

[95] J Kenedy and R. C. Eberhart "Particle swarm Optimization" *IEEE conference on neural networks, Perth Australia*, pp. 1942-1948, November 1995.

[96] J. Robinson and Y. Rahamat-Sammi "Particle swarm optimization in electromagnetics*" IEEE Transactions on Antennas and propagation*, vol. 52, no. 2, pp. 397-407, February 2004.

[97] S. Xu and Y. Rahamat-Sammi "Boundary Condition in Particle Swarm Optimization Revisited" *IEEE Transaction on Antenna and Propagation*, vol. 55, no. 3, pp. 760-765, March 2007.

[98] K. E. Parsopoulos and M. N. Varhatis "Recent approaches to global optimization problems through particle swarm optimization" *International Journal on Natural Computing*, vol. 1, no. 2-3, pp., June 2002.

[99] D. R. Smith and S. Schultz, "Determination of effective permittivity and permeability of metamaterials from reflection and transmission coefficients", *Physical Review Letters* 65 (2002), 195104-1 – 195104-5.

[100] X. Chen, T. M. Grzegorczyk, W. Bae-Ian, J. Pacheco, and J. A. Kong, "Robust method to retrieve the constitutive effective parameters of metamaterials", *Physical Review Letters* 70 (2004) 016680-1 – 016680-8.

[101] D. R. Smith, D. C. Vier, T. Koshney and C. M. Soukoulis, "Electromagnetic

parameter retrieval from inhomogeneous metamaterial", *Physical Review Letters* 71 (2005) 033617-1 – 033617-11.

[102] R. W. Ziolkowski, "Design, fabrication, and testing of double negative metamaterials", *IEEE Trans. Antennas and Prop*. 51 (2003) 1516-1529.

[103] R. Pandeeswari and S. Raghavan "Microstrip antenna with complimentary split ring resonator loaded ground plane for gain enhancement" *Microwave and Optical Technology Letters,* vol. 57, pp. 292-296, 2015.

[104] N. Ortiz, F. Falcone and M. Sorolla "Gain improvement of dual band antenna based on complimentary rectangular split ring resonator" *ISRN Communication and Networking*, vol. 2012, pp. 1-9, 2012.

[105] M. Ramzan and K. Topalli "A miniaturized patch antenna by using a CSRR loading plane" International Journal of Antennas and propagation, vol. 2015, pp. 1-9, 2015.

[106] I. Irfanullah, S. Nariyal, S. Roy, M. M. Masud, B. Ijaz and B. D. Braaten, "Analysis of the Noise Voltage Coupling (Crosstalk) between Right-Handed and Composite Right/Left-Handed (CRLH) Transmission Lines on Printed Circuit Boards," *IEEE Transactions on Electromagnetic Compatibility*, vol. 55, no. 4, Aug. 2013, pp. 788 - 797.

[107] B. D. Braaten, M. Reich and J. Glower, "A Compact Meander-Line UHF RFID Tag Antenna Loaded with Elements Found in Right/Left-Handed Coplanar Waveguide Structures," *IEEE Antennas and Wireless Propagation Letters,* vol. 8, pp. 1158-1161, 2009.

[108] S. I. Rosaline and S. Raghavan, "Design and analysis of a SRR superstrate for SAR reduction," *Journal of Electromagnetic waves and appl*., vol.29, No. 17, pp. 2330-2338, 2015.

[109] J. Zhu and G. V. Eleftheriades, "Dual-band metamaterial inspired small monopole antenna for WiFi applications, *Electronics Letters*, vol. 45, no. 22, pp. 1104–1106, 2009.

[110] F. J. Herraiz-Martinez, L. E. Garcia-Muinoz, D. Gonzalez- Ovejero, V. Gonzalez-Posadas, and D. Segovia-Vargas, "Dual frequency printed dipole loaded with split ring resonators," *IEEE Antennas and Wireless Propagation Letters,* vol. 8, pp. 137–140, 2009.

[111] J. Montero-de-Paz, E. Ugarte-Munoz, F. J. Herraiz-Martinez, V. Gonzaalez-Posadas, L. E. Garc´ıa-Muinoz, and D. Segovia- Vargas, "Multifrequency self-diplexed single patch antennas loaded with split ring resonators," *Progress in Electromagnetics Research*, vol. 113, pp. 47– 66, 2011.

[112] F. J. Herraiz-Martinez, F. Paredes, G. Zamora, F. Martin and J. Bonache, "Dual-band printed dipole antenna loaded with open complementary split-ring resonators (OCSRRs) for wireless applications," *Microwave and Optical Technology Letters*, vol. 54, no. 4, pp. 1014–1017, 2012.

[113] L. M. Si, W. Zhu and H. J. Sun "A compact, planar and CPW- fed metamaterial-inspired dual band antenna", *IEEE Antennas and Wireless Propagation Letters*, vol. 12, pp. 305-308,2013.

[114] Du. G, Tang. X and Xiao. F, "Tri band metamaterial inspired monopole antenna with modified S shaped resonator" *Progress in Electromagnetic Research Letters*, vol. 23, April 2011, pp. 39-48.

[115] Mahdy M. R. C,Zuboraj M. R. A, Ovi A. A. N and Matin M. A " Novel deign of triple band rectangular patch antenna loaded with metamaterial " *Progress in Electromagnetic Research Letters,* vol. 21, March 2011, pp. 99-107.

[116] Dai W. X, Wang Y. Z, Li. L and Liang H. C " Multiband rectangular microstrip antenna using a metamaterial inspired technique " *Progress in Electromagnetic Research Letters,* vol. 41, June 2013, pp. 87-95.

[117] Caloz C, Itoh T and Rennings A "CRLH metamaterial leaky wave and resonant antennas "*IEEE Antennas and Propagation Magazine*, vol. 50, Oct. 2008, pp. 25-39.

[118] Ryu Y, Park J, Lee J and Tae H " Multiband antenna using +1, -1 and 0 resonant mode of DGS dual composite right/left handed transmission line " *Microwave and Optical Technology Letters*, vol. 51, Jan. 2009, pp. 2485-2488.

[119] Cao W, Zhang B, Liu A, Yu T, Guo D and Pan X " Multi frequency and dual mode patch antenna based on electromagnetic band gap structure " *IEEE Transaction on Antennas and Propagation* , vol. 60, no. 12, Dec. 2012, pp. 6007-6012.

[120] Cao W, Liu A , Zhang B, Yu T, Guo D, Wei Y and Qian Z " Multiband multimode microstrip circular patch antenna loaded with metamaterial structures " *Journal of Electromagnetic Waves and Applications* , vol. 26, 2012, pp. 923-931.

[121] Cao W, Liu A, Zhang B, Yu T, Guo D and Wei Y " A dual band microstrip antenna with omnidirectional circularly polarized and unidirectional linearly polarized characteristics based on metamaterial structure " *Journal of Electromagnetic Waves and Applications* , vol. 26, 2012, pp. 274-283.

[122] C. A. Balanis: Antenna Theory - Analysis and Design, John Willey and Sons, New York, 1997.

[123] Anguera, J., L. Boada, C. Puente, C. Borja, and J. Soler, "Stacked H-shaped microstrip patch antenna," *IEEE Transactions on Antennas and Propagation*, vol. 52, no. 4, pp. 983–993, 2004.

[124] Moldovan, E., B. Lindmark, and P. S. attman, “Optimization of a stacked patch antenna for high directivity,” 13`emes Journ´eesInternationales de Nice sur les Antennes (JINA), pp. 317–372, 2004

[125] Foroozesh, A. and L. Shafai, “Investigation into the effects of the patch-type FSS superstrate on the high-gain cavity resonance antenna design,” *IEEE Transactions on Antennas and Propagation*, vol. 58, no. 2, pp. 258–270, 2010.

[126] Foroozesh, A. and L. Shafai, “On the characteristics of the highly directive resonant cavity antenna having metal strip grating superstrate,” *IEEE Transactions on Antennas and Propagation*, vol. 60, no. 1, pp. 78–91, 2012.

[127] Pirhadi, A., F. Keshmiri, M. Hakkak, and M. Tayarani, “Analysis and design of dual band high directivity EBG resonator antenna using square loop FSS as superstrate layer,” *Progress InElectromagnetics Research*, vol. 70, pp. 1–20, 2007.

[128] Cheype, C., C. Serier, M. Th`evenot, T. Mon´edi`ere, A. Reineix, and B. Jecko, “An electromagnetic bandgap resonator antenna,” *IEEE Transactions on Antennas and Propagation*, vol. 50, no. 9, pp. 1285–1290, 2002.

[129] Enoch. S, Tayeb. E, Sabourous. P, Vincent. P and Legay. H “A metallic fabry-parrot cavity directive antenna,” *IEEE Antennas and Propagation Magazine*, vol. 50, pp. 220–224, 2006.

[130] Wu. Q, Pan. P, Meng. Y,Li. W.L and Wu. J “A novel flat lens horn antenna designed based on zero refraction principle of metamaterials”, *Apply Physics Letters*, vol. 88, 2006.

[131] S. Enoch, G. Tayeb, P. Sabouroux, N. Gue´rin, and P. Vincent "A metamaterial directive emission," *Physical Review Letters* ,volume 21, pp. 1-4, November 2002.

[132] J. Brown, Artificial dielectrics having refractive indices less than unity, in: Proceeding of the IEE-Part-4 Institution Monographs, 100(5), 1953, pp. 51-62

[133] D. R. Smith, D. C. Vier, N. Kroll, S. Schultz “Direct calculation of permeability and permittivity for a left-handed matameterial” *Applied Physics Letters*, vol. 77, pp. 2246-2248, 2000.

[134] T. Wellend, R. Schuhmann, R. B. Greeegor, C. G. Parazzol, M. Vettor, D. R. Smith, D. C. Vier, S. Schultz “ Ab initio numerical simulation of left handed metamaterials: comparison of calculations and experiments “ *Journal of Applied Physics*, vol. 90, pp. 5419-5424, 2001.

[135] G. Dewar “A thin wire array and magnetic host structure with n<0 “*Journal of AppliedPhysics*, vol. 97, pp. 1011-1013, 2005.

[136] M. Hudlicka, J. Machac, S. I. Nefedov “A triple wire medium as an isotropic negative permittivity metamaterials “ *Progress on Electromagnetics Research*, vol. 65, pp. 233-246, 2006.

[137] P. Markos, C. M. Soukolis " Absorption losses in periodic arrays of thin metallic wires " *Optics letters*, vol. 28, pp. 846-848, 2003.

[138] A. Deetriadou, J. B. Pendry "Taming spatial dispersion in wire metamaterial"*Journal of Physics: Condensed Matter*, vol. 20, 2008.

[139] S. I. Maslovoski, M. G. Silveirinha "Nonlocal permittivity from a quastatic model for a class of wire media "*Physical Review Letters B*, vol. 80, pp. 2451011-2451019, 2009.

[140] A. K. Sarychev, V. M. Shalev, Comment on paper "Extremely low frequency plasmons in metallic mesostructures "

[141] P. A. Belov, S. A Tetrykov, A. J. Viitanen "Dispersion and reflection properties of artificial media formed by regular lattice of ideally conducting wires" *Journal of Electromagnetic Waves and Application*, vol. 16, pp. 1153-1170, 2002.

[142] S. I. Maslovoski, S. A Tetrykov, P. A. Belov "Wire media with negative effective permittivity: A quatatic model "*Microwave and Optical Technology Letters*, vol. 35, pp. 47-51, 2002.

[143] A. kumar, A. Majumder, S. Chatterjee, S. Das, S. Kar "A novel approach to determine the plasma frequency for wire media " *Metamaterials*, vol. 6, pp. 43-50, 2012.

[144] G. von Trentini, "Partially reflecting sheet arrays," *IRE Transactions on Antennas and Propagation*, vol.4, pp.666–671, 1956.

[145] H. Boutayeb, K. Mahdjoubi, A. C. Tarot, and T. A. Denidni, "Directivity of an antenna embedded inside a Fabry-Perot cavity: analysis and design," *Microwave and Optical Technology Letters*, vol.48, no.1, pp.12–17, 2006.